Università
Ca'Foscari
Venezia

Dottorato di ricerca
in Scienze Chimiche
Scuola di dottorato in Scienze e Tecnologie
Ciclo XXIV
(A.A. 2008/2009 - A.A. 2010/2011)

Advances in the Use of Nanoelectrode Ensembles in Analytical Chemistry and Molecular Diagnostics

SETTORE SCIENTIFICO DISCIPLINARE DI AFFERENZA: CHIM/01

Tesi di dottorato di Morena Silvestrini, matricola 955682

Coordinatore del Dottorato	**Tutore del dottorando**
Prof. Paolo Ugo	**Prof. Paolo Ugo**

Contents

List of Abbreviations

2D-NEE	Two dimensional ensembles of nanoelectrodes
3D-NEE	Three dimensional ensembles of nanoelectrodes
A	Ampere
A	Adenine
A_{act}	Active area (cm^2)
AFM	Atomic force microscopy
A_{geom}	Geometric area (cm^2)
AP	Alkaline phosphatase
AuNPs	Gold nanoparticles
AuNPs-NEE	NEE modified with AuNPs
BSA	Bovine serum albumin
BSA–NEE	NEE treated with BSA
C	Concentration (mol cm^{-3})
C	Cytosine
Cas	Casein
Cas–NEE	NEE treated with casein
C_{dl}	Double-layer capacitance (µF cm^{-2})
CV	Cyclic voltammetry
cyst-NEE	NEE modified with cysteamine
D	Diffusion coefficient (cm^2 s^{-1})
D^+	Cationic dye
DL	Detection limit
$_{ds}$DNA	Double-stranded DNA
DTT	Dithiothreitol
e^-	Electron
E	Potential
$E_{1/2}$	Half wave potential
EDC	*N*-Ethyl-*N*′-(3-dimethylaminopropyl) carbodiimide hydrochloride
EFM	Electrostatic force microscopy
E_{pb}	Backward peak potential
E_{pf}	Forward peak potential

F	Faraday constant (C mol^{-1})
f	Fractional electrode area
$FA^+PF_6^-$	(Ferrocenylmethyl) trimethylammonium hexafluorophosphate
FAD	Flavin adenine dinucleotide
FcCOOH	Ferrocenecarboxylic acid
FE-SEM	Field emission - Scanning electron microscopy
FNAB	1-Fluoro-2-nitro-4-azidobenzene
FPLC	Fast protein liquid chromatography
FTIR-ATR	Fourier transform infrared spectroscopy - Attenuated total reflectance
G	Guanine
GOx	Glucose oxidase
HAc	Acetic acid
HEPES	4-(2-Hydroxyethyl)-1-piperazineethanesulfonic acid
HER2	Human epidermal growth factor receptor 2.
HMDE	Hanging mercury drop electrode
HPLC	High-performance liquid chromatography
HRP	Horseradish peroxidase
I_b	Backward scan current
I_C or I_{cap}	Capacitive current
ICPMS	Inductively coupled plasma mass spectrometry
I_f	Forward scan current
I_F	Faradaic current
I_{lim}	Limiting current
I_p	Peak current
IR	Infrared
k°	Standard rate constant for heterogeneous electron transfer
$k°_{app}$	Apparent rate constant for heterogeneous electron transfer
m	Slope of the calibration plot
Med	Mediator
MES	2-Mercaptoethanesulfonic acid
MES–BSA–NEE	NEE pre-treated with MES, before the protein (BSA) treatment
MES–Cas–NEE	NEE pre-treated with MES, before the protein (casein) treatment
MES–NEE	NEE treated with MES
n	Number of electrons transferred

NEA	Nanoelectrode array
NEE	Nanoelectrode ensemble
PBE	Partially blocked surface electrodes
PBS	Phosphate buffer saline
PC	Polycarbonate
pI	Isoelectric point
PMA	Phosphomolybdic acid
K_a	Acid dissociation constant. $pK_a = -\log_{10} K_a$
PMMA	Poly(methyl methacrylate)
PS	Polystyrene
PVP	Polyvvynilpyrrolidone
q	Surface density of nanodiscs in a NEE (nanodiscs cm^{-2})
Q	Electric charge
QL	Quantification limit
r	Radius
RT	Room temperature
SAM	Self-assembled monolayer
SEM	Scanning electron microscopy
SPR	Surface Plasmon resonance
$_{ss}$DNA	Single-stranded DNA
sSMCC	Sulfosuccinimidyl 4-[*N*-maleimidomethyl]-cyclohexane-1-carboxylate
Sulfo-NHS	*N*-Hydroxysulfosuccinimide sodium salt
SWV	Square wave voltammetry
T	Thymine
TA	Thioctic acid
TA–NEE	NEE treated with TA
TEM	Transmission electron microscopy
THA	Thionin acetate
TO	Total overlap
UV	Ultraviolet
v	Scan rate
V	Volt
$W_{1/2}$	Half-peak width
ΔE_p	Separation between the peak potentials

ΔI_p	Difference between two peak current values
σ	Standard deviation
ϑ	Fraction of blocked electrode surface

Sommario

Obiettivo di questo lavoro di tesi è lo sviluppo di diverse applicazioni di ensemble di nanoelettrodi (NEE), sia in campo analitico che, in prospettiva, per la diagnostica molecolare.
I NEE vengono fabbricati tramite deposizione *electroless* di oro all'interno dei pori di membrane *track-etched* di policarbonato (PC), commercialmente disponibili. La membrana, in questo caso, funge da stampo (*template*) per la crescita delle nanofibre metalliche.
Grazie alla loro struttura geometrica, i NEE operano in regime diffusivo di *total overlap* (TO) e, di conseguenza, sono caratterizzati da un elevato rapporto segnale/rumore che permette di raggiungere limiti di rivelabilità più bassi, rispetto ad elettrodi convenzionali.
La prima applicazione analitica descritta in questa tesi, riguarda la determinazione elettrochimica dello ioduro in campioni di acqua e la comparazione delle prestazioni dei NEE, rispetto a quelle di convenzionali macro-elettrodi d'oro.
Essendo lo ioduro un analita elettroattivo, i metodi elettrochimici sono stati spesso utilizzati per la sua determinazione, in particolare metodi di stripping catodico. Con questo approccio, l'analisi prevede uno stadio di preconcentrazione dello ioduro, con formazione di uno ioduro insolubile sulla superficie elettrodica (tipicamente mercurio o argento), seguita da una scansione catodica di ridissoluzione/determinazione.
In questo lavoro di tesi, invece, viene utilizzato un metodo di rivelazione diretta che, non necessitando dello step di preconcentrazione, permette una determinazione più veloce dell'analita.
La bassa corrente capacitiva tipica dei NEE consente di raggiungere un limite di rivelabilità (DL) di 0.3 µM in acqua potabile e di 0.10 µM in acqua di laguna.
La seconda e più cospicua parte della tesi è focalizzata sullo sviluppo di diverse metodologie di funzionalizzazione dei NEE, per la fabbricazione di biosensori elettrochimici.
Innanzitutto, viene descritta la possibilità di prevenire adsorbimenti aspecifici di molecole biologiche, in particolare proteine, sulla superficie metallica dei nanoelettrodi, tramite preventiva protezione dei nanoelettrodi d'oro con monostrati auto-assemblati (SAMs) di tioli o disolfuri. Questa procedura può risultare utile per la fabbricazione di immunosensori o biosensori dove vengono impiegati sistemi proteici che tendono ad adsorbirsi facilmente sulla superficie elettrodica (in questo caso di oro), provocando interferenze nella trasduzione del segnale elettrochimico.

L'efficacia della protezione con SAMs è stata valutata tramite voltammetria ciclica, in funzione del pH della soluzione, utilizzando due differenti mediatori redox: il mediatore cationico ferroceniltetrametil ammonio (FA^+) e l'acido debole ferrocenilcarbossilico (FcCOOH), che dissocia
ad anione $FcCOO^-$ in soluzioni alcaline.

Successivamente, il ruolo protettivo dei monostrati è stato verificato analizzando il comportamento voltammetrico dei NEE immersi in soluzioni contenenti proteine (caseina e albumina di siero bovino, BSA), comparando i segnali registrati con NEE non modificati, con quelli funzionalizzati con SAMs. È stata inoltre condotta la caratterizzazione dei NEE protetti e non protetti con SAMs tramite microscopia a forza atomica (AFM), che ha permesso di caratterizzare la morfologia della superficie dei NEE, prima e dopo il trattamento con le macromolecole biologiche.

I NEE sono stati inoltre utilizzati per la fabbricazione di biosensori elettrochimici per la rivelazione di sequenze di DNA. Due sono le strategie messe a punto: l'immobilizzazione dello strato di rivelazione biologico sulla membrana di policarbonato che circonda i nanoelettrodi e la funzionalizzazione della superficie d'oro dei NEE.

Nel primo caso, singole catene oligonucleotidiche dotate di terminazioni amminiche, sono state immobilizzate sulla superficie polimerica, tramite la formazione di legami ammidici con i gruppi carbossilici presenti sul PC.

La quantità di funzionalità carbossiliche è stata inoltre aumentata, tramite ossidazione chimica del policarbonato con permanganato di potassio ($KMnO_4$), reagente dal forte potere ossidante. Aumentando la quantità di funzionalità carbossiliche sulla superficie di policarbonato è stato possibile immobilizzare un numero maggiore di macromolecole biologiche.

I risultati ottenuti hanno confermato la possibilità di immobilizzare sequenze di DNA sulla superficie del *template* e di rivelare l'ibridazione delle sequenze immobilizzate con oligonucleotidi complementari, tramite l'impiego di un marcatore enzimatico (glucosio ossidasi, GOx), preventivamente coniugato alle sequenze target complementari. È importante notare che la GOx è stata utilizzata raramente come marcatore enzimatico nella fabbricazione di biosensori elettrochimici per il DNA. Il sistema $_{ds}$DNA + enzima è stato rivelato elettrochimicamente operando in presenza del substrato dell'enzima (glucosio), utilizzando FA^+ come mediatore redox, disciolto nell'elettrolita, che funge da trasportatore di elettroni tra il sito attivo dell'enzima e la superficie dei nanoelettrodi.

Tramite questo approccio è stato possibile rivelare l'ibridazione di poche decine di picomoli di $_{ss}$DNA target, catturate dall'oligonucleotide sonda immobilizzato sulla superficie polimerica dei NEE.

Infine, si è studiata anche la possibilità di sfruttare la superficie d'oro dei NEE per la funzionalizzazione con sequenze nucleotidiche. L'utilizzo di NEE convenzionali (2D-NEE) in un approccio di questo tipo è condizionato negativamente dal fatto che l'area attiva disponibile per l'immobilizzazione dello strato biologico corrisponde solamente alla superficie dei nanoelettrodi ed è perciò molto piccola. Per superare questa limitazione, è stata proposta una nuova strategia atta ad aumentare la superficie attiva dei NEE attraverso l'assemblaggio di nanostrutture tridimensionali (3D-NEE).

A tal fine, sulla superficie dei nanoelettrodi d'oro sono state immobilizzate delle nanoparticelle di oro (AuNPs) utilizzando tioli bi-funzionali che agiscono da ponti molecolari tra i nano dischi d'oro e le AuNPs. Le nanoparticelle permettono l'aumento di area attiva dei NEE, mantenendone pressoché inalterate le prestazioni e le peculiarità analitiche tipiche.

Le strutture complesse così ottenute sono state utilizzate per la fabbricazione di biosensori. Singole sequenze nucleotidiche tiolate sono state infatti immobilizzate sulla superficie metallica dei 3D-NEE e, successivamente, sono state ibridate con sequenze complementari marcate con GOx, come nel caso precedente.

I risultati preliminari ottenuti hanno confermato la possibilità di modificare facilmente NEE convenzionali con nanoparticelle d'oro, al fine di fabbricare 3D-NEE utili per applicazioni sensoristiche o biosensoristiche.

Seguendo questa procedura, le strutture tridimensionali vengono prodotte senza etching (chimico o al plasma) del polimero evitando, di conseguenza, trattamenti che possono provocare un peggioramento delle prestazioni dei NEE.

Inoltre, le nanoparticelle non bloccano il trasferimento elettronico tra nanoelettodi d'oro e specie redox in soluzione e permettono l'immobilizzazione sulla superficie dei nanoelettrodi di un maggior numero di molecole elettroattive o biologiche, rispetto a 2D-NEE convenzionali.

Goal of the thesis

The goal of this thesis is to exploit the capabilities of Nanoelectrode Ensembles (NEEs) in order to extend their application field.

NEEs show remarkable advantages in comparison with conventional electrodes, thanks to their particular geometry. This distinctive feature makes them suitable for different uses, some of which will be described hereafter.

These devices can be used for the direct determination of trace analytes in real samples. By exploiting the main advantage of NEEs, that is the high signal-to-background current ratio, it is indeed possible to reach by direct voltammetry detection limits (DLs) at the submicromolar range.

In this thesis, the use of NEEs for the detection of trace iodide in water samples, wants to underline the possibility of a successful direct electrochemical measurement of analytes at micromolar concentrations, without the addition of any time-consuming preconcentration step. In this way, the measurements become faster and easier. This is the topic dealt in chapter 3.

Another goal, to which a great part of the thesis is devoted, is the development of techniques and methods able to exploit NEEs characteristics in order to develop high-performance electrochemical biosensors.

NEEs are used as platforms suitable for the fabrication of biosensors where either, the template membrane which surrounds the nanoelectrodes or the nanoelectrodes themselves, are exploited for the immobilization of a biorecognition layer.

When the polymeric surface of NEEs has to be functionalized with macromolecules that easily adsorb onto the gold nanoelectrodes, therefore poisoning the metal surface, it is important to find a way to avoid this undesired adsorption. An useful method for the protection of the NEE surface is described in chapter 4.

The fabrication of NEE-based biosensors for DNA detection has also been faced, developing different strategies and chemistry to increase the efficiency of functionalization.

For the functionalization of the polymer it is important to exploit its natural reactivity with respect to the probe DNA sequences or, eventually, to increase such a reactivity with suitable activation procedures (chapter 5).

While the polymeric surface constitutes the majority of the geometric area of a NEE, the small metal (gold) surface can be a limitation for the immobilization of DNA strands. For this reason, the possibility to increase the active area of a NEE by structures provided with high surface area,

has been studied (chapter 6). In particular, preliminary applications of these 3D-NEEs as sensors or biosensors have been faced.

Advantages and limits of these approaches are compared and discussed, together with relevant prospects and further developments.

1. Nanoelectrode ensembles

Nanoelectrode ensembles (NEEs) are nanostructured electrochemical devices which find application in a wide range of fields, ranging from nanosensors to bio-analytical devices, from energy storage to magnetic materials [1,2].

The definition of "ensembles" as synonymous of random arrays of nanoelectrodes, was firstly introduced by C.R. Martin in the 1995 [3].

Typically, NEEs are prepared by template deposition of metal nanoelements within the pores of a microporous membrane [3].

The polymeric membranes most widely used to this goal are fabricated by the *track-etching* method which consists of two different steps. In the first step (the *tracking* step), a thin polymeric membrane is tracked by nuclear fission fragments of heavy elements such as californium or uranium, or by accelerated ion beams. The tracking of the membrane is then followed by chemical *etching*, during which the pore formation takes place. The removal of the tracked zones is achieved by a chemical etching agent, typically a solution of a strong alkali.

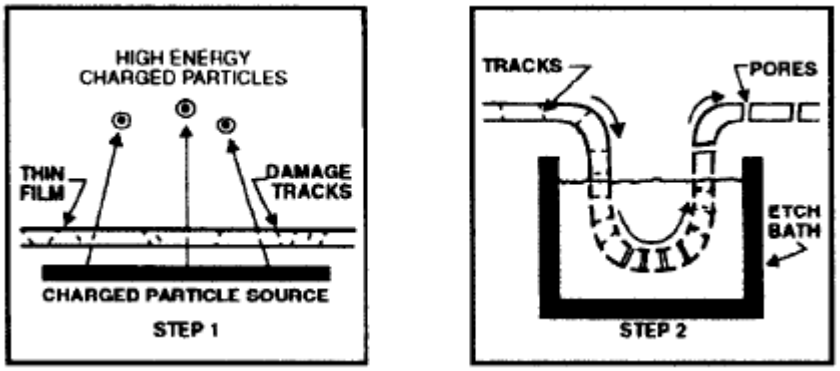

Figure 1. Scheme of fabrication of track-etch polymeric membranes

The time of tracking determines the pore density [4,5], while the chemical etching influences the pores size and shape [4,6,7]. The polymeric materials most widely used to fabricate track-etched membranes are polycarbonate, polyethylene terephthalate and polyimide [4].

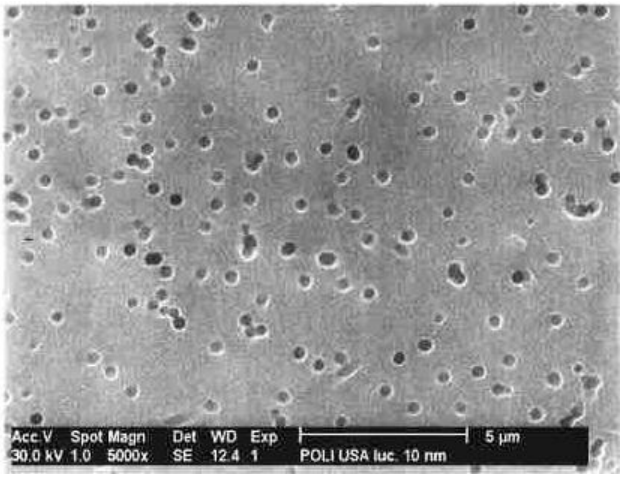

Figure 2. SEM image of a commercially available track-etched polycarbonate membrane.

1.1. Electroless deposition of metals

NEEs can be obtained both by electrochemical and chemical deposition of a metal in the pores of a track-etched membrane. In this thesis we will use the electroless (chemical) method, therefore we will focus only on it.

Electroless metal deposition involves the use of chemical reducing agents which allow the plating of a metal from a solution onto a specific surface. The kinetic of this process plays a key role since the homogeneous electron transfer from the reducing agent to the metal ions is very slow respect to the reduction on the surface. A catalyst that accelerates the rate of ion reduction is then applied to the surface to be coated. As a consequence, the metal is reduced preferentially at the surface incorporating the catalyst so that only the surface of interest, activated with the catalyst, is finally plated. The thickness of the metal layer can be controlled by varying the plating time [1].

The electroless deposition of gold [3] consists of three different steps. The first is the "sensitization" of the membrane. During this process, Sn^{2+} is applied to the surface (pore walls plus outer faces of the membrane) of the template by immersion of the membrane into an acidic solution containing $SnCl_2$. The adhesion of the cations occurs through coordination with amino and carbonyl functionalities probably of the polyvynilpyrrolidone (PVP) which is added as wetting agent to commercial membranes (PC is hydrophobic, but impregnation with PVP makes the surface hydrophilic).

The sensitized membrane is subsequently activated by immersion into an aqueous silver-ammonia solution: during this step the surface bound Sn(II) is oxidized to Sn(IV) and Ag^+ is reduced to elemental Ag, according to the reaction

$$Sn^{2+} + 2\,Ag^{+} \rightarrow Sn^{4+} + 2\,Ag^{0}$$

As a result, the pore walls and both membrane faces are coated with Ag nanoparticles.
The Ag-coated membrane is finally immersed into an Au plating bath, where the silver particles are galvanically displaced by gold and all the surface is coated with Au particles.

$$Au^{+} + Ag^{0} \rightarrow Au^{0} + Ag^{+}$$

These particles act as catalytic sites for the further reduction of Au(I) on the membrane surfaces, performed using formaldehyde as the reducing agent.

$$2\,Au^{+} + CH_2O + 3\,OH^{-} \rightarrow 2\,Au^{0} + HCOO^{-} + 2\,H_2O$$

With this procedure, the metal growth starts from the pore walls to continue up to the complete filling of the porosities. This is the reason why stopping the deposition after a short time, Au nanotubes can be obtained [8-10], while, the complete filling to obtain nanowires is achieved if the plating step is extended up to 24 h. In order to slow down the kinetics of the deposition, the plating is performed at 0° C. The scheme of the structure of a NEE is shown in Fig. 3.

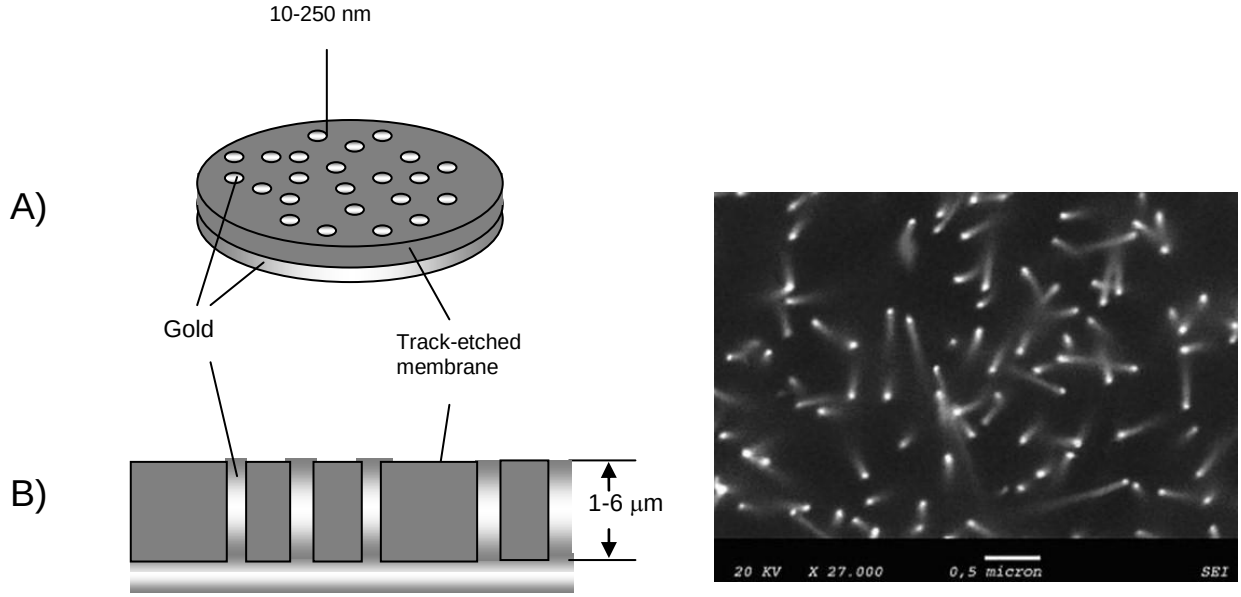

Figure 3. Scheme of a nanoelectrode ensemble in a template membrane (sx): A) overall view; B) lateral section; SEM image of a NEE made from a PC membrane, with nominal pore diameter of 30 nm (dx).

The electroless plating bath can be composed by a commercial solution containing sodium gold sulfite, $Na_3[Au(SO_3)_2]$ (Oromerse Part B, from Technics Inc.) [3], or home-made as explained in chapter 6.

1.2. Electrochemical properties of NEEs

From a voltammetric viewpoint, NEEs can be considered as ensembles of extremely small disk-shaped ultramicroelectrodes separated by an electrical insulator interposed between them. An ultramicroelectrode is considered as an electrode with at least one dimension comparable or lower than the thickness of the diffusion layer (typically < 25 μm). At such small dimensions, edge effects from the electrode become relevant and diffusion from the bulk solution to the electrode surface is described in terms of radial geometry instead of the simpler linear geometry used for larger (> 100 μm) electrodes. Under radial diffusion control, the voltammogram displays a typical sigmoidal shape; a limiting current (I_{lim}) instead of a peak, is the relevant analytical parameter related directly to the analyte concentration.

The density (q) of nanodisks/surface in a NEE is dramatically large (10^6-10^8 elements/cm^2); for this reason, all the nanoelectrodes are statistically equivalent and the different contribution of the elements at the outer border of the ensemble is negligible [11,12], even in NEEs of overall area as small as 10^{-2}-10^{-3} cm^2 [11].

NEEs can exhibit three distinct voltammetric response regimes depending on the scan rate or reciprocal distance between the nanoelectrode elements [13,14]. When radial diffusion boundary layers overlap totally (radius of diffusion hemisphere larger than average hemidistance between electrodes, slow scan rates) NEEs behave as planar macroelectrodes with respect to Faradaic currents (total overlap conditions). When diffusion hemispheres become shorter (higher scan rates), the current response is dominated by radial diffusion at each single element (pure radial conditions). At very high scan rates, the linear active regime is reached in which the current response is governed by linear diffusion to the individual nanodisk.

Fig. 4 shows the two most common voltammetric behaviors encountered for the total overlap and pure radial regimes; being characterized by the higher signal/background current ratios (see below), these two regimes are those typically used for analytical and sensing applications. However, total overlap (TO) regime is the regime usually observed at NEEs prepared from commercial track-etched membranes, with high pore density [3]. Transition from one regime to the other as a function of nanoelements distance was demonstrated experimentally [13] using specially-made membranes.

Recently, it was shown that the pure radial regime can be achieved when using NEEs (made with commercially available membranes) in high viscosity ionic liquids [15,16].

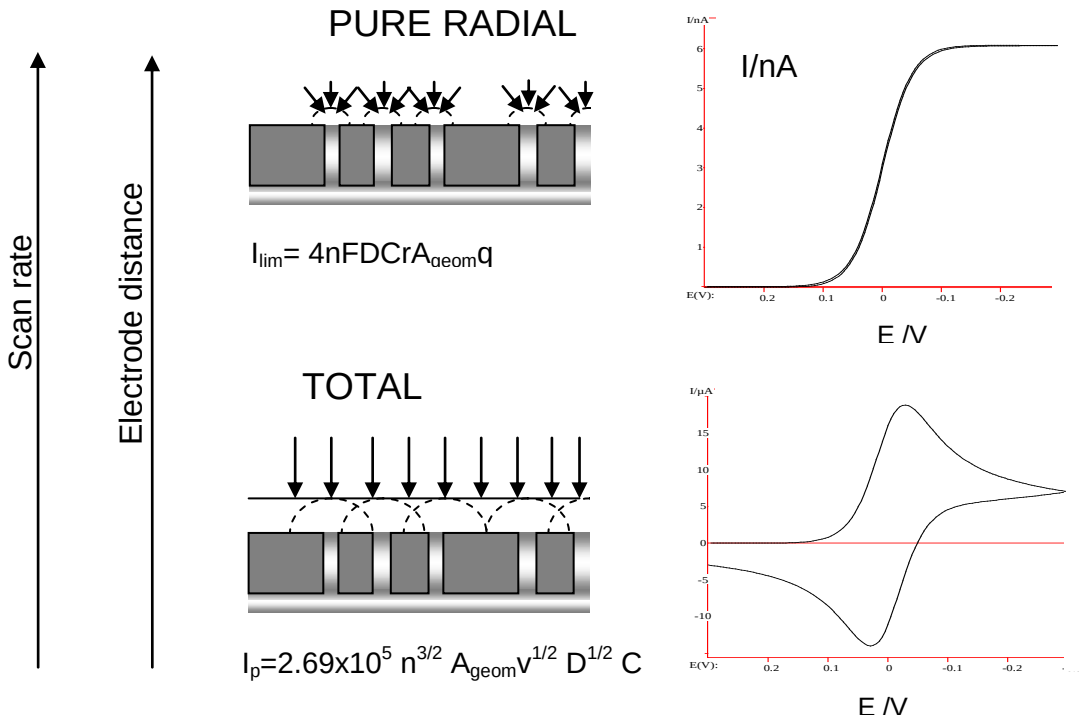

Figure 4. Typical diffusive regimes observed at nanoelectrode ensembles as a function of the scan rate and/or nanoelectrodes distance. See the list of abbreviations for symbols in the equations.

Under TO conditions, the Faradaic current (I_F) is proportional to the geometric area of the electrode (A_{geom}, nanodisks plus insulator), according to the following equation:

$$I_F = 2.69 \times 10^5 \, n^{3/2} \, A_{geom} \, D^{1/2} \, C^* \, v^{1/2} \qquad (1)$$

where D is the diffusion coefficient (cm^2 sec^{-1}), C^* is the redox species bulk concentration (mol cm^{-3}) and v is the scan rate (V sec^{-1}).

On the other hand, the capacitive current (Ic) is proportional only to the active area (A_{act}), which corresponds to the summation of the area of all the nanodisks exposed to the sample solution. In voltammetry, Ic is the main component of the background current and it is expressed by the equation (2):

$$I_C = v\ A_{act}\ C_{dl} \qquad (2)$$

where C_{dl} is the double-layer capacitance of the metal nanodisks of the NEE.

Typical Ic values are in the range between 1 and 2 nA (based on C_{dl} values between 20 and 40 $\mu F\ cm^{-2}$) [17].

The Faradic-to-background current ratios at a NEE and a conventional electrode with the same geometric area are compared by the equation (3):

$$(I_F/I_C)_{NEE} = (I_F/I_C)_{CONV} \times A_{geom}/A_{act} \qquad (3)$$

This ratio at the NEE is higher than that at the conventional electrode by a factor that is the reciprocal of the fractional electrode area (f):

$$f = A_{act} / A_{geom} \qquad (4)$$

Since the fractional area is an order of 10^{-2} 10^{-3}, signal to background current ratios at NEE are 2-3 order of magnitude higher than at conventional electrodes of the same geometric area. As a consequence detection limits at NEEs are 2-3 orders of magnitude lower than with conventional electrodes [3,18,19].

It was shown that improvements in signal/background current ratios at NEEs are independent on the total geometric area of the ensemble [11]; this is true if the fractional area is kept constant and if the dimensions of the ensemble are lowered to a size still large enough to contain a large number of nanoelements (for instance, NEE with A_{geom} of 0.005 cm^2 contains 4.8×10^6 nanoelectrodes). Note that NEEs warrant such an independence on the ensemble size for overall geometric areas much lower than those required for achieving comparable results with arrays of micrometer sized electrodes [12]. This is particularly attractive when thinking to apply the advantages of the use of arrays/ensembles of micro-nanoelectrodes to analyze samples of very small volume or for “in vivo” biomedical applications.

For a given geometric area, it is evident that the I_F/I_C is maximum when the TO regime is operative, being lower in the case of a pure radial regime. In this case, in fact, only a certain percentage of the geometric area of the ensemble contribute to producing a Faradaic current while, in the total overlap regime, this percentage is 100%. On the other hand, it is worth

stressing that for NEEs or NEAs with the same active area, higher Faradaic currents are achieved when operating under pure radial conditions [12]; this is the regime of choice for obtaining the maximum improvement of detection limits when there is no constrain in increasing the distance between the nanoelectrode elements
and/or the overall geometric area of the ensemble.

It was demonstrated that NEEs can be used not only as bare electrodes, but also as polymer coated devices [18]. For instance, the overall surface of a NEE (insulator and nanodisks) can be easily coated by a thin layer of an ionomer coating. In the cited literature example [18], the ionomer of choice was the polyestersulphonate Eastman AQ55®, which was applied as a water dispersion, i.e. using a solvent which does not damage the NEE surface (the polycarbonate template can be damaged by organic solvents). Really, such an approach showed that it was possible to combine successfully the preconcentration capabilities of ionomer coated electrodes with the increased Faradaic/capacitive current ratio typical of NEEs. From a detection limit viewpoint, it was advantageous to use polymer-coated NEEs operating under total overlap conditions and not under radial diffusion control, in order to keep as low as possible the negative effect of the decrease of (apparent) diffusion coefficients related to the ion-exchange incorporation of the redox analyte. As said before, in the total overlap regime, responses obey the Randles-Sevcik equation with peak currents depending on $D^{1/2}$ and not directly on D, as it is the case for the pure radial diffusive regime [20].

The ability of NEEs to furnish well resolved cyclic voltammograms for trace redox species has interesting consequences also for adsorption related problems, as in the case of small organic redox molecules and some biomacromolecules as well. If adsorption is concentration dependent, then lowering the solution concentration below the adsorption limit can sometime overcome the problem. This was demonstrated to be the case for some phenothiazines [19], commonly used as redox mediators in biosensors, and for the heme-containing enzyme cytochrome *c* [21].

An important characteristic of NEEs is that electron transfer kinetics appear slower than at a conventional electrode with continuous metallic surface [3]. Being composed of a large number of nanodisks metal elements surrounded by a large surface of insulating material (the guest membrane), NEEs act indeed as electrodes with partially blocked surface (PBE); the nanodisks electrodes are the unblocked surface and the template membrane is the blocking material. According to the pioneering model elaborated by Amatore et al. [22], the current response at this kind of electrodes is identical to that at a naked electrode of the same overall geometric area, but with a smaller apparent standard rate constant for the electron transfer which decreases as the

coverage with the blocking agent increases. Such an apparent rate constant ($k°_{app}$) is related, in fact, to the true standard charge transfer rate constant (k°), by the relationship [22]:

$$k°_{app} = k°(1 - \vartheta) = k° f \qquad (5)$$

where ϑ is the fraction of blocked electrode surface and f is the fraction of the electrode surface that is Au nanodisks (see eq. 4).

Such a dependence has two different practical consequences. From a mechanistic viewpoint, it is an advantage since it means that with NEEs it is easier to obtain experimentally very large k° values [23]. What is measured at NEE is indeed the smaller $k°_{app}$, which can be converted into the larger k° by means of eq. 5 [19,24].

From an analytical viewpoint, the operativeness of eq. 5 means that, at NEEs, high Faradaic current signals are obtained only for redox systems that behave "very" reversibly [3]. In cyclic voltammetry, the reversibility depends on k° and the scan rate; at a regular electrode a redox system gives a reversible voltammetric pattern when $k° > 0.3\ v^{1/2}$ cm s^{-1} [23]. At NEEs k_{app} substitutes k°; this means that at a NEE a redox system gives a reversible voltammetric pattern when $k° > k_{app}/f$, i.e. $k° > 3 \times 10^2\ v^{1/2}$ cm s^{-1} when, for instance, f is 10^{-3} [25,26]. With fixed pore density, the excessive lowering of the nanodisks diameter can increase the irreversibility problem. This is a limitation to be seriously taken into account when trying to optimize NEEs for analytical application, since it is important to consider the contrasting effect both of the increased I_F/I_C value and the apparent slowing down of the electron transfer kinetics. On the other hand, it is worth pointing out that the high sensitivity of NEEs to electron transfer kinetics can be even turned into an advantage, to avoid the effect of interfering substances when the interferences are sluggish redox couples while the analyte is an electrochemically (very) reversible redox species.

Further understanding of the electrochemical behavior of NEEs will probably take advantage of recent studies devoted to modeling by digital simulation the voltammetric behavior of regular [27] and random arrays [28] of ultramicroelectrodes.

2. Electrochemical biosensors

A biosensor is defined as an analytical device composed by two main elements, in close proximity to each other: a biological recognition element and a transducer which converts the recognition event into a measurable signal [29]. In electrochemical biosensors, the transducer is an electrode. Electrochemical biosensors can be divided in two categories, depending on the nature of the recognition process: electrocatalytic biosensors and affinity biosensors [30].

The formers are mainly based on the coupling of an enzymatic layer with a suitable sensing device. Such a combination joins the specificity of the catalytic protein with the sensitivity of the transducer. In fact, enzymes are biological catalysts with extreme specificity for a substrate (or a group of substrates) which they interact with, generating the relative products. The process follows, in the majority of cases, the Michaelis-Menten kinetics model [31] and can be studied by following the kinetic signal measured.

Affinity electrochemical biosensors exploit the interaction between a recognition molecule and its specific *target*, to produce the detectable signal. The recognition event is strongly influenced by the characteristics (e.g., shape and size) of the interacting biomolecules and high specificity and affinity are required to ensure a strong and stable interaction [30].

Sensing element and target can interact by several kinds of affinity systems, such as antibody-antigen complexes or the formation of the DNA double helix by hybridization between a probe and its complementary target. This interaction can be detected by direct electrochemistry by a combination of electrochemical and mass signal changes (with the Electrochemical Quartz Crystal Microbalance), or by detecting the electrochemical signal of a suitable electroactive or redox enzyme label [32,33].

In the latter case, the enzymatic label is typically bound to the analyte, exploiting its electrocatalytic properties to detect the formation of the probe-analyte complex. The electrocatalytic signal of the label will be indeed detected only when the biorecognition event (that is the binding between the probe and the enzyme-labeled analyte) has been successful. In this case, the characteristics of the affinity biosensor intersects with those of an electrocatalytic sensor.

It is worth noting that, in the past, different ways to define a biosensor have been proposed; below some of them are reported.:

"...small-sized devices comprising a recognition element, a transduction element, and a signal processor capable of continuously and reversibly reporting a chemical concentration" [34]
"…device that incorporates a biological sensing element in close proximity or integrated with the signal transducer…" [35]

"…biosensors comprise an analyte selective interface in close proximity or integrated with a transducer, whose function it is to relay the interaction between the surface and analyte either directly or through a chemical mediator…" [36].

In 1996 the Physical Chemistry and Analytical Chemistry Divisions of IUPAC proposed a more precise definition of a biosensor:

"…A biosensor is a self-contained integrated device that is capable of providing specific quantitative or semi-quantitative analytical information using a biological recognition element (biochemical receptor) which is retained in direct spatial contact with a transduction element" [37].

In this thesis we will use specifically the IUPAC recommendation to define what should be considered as a biosensor.

2.1. Electrochemical enzyme biosensors

Electrochemical enzyme-based sensors are devices useful for the study and monitoring of several substrates of great relevance in environmental, food and medical fields.
The first example of enzyme biosensor was introduced by Clark and Lyons in 1962, when was coined the term *enzyme electrode* [38]. In that case, a transducer composed by an amperometric oxygen electrode covered by an inner oxygen semi-permeable membrane, by a thin layer of glucose oxidase (GOx) and by an outer dialysis membrane, was used for glucose detection. The substrate (i.e. glucose) diffused through the membrane that retained the protein and then, reacting with the enzyme, it was converted to gluconolactone with the consequent lowering of the oxygen concentration:

$$\text{glucose} + \text{GOx}(\text{FAD}^+) \rightarrow \text{gluconolactone} + \text{GOx}(\text{FADH}_2)$$
$$\text{FADH}_2 + \text{O}_2 \rightarrow \text{FAD}^+ + \text{H}_2\text{O}_2$$

where FAD^+/ $FADH_2$ is the cofactor of GOx. It is important to note that the kinetics conditions make the overall rate of the process dependent on the concentration of glucose in the sample.

This device allowed the indirect measurement of glucose by monitoring the decrease of the amperometric signal relevant to O_2 reduction. The Clark's technology was developed in 1975 with the first commercial glucose biosensor (Yellow Springs Instrument Company analyzer - Model 23A YSI analyzer).

In 1967, Updike and Hicks expanded Clark's biosensing principle, developing an amperometric sensor constituted by GOx immobilized in a polyacrilamide gel coating an oxygen electrode, for the determination of glucose concentration in biological fluids [39].

Since then, the development of many kinds of biosensors took place. For example, Guilbault and Montalvo described a potentiometric sensor for urea detection based on urease immobilized in a layer of acrylamide gel, deposited on the surface of a glass electrode [40]. In presence of the enzyme, urea is decomposed to ammonium ion, changing the pH at the surface of the glass electrode. Again, Guilbault in 1973 described a method for the amperometric anodic detection of hydrogen peroxide (see the reaction reported below) generated by the reaction between GOx and glucose [41]:

$$H_2O_2 \rightarrow O_2 + 2H^+ + 2e^-$$

This enzyme electrode was fabricated by physical entrapment of GOx on a metal electrode by a polyacrylamide gel or by a cellophane membrane.

Permselective layers, such as electro-polymerized films [42,43] or Nafion and cellulose acetate [44], has been exploited both for keeping the recognition layer in contact with the electrode surface, as well as to minimize the access of other electroactive species present in biological fluids, such as ascorbic and uric acid [45]. These and other oxidizable constituents of biological fluids can interfere with the measurements, for example when high potentials are applied for the detecting H_2O_2.

All the devices described above are called *first-generation biosensors*; they detect directly the substrate or the product of the enzymatic reaction. However, some limits arise from the fact that the electrochemical behavior of both O_2 and H_2O_2 are far from being perfectly reversible; moreover, changes in the concentration of dissolved oxygen due to reasons different from the operativeness of the GOx catalyzed reaction, can influence the sensor response. An improvement to overcome both these limiting factors was achieved by introducing small electroactive molecules, called *mediators*, which act as artificial electron acceptor, so replacing oxygen. They

operate shuttling electrons from the redox site of the enzyme to the surface of the working electrode (*second-generation biosensors*) [46,47]. Organic and organometallic redox compounds, such as ferrocene and quinone derivatives, ruthenium complexes, ferricyanide, phenoxazine compounds and organic conducting salts have been used as electron mediators [48-51]. Ferrocene and its derivatives are the most used for this purpose, because of their reversibility and rapidity in electron transfer [52]. In the oxidized form, they act as electron acceptors for *flavoproteins* [53], that are oxidase enzymes which contain a FAD group (flavin adenine dinucleotide, two-electron redox site [54]) as redox cofactor.

The most important and widespread application of ferrocene and its derivatives as mediators has been for the amperometric determination of glucose. The mediator is reduced by direct reaction with the cofactor of GOx and then it is regenerated electrochemically at the electrode surface. The general scheme of the mediated detection of glucose is reported here:

$$\text{glucose} + \text{GOx}(\text{FAD}^+) \rightarrow \text{gluconolactone} + \text{GOx}(\text{FADH}_2)$$

$$\text{FADH}_2 + 2\ \text{Med}_{(ox)} \rightarrow \text{FAD}^+ + 2\ \text{Med}_{(red)} + 2\ \text{H}^+$$

$$\text{Med}_{(red)} \rightarrow \text{Med}_{(ox)} + e^-$$

where $\text{Med}_{(ox)}$ and $\text{Med}_{(red)}$ are the oxidizing and reducing forms of the mediator, respectively.

Cass et al. [55] used ferrocene monocarboxylic acid to shuttle electrons from the immobilized enzyme to a graphite electrode. In presence of both substrate and enzyme, the shape of the voltammogram changed and a catalytic current was observed. It is important to note that this behavior was particularly evident at slow scan rates (Figure 5).

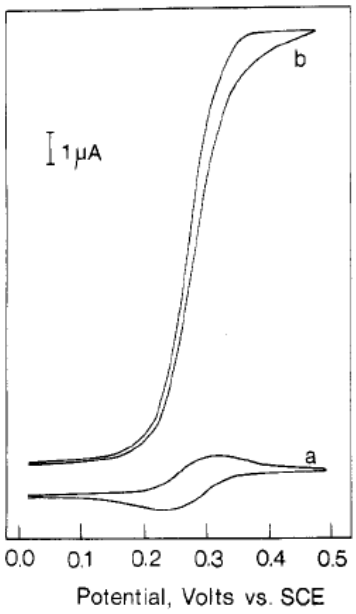

Figure 5. Cyclic voltammograms of ferrocene monocarboxylic acid in the presence of D-glucose, before (a) and after (b) the addition of GOx. Scan rate 1 mV/s [55].

The direct communication between redox protein and electrode can be further facilitated by chemical modification of the enzyme with electron-relay groups. In fact, glucose oxidase does not transfer electrons directly to the electrode because its flavin redox center is deeply buried within the polypeptide chain. Such a shell produces a spatial separation of the electron donor-acceptor pair, consequently hindering the direct electron transfer with the electrode surface [56]. Degani and Heller bound covalently a specific mediator (ferrocenecarboxylic acid) to the protein backbone of the enzyme, in order to promote the electron exchange with the active site of GOx [57]. A very efficient communication between the enzyme and the electrode was also achieved by the reconstitution of apo-flavoenzymes onto FAD-containing monolayers immobilized on the electrode surface [58]. An alternative approach was proposed by Heller and coworkers who bound covalently the enzyme to a redox-polymer deposited on the electrode surface [59]. This allowed to achieve the direct electrochemical connection between the enzyme and the transducer, so that electrons can flow from the active site through the polymer to the electrode. This flow was favored by a cross-linkable metal complex that acted as electron relay.

Recent efforts are devoted to the development of *third-generation biosensors* which are based on the direct electron transfer with the proteins, without the presence of any mediator [60,61]. These sensors allow to obtain better selectivity by working in a potential windows close to the redox potential of the enzyme itself, consequently avoiding interfering reactions [45,62]. Moreover, they are advantageous for *in vivo* detection, due to their simplicity.

However, efficient direct electron transfer at conventional electrodes has been reported only for few redox enzymes, such as Horseradish Peroxidase [63], Cytochrome c [64] and Hemoglobin [65].

The scheme below summarizes the main features of the three different generations of biosensors described above.

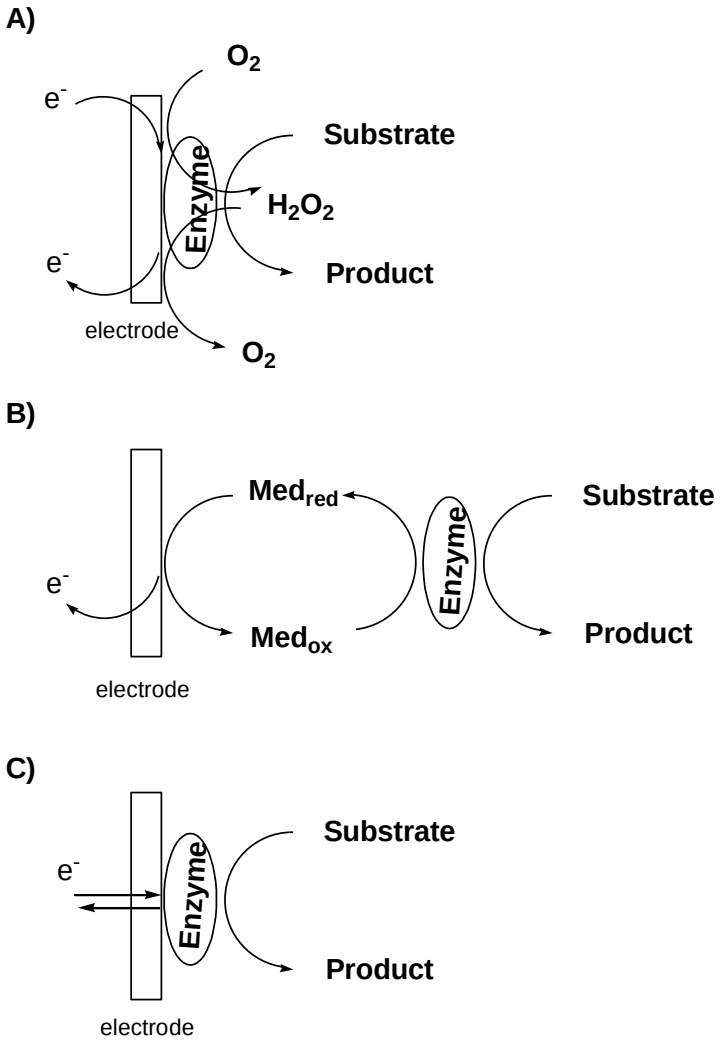

Figure 6. Representation of the three generations of electrochemical biosensors [62]: A) first, B) second; C) third generation biosensors.

2.2. DNA-based biosensors

DNA detection, in particular the determination of the presence of certain nucleotide sequences (genes), plays an important role in several fields, such as clinical diagnostic, biology, forensic science, etc. The progressively increasing interest direct to the detection of specific viral and

plasmid DNA sequences and the necessity to work with small amounts of analyte, still encourages the development of advanced DNA biosensors, provided with high sensitivity and specificity.

DNA biosensors can be defined as diagnostic tools which combine a biological recognition layer, composed namely by single-stranded DNA sequences ($_{ss}$DNA), with the transducer which converts the bio-recognition event into a readable and quantifiable signal [66]. In this case, the detectable event is usually the hybridization of the $_{ss}$DNA probe with the complementary sequence present in the target (analyte), to form the well known DNA double helix structure, clarified more than 50 years ago by Watson and Crick [67].

Biochemical assays for DNA characterization are mainly based on the formation of *arrays* of different probes (each with different nucleic acid sequences) onto the surface of a solid support.

The *Southern blotting* procedure was introduced in 1975 by E.M. Southern and combines a separation step with a subsequent recognition step [70].

In this method, summarized in Figure 7, double-stranded DNA ($_{ds}$DNA) fragments, produced by treatment of DNA with restriction nuclease, are denaturated, separated by electrophoresis, transferred from the gel to a nitrocellulose membrane, hybridized and detected by using suitable radioactive, fluorescent or chemiluminescent labels [71,72].

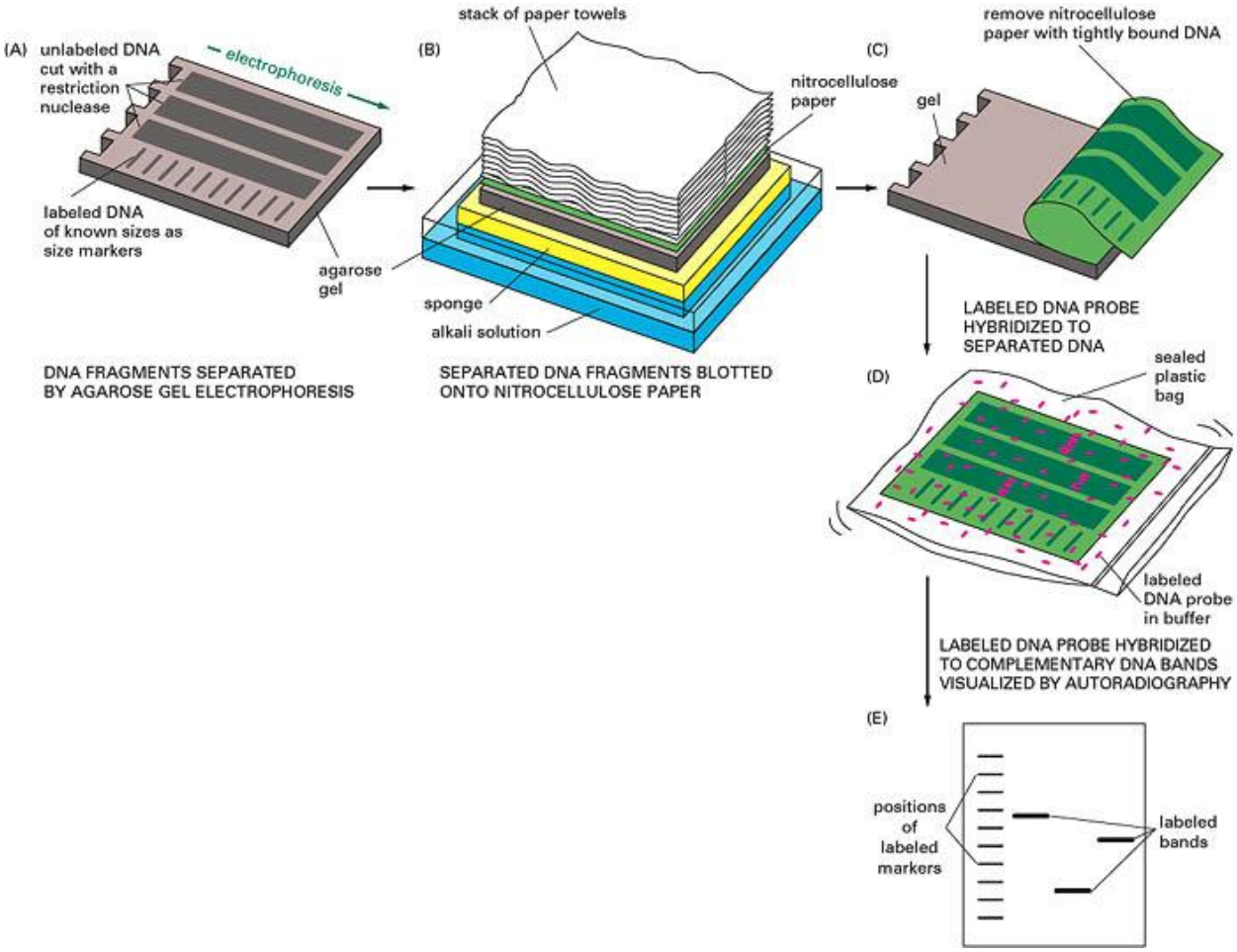

Figure 7. Detection of RNA or DNA fragments by gel-transfer hybridization method [73]. Note that radiographic detection can be replaced by other chemical or fluorescence methods.

The same procedure applied to RNA instead of DNA is called *Northern blotting* [74].

How declared by Southern, using porous membranes it is possible to immobilize quite large amounts of macromolecules on a small area, since the porosity provides a wide surface for binding. On the contrary, the shapes of the spots are not well defined and the amount of oligonucleotides deposited is not easy to control accurately [75].

In the *dot blot* method described by Kafatos et al. [68], a number of unknown DNA sequences are spotted on a suitable surface and subsequently, hybridized with radioactive complementary probes. A variation at this protocol, the so-called *reverse dot blot*, was introduced in 1989 by Saiki et al. [69]. In such a procedure, the known probes are immobilized on a polymeric membrane and then hybridized with labeled targets.

The request of miniaturized devices, that allow a rapid and simultaneous detection of multiple analytes in a single measurement, has favored the development of the so-called *DNA-*

microarrays [76]. Despite their limited dimensions, these systems can detect thousand of genes in a single measurement [77].

In the microarrays, the biological molecules are linked, with a predetermined spatial order, to a 2-D surface (glass, plastic or silicon supports), to which the labeled targets are added. On the spots where hybridization takes place, the label will be bound. The label signal (typically fluorescence) is detected in a following step, performed e.g. by fluorescent microscopy read-out. On the contrary, on DNA biosensors, the immobilization of the biomolecules is achieved directly onto the transducer surface [78].

As said above, one of the most used methods for detecting DNA hybridization is fluorescence [79-81]. Even if the fluorescence method is quite simple, it requires expensive and not easily portable instrumentation. Moreover, some fluorescent dye, such as ethidium bromide, are toxic.

Other detection methods, applied to DNA biosensors or microarrays, are based on fiber-optics [82,83], surface plasmon resonance (SPR) [84], raman spectroscopy [85,86], quartz crystal microbalance measurements [87,88], chemiluminescence [89], atomic force microscopy [90].

2.2.1. Electrochemical DNA biosensors

In order to reduce further the size and cost of the instrumentation needed in DNA hybridization detection, several bio-electrochemical devices have been proposed [77,91-93].

Electrochemical biosensors offer several advantages with respect to other assays, because they are portable, cheaper and the measurements are faster and easier [91]. Electrochemical sensors are furthermore provided with high sensitivity, they allow high performances with low background and

can be miniaturized down to nm-size.

All these devices should be able to detect viral, bacterial or mutant genes associated with specific human diseases also in biological fluids, such as blood, serum or tissues.

The immobilization of the recognition molecules onto the transducer surface influences the performances of the biosensors, since the surface modification procedure must be compatible with the sensing methodology. Moreover, the immobilization of the probe sequences should assure high reactivity, orientation and/or accessibility to the complementary strands as well as stability of the interaction with the surface [92].

The first studies concerning electrochemical electron transfer to DNA date back to the 1960s [94-96].

For many years, the electrochemistry of nucleic acids was studied at mercury electrodes [97-99],

but in more recent years other conducting materials, such as carbon, polymers and gold as well as several kinds of immobilization procedures, have been used for the electrochemical characterization of single-stranded or double-stranded DNA [100-105].

In principle, the DNA hybridization event can be detected directly using label-free approaches. These methods consist in the direct hybridization characterization by detecting the signal produced by the oxidation of guanine or adenine bases present in the DNA structure [106-108] or from changes in electrochemical parameters (e.g., capacitance or conductivity), induced by hybridization [109,110].

The formation of the double helix structure can be also detected following the electrochemistry of specific intercalating molecules, such as some metal complexes [111,112] or aromatic compounds [113,114]. These intercalators interact in several binding modes with the oligonucleotide structure [114-116] and allow one to discriminate $_{ss}$DNA from $_{ds}$DNA [117,118] with the capability even to detect single-base mismatches [119-121].

Methylene blue (MB) is one of the intercalator most widely used for the electrochemical detection of DNA, thanks to its low oxidation potential which allows to minimize electroactive interferences [122]. Moreover, it produces different voltammetric signals before and after hybridization [123,118].

Other frequently used intercalators are organic complexes of Co(III) [124-126], Fe(II) [127], Ru(II) [127,128], Os(II) [129].

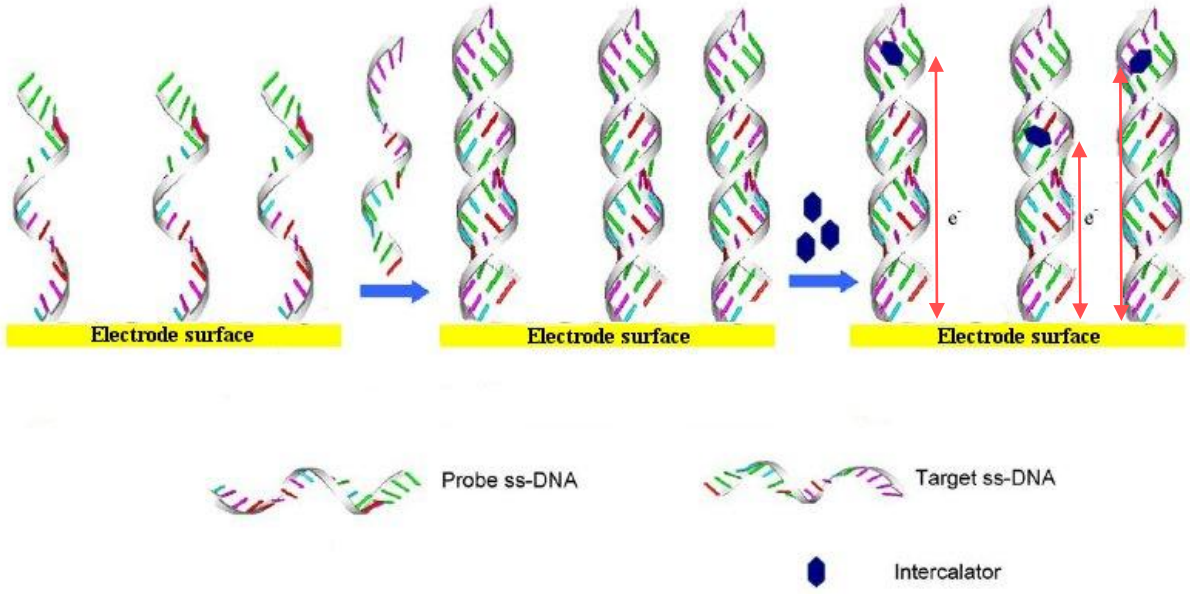

Figure 8. General scheme of a DNA-based electrode, with intercalation for the detection of the hybridization event (modified image from ref. [130]).

The target sequence can be also labeled with redox-active molecules, such as enzymes, that allow the indirect detection of the hybridization event by the introduction of an electroactive mediator in solution [131,132]. An electrocatalytic signal is measured only when the labeled target interacts with the complementary sequence, previously immobilized onto the electrodic surface.

Two enzymes widely used for this purpose are alkaline phosphatase (AP) [133,134] and horseradish peroxidase (HRP) [135,136].

Nanoparticles has also been used as markers for the electrochemical detection of the double helix formation [137,138].

The use of nanoscale materials, namely nanoparticles [137,139], nanotubes [140,141] and nanowires [142], has facilitated recently the development of ultrasensitive electrochemical biosensors, characterized by high surface area, optimal electrochemical properties and, in many cases, biocompatibility.

2.2.2. Electrochemical DNA biosensors based on NEEs

The only previous example of use of NEEs as platforms for the fabrication of DNA-based biosensors was developed by Gasparac et al. in 2004 [143,144]. In that case, 3D-NEEs were obtained by partial etching of the polycarbonate surface with oxygen plasma. This treatment allowed to increase the active area of conventional 2D-NEEs that was then exploited for the immobilization of the biorecognition layer. In fact, after etching the nanowires were exposed of approximately 150-250 nm length.

Subsequently, the exposed nanoelectrodes were functionalized with thiolated DNA and the amount of macromolecules immobilized was detected by an electrocatalytic reaction between a primary acceptor, namely $Ru(NH_3)_6^{3+}$ and a secondary acceptor, namely $Fe(CN)_6^{3-}$ (Figure 9).

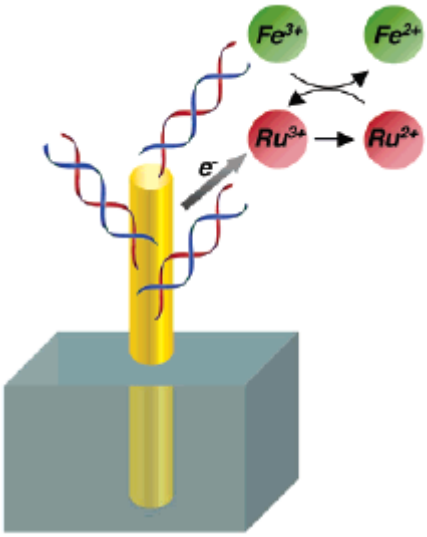

Figure 9. Schematic representation of Ru(III)/Fe(III) electrochemical detection at a 3D-NEE [143].

The first ion was reduced at the electrode surface and then reoxidized by excess of the anion, producing a catalytic electrochemical process. By increasing the concentration of negatively charged phosphate groups at the Au surface of NEEs, by hybridization with complementary sequences, the local concentration of $Ru(NH_3)_6^{3+}$ increases as well. The result was an evident increase in the final electrocatalytic signal, after hybridization. Note that the etching process used to expose the nanowires to increase the yield of functionalization respect to 2D-NEEs.
However, how said before, etching of the PC membrane causes an increase in active area [145], with a subsequent decrease in the signal/background current ratio.

In this thesis (chapters 5 and 6), two new approaches for the fabrication of DNA biosensors based on NEEs are proposed. In the first, the $_{ss}$DNA probe is immobilized on the PC membrane which surrounds the nanoelectrodes. In the second approach, the probe is bound to gold nanoparticles, pre-bound (by a suitable linker) onto the gold surface of the nanoelectrodes of a NEE.

References

[1] C.R. Martin, D.T. Mitchell, in *Electroanalytical Chemistry: a Series of Advances*, edited by A.L. Bard, I. Rubinstein, Marcel Dekker Inc., New York **vol. 21** (1999), 1.

[2] L.M. Moretto, S. Panero, B. Scrosati, P. Ugo, in *Handbook of Electrochemical Nanotechnology*, edited by Y. Lin, H.S. Nalwa, ASP, Stevenson Ranch **vol. 1** (2009), 87.

[3] V.P. Menon, C.R. Martin, *Anal. Chem.* **67** (1995), 1920.

[4] P. Apel, *Radiat. Meas.* **34** (2001), 559.

[5] N. Li, S. Yun, C.C. Harrel, C.R. Martin, *Anal. Chem*. **76** (2004), 2025.

[6] Z. Siwy, A. Fulinski, *Phys. Rev. Lett*. **198** (2002),103.

[7] Z. Siwy, D. Dobrev, R. Neumann, C. Trautmann, K. Voss, *Appl. Phys. A* **76** (2003), 781

[8] M. Wirtz, C.R. Martin, *Adv. Mater*. **15** (2003), 455.

[9] P. Ugo, L. M. Moretto, in *Handbook of Electrochemistry*, Ed. C. G. Zoski, Elsevier, **2007**, Cap. 16, Sezione 16.2.

[10] M. De Leo, F. C. Pereira, L. M. Moretto, P. Scopece, S. Polizzi, P. Ugo, *Chem. Mater.*, **2007**, *19*, 5955.

[11] L.M. Moretto, N. Pepe, P. Ugo, *Talanta* **62** (2004), 1055.

[12] H.J. Lee, C. Beriet, R. Ferrigno, H.H. Girault, *J. Electroanal. Chem.* **502** (2001), 138.

[13] J.C. Hulteen, V.P. Menon, C.R. Martin, *J. Chem. Soc. Faraday Trans.* **92** (1996), 4029.

[14] J.F. Cheng, L.D. Whiteley, C.R. Martin, *Anal. Chem.* **61** (1989), 762.

[15] M. De Leo, L.M. Moretto, O. Buriez, P. Ugo, *Electroanalysis* **21** (2009), 392.

[16] P. Ugo, L.M. Moretto, M. De Leo, A.P. Doherty, C. Vallese, S. Pentlavalli, *Electrochim. Acta* **55** (2010), 2865.

[17] R. Greef, R. Peat, L.M. Peter, D. Pletcher, J. Robinson, *Instrumental Methods in Electrochemistry*, Ellis Horwood Ltd., Chichester, UK (1985).

[18] P. Ugo, L.M. Moretto, S. Bellomi, V.P. Menon, C.R. Martin, *Anal. Chem.* **68** (1996), 4160.

[19] B. Brunetti, P. Ugo, L.M. Moretto, C.R. Martin, *J. Electroanal. Chem.* **491** (2000), 166.

[20] S. Daniele, P. Ugo, C. Bragato, G.A. Mazzocchin, *J. Electroanal. Chem.* **418** (1996), 29.

[21] P. Ugo, N. Pepe, L.M. Moretto, M. Battagliarin, *J. Electroanal. Chem.* **560** (2003), 51.

[22] C. Amatore, J.M. Saveant, D. Tessier, *J. Electroanal. Chem*. **147** (1983), 39.

[23] A.J., Bard, L. Faulkner, *Electrochemical Methods*, Wiley, New York (2000), 18.

[24] E. Sabatani, J. Rubinstein, *J. Phys. Chem.* **91** (1997), 6663.

[25] P. Ugo, L.M. Moretto, F. Vezzà, *ChemPhysChem* **3** (2002), 917.

[26] P. Ugo, L.M. Moretto, F. Vezzà, in *Sensors Update*, edited by H. Baltes, G.K. Fedder, J.G. Korvink, , Wiley-VCH, Weinheim **12** (2003), 121.

[27] B.A. Brookes, T.J. Davies, A.C. Fisher, R.G. Evans, S.J. Wilkins, K. Yunus, J.D. Wadhawan, R.G. Compton, *J. Phys. Chem. B* **107** (2003), 1616.

[28] T.J. Davies, B.A. Brookes, A.C. Fisher, K. Yunus, S.J. Wilkins, P.R. Greene, J.D. Wadhawan, R.G. Compton, *J. Phys. Chem. B* **107** (2003), 6431.

[29] P.R. Coulet, in *Biosensor principles and applications*, edited by L.J. Blum, P.R. Coulet, Marcel Dekker Inc., New York (1991).

[30] J. Wang, *Analytical Electrochemistry*, 3rd edition, Wiley-VCH (2006), 201.

[31] P.N. Bartlett, C.-S. Toh, in *Biosensors*, 2nd edition, edited by J.M. Cooper, A.E.G. Cass, Oxford University press (2004), 59.

[32] J. Yakovleva, J. Emnéus, in *Bioelectrochemistry. Fundamentals, Experimental Techniques and Applications*, edited by P.N. Bartlett, Wiley-VCH (2008), 377.

[33] E. Palecek, M. Fojta, in *Bioelectronics*, edited by I. Willner, E. Katz, Wiley-VCH, Weinheim (2005), 127.

[34] O.S. Wolfbeis, *Fresenius' J. Anal. Chem*. **337** (1990), 522.

[35] E.A.H. Hall, *Biosensors*, Prentice-Hall, Englewood Cliffs, New Jersey (1991).

[36] E.A.H. Hall, in *Biosensors and Chemical Sensors*, edited by P.G. Edelman, J. Wang, ACS Symposium Series #487, American Chemical Society, Washington, DC (1992).

[37] D.R. Thévenot, K. Toth, R.A. Durst, G.S. Wilson, *Pure Appl. Chem*. **71** (1999), 2333.

[38] L.C.Jr. Clark, C. Lyons, *Ann. NY Acad. Sci* **102** (1962), 29.

[39] S.J. Updike, G.P. Hicks, *Nature* **214** (1967), 986.

[40] G.G. Guilbault, J. Montalvo, *JACS* **91** (1969), 2164.

[41] G.G. Guilbault, G. Lubrano, *Anal. Chim. Acta* **64** (1973), 439.

[42] S. Emr, A. Yacynych, *Electroanalysis* **7** (1995), 913.

[43] C. Malitesta, F. Palmisano, L. Torsi, P. Zambonin, *Anal. Chem*. **62** (1990), 2735.

[44] Y. Zhang, Y. Hu, G.S.Wilson, D. Moatti-Sirat, V. Poitout, G. Reach, *Anal. Chem*. **66** (1994), 1183.

[45] J. Wang, *Chem. Rev*., **108** (2008), 814.

[46] G.S. Wilson, Y. Hu, *Chem. Rev.* **100** (2000), 2693.

[47] V. Saxena, B.D. Malhotra in *Advances in biosensors: Perspectives in biosensors*, edited by B.D. Malhotra, A.P.F. Turner, Elsevier **vol. 5** (1993), 63.

[48] J. Ohara, R. Rajagopapan, A. Heller, *Anal. Chem*. **66** (1994), 2451.

[49] B. Persson, L. Gorton, *J. Electroanal. Chem*. **292** (1990), 115.

[50] S.P. Hendry**,** M.F. Cardosi**,** A.P.F. Turner**,** E.W. Neuse, *Anal. Chim. Acta* **281** (1993), 453.

[51] E.V. Ivanova, V.S. Sergeeva, J. Oni, C. Kurzawa, A.D. Ryabov, W. Schuhmann, *Bioelectrochemistry* **60** (2003), 65.

[52] J. Frew, H.A. Hill, *Anal. Chem*. **59** (1987), 933A.

[53] A.E.G. Cass, G. Davis, M.J. Green, H.A.O. Hill, *J. Electroanal. Chem*. **190** (1985), 117.

[54] C. Walsh, *Acc. Chem. Res*. **13** (1980), 148.

[55] A.E.G. Cass, G. Davis, G.D. Francis, H.A.O. Hill, W.J. Aston, I.J. Higgins, E.V. Plotkin, L.D.L. Scott, A.P.F. Turner, *Anal. Chem*. **56** (1984), 667.

[56] J. Wang, *Electroanalysis* **13** (2001), 983.

[57] Y. Degani, A. Heller, *J. Phys. Chem*. **91** (1987), 1285.

[58] I. Willner, E. Katz, B. Willner, *Electroanalysis* **9** (1997), 965.

[59] B. A. Gregg, A. Heller, *Anal. Chem*. **62** (1990), 258.

[60] U Wollenberger, in *Biosensors and modern biospecific analytical techniques*, edited by L. Gorton, Elsevier **vol. 44** (2005), 65.

[61] W. Zhang, G. Li, *Analytical Sciences* **20** (2004), 603.

[62] R.S. Freire, C.A. Pessoa, L.D. Mello, L.T. Kubota, *J. Braz. Chem. Soc.* **14** (2003), 230.

[63] E.E. Ferapontova, V.G. Grigorenko, A.M. Egorov, T. Börchers, T. Ruzgas, L. Gorton, *Biosens. Bioelectron.* **16** (2001), 147.

[64] M.J. Eddowes, H.A.O. Hill, *J. Chem. Soc. Chem. Comm.*(1977), 771b.

[65] J. Yang, N. Hu, J.F. Rusling, *J. Electroanal. Chem.* **463** (1999), 53.

[66] S. Cagnin, M. Caraballo, C. Guiducci, P. Martini, M. Ross, M. SantaAna, D. Danley, T. West, G. Lanfranchi, *Sensors* **9** (2009), 3122.

[67] J.D. Watson, F.H.C. Crick, *Nature* 171 (1953), 737.

[68] F.C. Kafatos, C.W. Jones, A. Efstratiadis, *Nucleic Acids Res.* **7** (1979), 1541.

[69] R.K. Saiki, P.S. Walsh, C.H. Levenson, H.A. Erlich, *Proc. Natl. Acad. Sci. USA* **86** (1989), 6230.

[70] E.M. Southern, *J. Mol. Biol.* **98** (3) (1975), 503.

[71] D. Voet, J.G. Voet, *Biochimica,* Zanichelli (1993), 925.

[72] E. Southern, *Nat. Protoc.* **1** (2006), 518.

[73] B. Alberts, A. Johnson, J. Lewis, M. Raff, K. Roberts, P. Walter, *Molecular Biology of the Cell*, 5th edition, Garland Science, Taylor and Francis group (2008), 538.

[74] G.M. Wahl, J.L. Meinkoth, A.R. Kimmel, *Meth. Enzym.* **152** (1987), 572.

[75] E.M. Southern, *Methods Mol. Biol.* **170** (2001),1.

[76] M.J. Heller, *Annu. Rev. Biomed. Eng*. **4** (2002), 129.

[77] J. Lamartine, *Mater. Sci. Eng. C* **26** (2006), 354.

[78] A. Sassolas, B.D. Leca-Bouvier, L.J. Blum, *Chem. Rev.* **108** (2008), 109.

[79] X. Fang, X. Liu, S. Schuster, W. Tan, *J. Am. Chem. Soc.* **121** (1999), 2921

[80] S. Nagl, M. Schaeferling, O.S. Wolfbeis, *Microch. Acta* **151** (2005), 1.

[81] M. Schaferling, S. Nagl, *Anal. Bioanal. Chem.* **385** (2006)**,** 500.

[82] K. Kuhn, S.C. Baker, E. Chudin, M.H. Lieu, S. Oeser, H. Bennett, P. Rigault, D. Barker, T.K.

McDaniel, M.S. Chee, *Genome Res.* **14** (2004), 2347.

[83] J.H. Watterson, S. Raha, C.C. Kotoris, C.C. Wust, F. Gharabaghi, S.C. Jantzi, N.K. Haynes, N.H. Gendron, U.J. Krull, A.E. Mackenzie, P.A. Piunno, *Nucl. Acid. Res.* **32** (2) (2004)**,** e18.

[84] T.T. Goodrich, H.J. Lee, R.M. Corn, *Anal. Chem.* **76** (2004), 6173.

[85] M. Culha, D. Stokes, L.R. Allain, T. Vo-Dinh, *Anal. Chem.* **75** (2003), 6196.

[86] Y.C. Cao, R. Jin, C.A. Mirkin, *Science* **297** (2002), 1536.

[87] I. Willner F. Patolsky, Y. Weizmann, B. Willner, *Talanta* **56** (2002), 847.

[88] D. Dell'Atti, M. Zavaglia, S. Tombelli, G. Bertacca, A.O. Cavazzana, G. Bevilacqua, M. Minunni, M. Mascini, *Clin. Chim. Acta* **383** (2007), 140.

[89] V. Pavlov, Y. Xiao, R. Gill, A. Dishon, M. Kotler, I. Willner, *Anal. Chem.* **76** (2004), 2152.

[90] F. Bano, Lj. Fruk, B. Sanavio, M. Glettenberg, L. Casalis, C.M. Niemeyer, G. Scoles, *Nano Lett.* **9** (7) (2009), 2614.

[91] O.A. Sadik, A.O. Aluoch, A. Zhou, *Biosens. Bioelectron.* **24** (2009), 2749.

[92] F. Lucarelli, G. Marrazza, A.P. Turner, M. Mascini, *Biosens. Bioelectron.* **19** (2004), 515.

[93] J. Wang, *Anal. Chim. Acta* **469** (2002), 63.

[94] D.D. Eley, D.I. Spivey, *Trans. Faraday Soc*. **58** (1962), 411.

[95] C.Y. Liang, E.G. Scalco, *J. Chem. Phys*. **40** (1964), 919.

[96] R.S. Snart, *Biopolymers* **6** (1968), 293.

[97] E. Paleček, *Electroanalysis* **8** (1996), 7.

[98] E. Paleček, M. Fojta, F. Jelen, V. Vetterl, in *Encyclopedia of Electrochemistry*, edited by A.J. Bard, M. Stratsmann, Wiley-VCH Weinheim (2002), 365.

[99] E. Paleček, M. Tomschik, V. Stankova, L. Havran, *Electroanal*ysis **9** (1997), 990.

[100] V. Brabec, G. Dryhurst, *J. Electroanal. Chem. Interfacial Electrochem.* **89** (1978), 161.

[101] V. Brabec, *Bioelectrochem. Bioenerg.* **8** (1981), 437.

[102] J. Wang, X. Cai, C. Jonsson, M. Balakrishnan, *Electroanalysis* **8** (1996), 20.

[103] G. Marrazza, L. Chianella, M. Mascini, *Biosens. Bioelectron*. **14** (1999), 43.

[104] M.I. Pividori, A. Merkoçi, S. Alegret, *Biosens. Bioelectron*. **15** (2000), 291.

[105] D.J. Caruana, in *Biosensors*, second edition, edited by J.M. Cooper and A.E.G. Cass, Oxford University Press (2004), 19.

[106] K. Kerman, Y. Morita, Y. Takamura, E. Tamiya, *Electrochem. Commun*. **5** (2003), 887.

[107] P. De los Santos-Alvarez, M.J. Lobo-Castanon, A.J. Miranda-Ordieres, P. Tunon-Blanco, *Anal. Chem.* **74** (2002), 3342.

[108] D. Ozkan, A. Erdem, P. Kara, K. Kerman, B. Meric J. Hassmann, M. Ozsoz, *Anal. Chem.* **74** (2002), 5931

[109] C. Berggren, P. Stalhandske, J. Brundell, G. Johansson, *Electroanalysis* **11** (1999), 156.

[110] H. Korri-Youssoufi, F. Garnier, P. Srivtava, P. Godillot, A. Yassar, *J. Am. Chem. Soc*. **119** (1997) 7388.

[111] M.-Y. Wei, L.-H. Guo, P. Famouri, *Microchim Acta* **172** (2011), 247.

[112] B.M. Zeglis, V.C. Pierre, J.K. Barton, *Chem. Commun*. **44** (2007), 4565.

[113] S. Girousi, V. Kinigopoulou, *Cent. Eur. J. Chem*. **8** (2010), 732.

[114] H. Ihmels, D. Otto, *Top. Curr. Chem*. **258** (2005), 161.

[115] B.A.D. Neto, A.A.M. Lapis, *Molecules* **14** (2009), 1725.

[116] S.O. Kelley, J.K. Barton, *Bioconj. Chem*. **8** (1997), 31.

[117] S. Liu, J. Ye, P. He, Y. Fang, *Anal. Chim. Acta* **335** (1996), 239.

[118] W. Yang, M. Ozsoz, D.B. Hibbert, J.J. Gooding, *Electroanalysis* **14** (2002), 1299.

[119] E.L.S. Wong, J.J. Gooding, *Anal. Chem*. **75** (2003), 3845.

[120] S.O. Kelley, E.M. Boon, J.K. Barton, N.M. Jackson, M.G. Hill, *Nucl. Acids Res.* **27** (1999), 4830.

[121] E.M. Boon, D.M. Ceres, T.G. Drummond, M.G. Hill, J.K. Barton, *Nature Biotech*. **18** (2000), 1096.

[122] O.A. Loaiza, S. Campuzano, M. Pedrero, J.M. Pingarrón, *Talanta* **73** (2007), 838.

[123] A. Tani, A.J. Thomson, J.N. Butt, *Analyst* **126** (2001), 1756.

[124] M.T. Carter, A.J. Bard, *J. Am. Chem. Soc*. **109** (1987**),** 7528.

[125] A. Erdem, B. Meric, K. Kerman, T. Dalbasti, M. Ozsoz, *Electroanalysis* **11** (1999), 1372.

[126] M.T. Carter, M. Rodriguez, A.J. Bard, *J. Am. Chem. Soc* **111** (1989), 8901.

[127] D.H. Johnston, K.C. Glasgow, H.H. Thorp, *J. Am. Chem. Soc*. **117** (1995), 8933.

[128] D.H. Johnston, H.H. Thorp, *J. Phys. Chem.* **100** (1996), 13837.

[129] K. Maruyama, Y. Mishima, K. Minagawa, J. Motonaka, *Anal. Chem.* **74** (2002), 3698.

[130] E.L.S. Wong, F.J. Mearns, J.J. Gooding, *Sensor. Actuat. B* **111–112** (2005), 515.

[131] F. Azek, C. Grossiord, M. Joannes, B. Limoges, P. Brossier, *Anal. Biochem.* **284** (2000), 107.

[132] G. Carpini, F. Lucarelli, G. Marrazza, M. Mascini, *Biosens. Bioelectron.* **20** (2004), 167.

[133] P. Kara, A. Erdem, S. Girousi, M. Ozsoz, *J. Pharm. Biomed. Anal.* **38** (2005), 191.

[134] F. Farabullini, F. Lucarelli, I. Palchetti, G. Marrazza, M. Mascini, *Biosens. Bioelectron.* **22** (2007), 1544.

[135] A.L. Ghindilis, M.W. Smith, K.R. Schwarzkopf, K.M. Roth, K. Peyvan, S.B. Munro, M.J. Lodes, A.G. Stöver, K. Bernards, K. Dill, A. McShea, *Biosens. Bioelectron.* **22** (2007), 1853.

[136] L. Tang, G. Zeng, G. Shen, Y. Li, C. Liu, Z. Li, J. Luo, C. Fan, C. Yang, *Biosens. Bioelectron.* **24** (2009), 1474.

[137] M.T. Castaneda, S. Alegret, A. Merkoci, *Electroanalysis* **19** (2007), 743.

[138] F. Wang, S. Hu, *Microchim. Acta* **165** (2009), 1.

[139] S.S. Agasti, S.Rana, M.-Hwan Park, C.K. Kim, C.-C. You, V.M. Rotello, *Advanced Drug Delivery Reviews* 62 (2010), 316.

[140] A. Erdem, P. Papakonstantinou, H. Murphy, *Anal. Chem.* **78** (2006), 6656.

[141] T.I. Abdullin, I.I. Nikitina, D.G. Ishmukhametova, G.K. Budnikov, O.A. Konovalova, M.K. Salakhov, *J. Anal. Chem.* **62** (2007), 599.

[142] N.N. Zhu, Z. Chang, P.G. He, Y.Z. Fang, *Electrochim. Acta* **51** (2006), 3758.

[143] R. Gasparac, B.J. Taft, M.A. Lapierre-Devlin, A.D. Lazareck, J.M. Xu, S.O. Kelley, *J. Am. Chem. Soc.* **126** (2004), 12270.

[144] M.A. Lapierre-Devlin, C.L. Asher, B.J. Taft, R. Gasparac, M.A. Roberts, S.O. Kelley, *Nano Lett.* **5** (6) (2005), 1051.

[145] M. De Leo, A. Kuhn, P. Ugo, *Electroanalysis* **19** (2007), 227.

Nanoelectrode Ensembles for the Direct Voltammetric Determination of Trace Iodide in Water

1. Introduction

Iodine is an essential component required by the thyroid gland to produce two iodized hormones, thyroxine and tri-iodothyronine, which are used by the body during metabolism. The human body does not need much iodine and, in average, it contains around 20-25 mg of the element. When starved for iodine, the thyroid gland swells and this causes goiter.

Iodine is a trace element present in seawater and sea products, mainly in the form of iodide or iodate anions [1]. The most common sources of iodine intake for human beings are table salt and seafood, but also plants grown in iodine rich soils. Problems arise in certain parts of the world where the soil contain no iodine; this causes iodine deficiencies in the diet and consequent health problems [2,3].

Various methods have been proposed for iodide determinations such as spectrophotometry [4], ICPMS [5], capillary electrophoresis [6,7], ion-chromatography and HPLC [8-10], the latter being probably the most widely used.

By taking advantage of the electroactivity of iodide, electrochemical methods have been often applied to this goal, in particular cathodic stripping methods, following electrolytic preconcentration of iodide in the form of insoluble salts deposited on the surface of a suitable electrode material, typically mercury or silver [11-14], but also at modified electrodes [15,16]. However, from the viewpoint of quick analytical control in the environment, direct methods (which could avoid a pre-concentration step) might be preferable. Recent researches [17-22] showed that the use of the NEEs can improve the performances of electrochemical determinations thanks to dramatically higher signal to background current ratios with respect to other electrode systems and this was demonstrated also in relation to the direct determination of iodide with NEEs [23].

The NEEs used in our laboratory are prepared by electroless deposition of gold electrode elements within the pores of a microporous track-etch polycarbonate membrane [24]. The diameter and length of the pores in the template determine the geometrical characteristics of the metal nanostructure, with radii as small as 30 nm. The introduction of the use of pre-formed microporous membranes as template for the synthesis of nanomaterials [21] was somehow revolutionary since it made accessible to almost any laboratory a simple but effective procedure

for the easy preparation of nanomaterials. What is needed for the membrane based synthesis of nanomaterials is, in fact, very simple apparatus, such as apparatus for metal deposition and basic electrochemical instrumentation.

In the present work we examine the use of NEEs for the direct electroanalysis of iodide in water samples, comparing the analytical performances of NEEs with conventional gold-disk electrodes also in waters from the marine environment, such as lagoon waters.

2. Experimental

2.1. Materials

Polycarbonate filtration membranes (SPI-Pore, 47 mm filter diameter, 6 μm filter thickness) with a nominal pore diameter of 30 nm and coated with the wetting agent polyvinylpyrrolidone were used as the templates to prepare the NEEs. Commercial gold electroless plating solution (Oromerse Part B, Technic Inc.) was diluted (40 times with water) prior to use. All other reagents were of analytical grade and were used as received. Purified water was obtained using a Milli-Ro plus Milli-Q (Millipore) water purification system.

2.2. Electrochemical measurements and instrumentation

All electroanalytical measurements were carried out at room temperature (22 ± 1 °C) using a three electrodes single-compartment cell equipped with a platinum coil counter electrode and an Ag/AgCl (KCl saturated) reference electrode. All potential values are referred to this reference electrode.

Voltammetric measurements with NEEs and Au electrodes were performed with a CH-660A (CHIIJ Cambria Scientific, UK) instrument controlled by its own software. Cathodic stripping measurements at the hanging mercury drop electrode (HMDE) were performed using the EG&G Parc model 303A Static Mercury Drop Electrode in conjunction with an EG&G Parc model 394 Electromechanical Trace Analyzer, controlled by its own software. In this case, the sample solutions were carefully degassed by bubbling nitrogen before each measurement.

2.3. Electrode preparation

The nanoelectrode ensembles were prepared using the electroless plating procedure described previously [21], with some modifications. In particular, the method described in ref. [24,25] was followed. Briefly, after wetting for 2 h in methanol, the polycarbonate template membrane was sensitized with Sn^{2+} by immersion into a solution that was 0.026 M in $SnCl_2$ and 0.07 M in trifluoroacetic acid in 50:50 methanol-water for 5 minutes. After rinsing with methanol for 5 min, the sensitized membrane was immersed for 10 min in 0.029 M $Ag[(NH_3)_2]NO_3$. The membrane was then immersed into the Au plating bath which was 7.9×10^{-3} M in $Na_3Au(SO_3)_2$, 0.127 M in Na_2SO_3. After waiting 30 minutes, 0.625 M formaldehyde was added to the plating bath; this delay time was introduced here since it allows one to separate the formation of the first gold nuclei (produced by galvanic displacement of metallic Ag° nuclei with Au° nuclei) from the following catalytic growth of these nuclei by further gold deposition caused by formaldehyde. The temperature of the bath was 0-2 °C. Electroless deposition was allowed to proceed for 15 hours, after which an additional 0.3 M formaldehyde was added. Deposition was continued for another 9 hours, after which the membrane was rinsed with water and immersed in 10% HNO_3 for 12 hours. The membrane was then rinsed again with water and dried.

The final assembly of the NEE (for obtaining electrodes handy for use in an electrochemical cell) followed a previous method [26], reported herein. Briefly: the gold layer on the smoother face of the membrane is removed by peeling with scotch tape, in order to expose the head of the gold nanowires inside the pores; a small piece (approximately 8 mm × 8 mm) of golden membrane is then attached to a suitable conductive substrate; all the surface of the NEE is insulated with a film of plastics (Monokote by Topflite), apart a hole (3 mm diameter) which defines the geometric area of the ensemble (A_{geom}, = 0.07 cm^2). Good sealing between the nanoelectrodes and the polycarbonate is assured by heating the NEE at 150 °C for 15 min.

The average diameter of the nanodisks in these NEEs was measured by SEM and is 50 ± 10 nm [18].

A schematic drawing of a NEE is shown in Fig. 1.

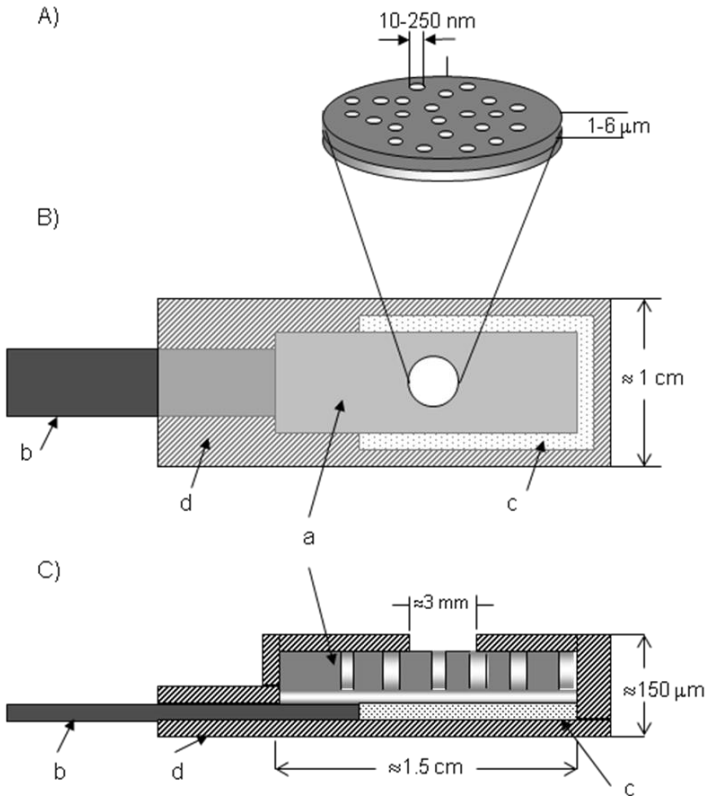

Figure 1. Scheme of an Au-NEE prepared using a track-etched polycarbonate membrane as template [26]. A). Particular of the section of the active area; B) top view, C) section of the all NEE ready for use as working electrode. a: track-etched golden membrane; b: copper adhesive tape with conductive glue to connect to instrumentation; c: aluminum adhesive foil with non-conductive glue; d: insulating tape. Not all details (namely, the nanoelectrodes dimension) are in scale.

Conventional millimeter-sized gold disk electrodes were prepared from a golden glass plate (thickness 1 mm) coated with nickel 80 Å, chromium 20 Å and gold 3900 Å on the outer surface. They were purchased from ACM France. The golden plate was cut into slides (ca. 2.5 cm × 1.0 cm) and the geometric area of the electrodes (0.07 cm^2) was defined, as it was made for the NEE, by the diameter of a hole punched in a strip of insulating tape which covers all the golden surface apart the hole. The electrical contact was made with a copper tape before placing the insulating tape.

Before each set of measurements, the surface of the Au-disk electrode and NEEs was cleaned electrochemically by cycling in 0.5 M H_2SO_4 between -0.1 V and 1.5 V at 100 mV/s.

2.4. Lagoon water samples

Lagoon waters were collected sampling at about 25 cm depth in preconditioned bottles, in the north area of the Venice lagoon, close to Lido portal, where the waters present an average salinity of 34 ‰ and pH 8.0. Samples were filtered through 0.45 μm Millipore membrane and acidified to pH 1 with some drops of sulphuric acid.

3. Results and discussion

3.1 Preliminary considerations

NEEs can be considered as ensembles of disk ultramicroelectrodes separated by an electrical insulator interposed between them. An ultramicroelectrode is considered as an electrode with at least one dimension comparable or lower than the thickness of the diffusion layer (typically < 25 μm). At such small electrodes, edge effects from the electrode become relevant and diffusion from the bulk solution to the electrode surface is described in terms of radial geometry instead of the simpler linear geometry used for larger (> 100 μm) electrodes. A NEE can be considered as a very large assembly of very small ultramicrolectrodes confined in a rather small space. Since the number of nanodisks elements per unit surface of the ensemble is large (in our case 6.5×10^8 nanodisks/cm^2 [18]), all the nanoelectrodes are statistically equivalent and the different contribution of the elements at the outer range of the ensemble can be considered negligible [19,27].

With respect to diffusing redox analytes, NEEs can exhibit two limit voltammetric response regimes which are ruled by the scan rate and/or by the reciprocal distance between the nanoelectrode elements [28]. When radial diffusion boundary layers overlap totally (radius of diffusion hemisphere larger than average hemi-distance between electrodes and/or slow scan rates) NEEs behave as planar macroelectrodes with respect to Faradaic currents (total overlap conditions, see Fig. 2a).

When diffusion hemispheres become shorter than the hemi-distance between the nanoelectrodes (larger distance between the nanodisks and/or higher scan rates), the current response is dominated by radial diffusion at each single element; under these conditions, the pure radial regime is achieved (see Fig. 2b). Really at very high scan rates, a so-called linear active regime can be reached [20], however, this regime is not encountered commonly in the experimental

practice, apart for recessed electrodes. Being characterized by the highest signal/background current ratios (see below), the total overlap and pure radial regimes are the regimes typically used for analytical and sensing applications.

Because of the geometrical characteristics, using NEEs obtained by commercial track-etched membranes as templates, the prevailing diffusion regime is the total overlap regime [20,21]. Transition from total overlap to the pure radial control as a function of nanoelements distance or scan rate was demonstrated experimentally by Martin and coworkers using specially made membranes [28] and by Ugo and coworkers with commercial membranes, but operating in high viscosity media [29].

Under total overlap diffusion regime, NEEs show enhanced electroanalytical detection limits, relative to a conventional millimeter-sized electrode. This is because the Faradaic current (I_F) at the NEE is proportional to the total geometric area (A_{geom}, nanodisks plus insulator area) of the ensemble (eq. 1, chapter 1), while the double-layer charging current (I_C) is proportional only to the area of the electrode elements (eq. 2, chapter 1) [21]. Faradaic-to-capacitive currents at NEEs and conventional electrodes with the same geometric area are related by eq. 3 on chapter 1 [20,21]:

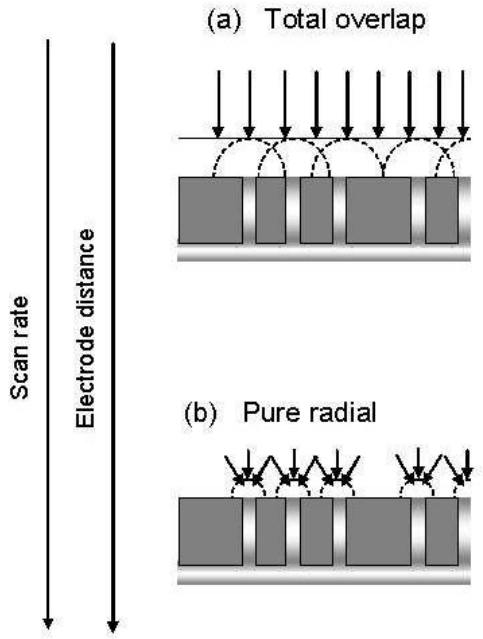

Figure 2. Schematic drawing of the typical diffusive regimes observed at nanoelectrode ensembles as a function of the scan rate and/or nanoelectrodes distance. (a) Total overlap regime; (b) Pure radial regime.

This ratio at the NEE is higher than the relevant ratio at a conventional electrode of the same geometric area for a proportionality factor that is the reciprocal of the fractional electrode area (f) (equation 4, chapter 1).

Typical f values for NEEs are between 10^{-3} and 10^{-2}. Faradaic currents at NEEs are equal to those recorded at macro electrodes of the same geometric area, however at NEEs background currents are dramatically lowered. Such an improvement in the Faradaic to capacitive currents ratio explains why detection limits (DLs) at NEEs can be from 1 to 3 orders of magnitude lower than with conventional electrodes [17,21,30].

3.2 Cyclic voltammetry of iodide in tap water

Fig. 3, full lines, compares the cyclic voltammograms recorded at an Au-disk electrode in tap water acidified with sulfuric acid, pH 1.0, spiked with 50 μM iodide (Fig. 3a) and at a NEE at ten times lower iodide concentration, that is 5 μM (Fig. 3b). The CVs are characterized by an oxidation peak with associated return peak both at the Au-disk and at the NEE. Oxidation peak currents scale linearly with the square root of the scan rate (not shown); this evidence agrees with the occurrence of a diffusion controlled process.

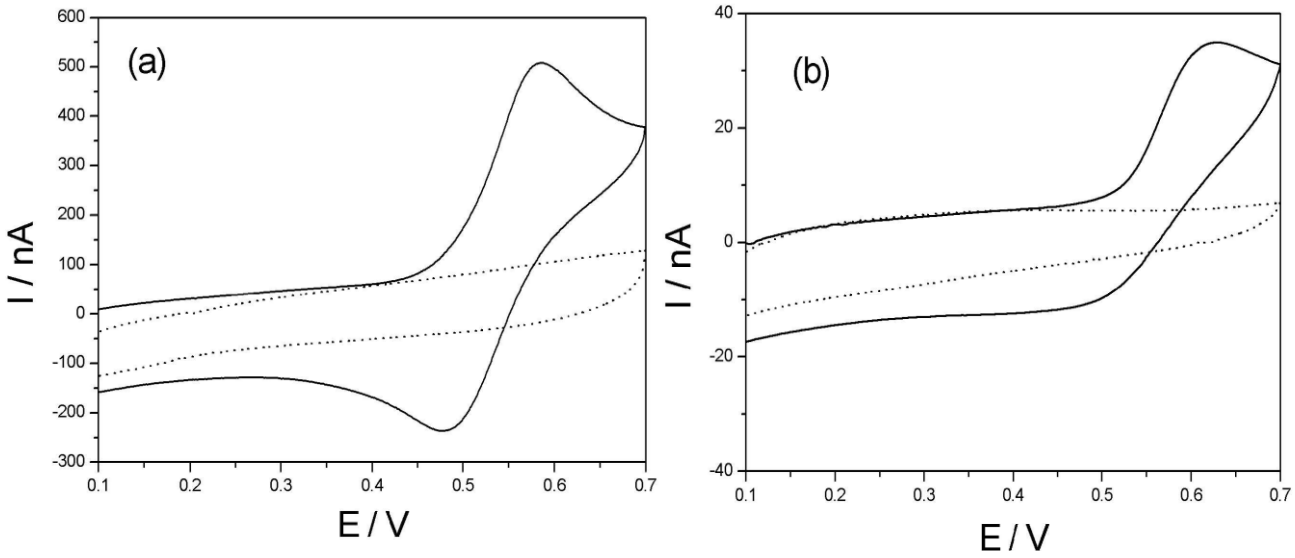

Figure 3. Cyclic voltammograms recorded at 20 mVs^{-1} in tap water, 0.1 M sulphuric acid solution, pH 1.0, before (·····) and after addition (——) of: (a) 50 μM KI at an Au-disk millimeter-sized electrode; (b) 5 μM KI at a NEE.

For NEEs, the peak shape of the voltammogram together with the linear dependence of I_p on $v^{1/2}$ indicate the operativeness of the total overlap regime with respect to diffusion of iodide to the ensemble of nanolectrodes. $E_{1/2}$ values, calculated as $(E_{pf} + E_{pb})/2$ (where the f and b subscripts indicate the forward and backward peaks, respectively) were 0.548 V vs. Ag/AgCl at the NEE and 0.524 V vs. Ag/AgCl at the Au-disk. Forward to backward peak separation (ΔE_p) values were of the order of 150 mV at the NEE and 80 mV at the Au macro (both at 20 mV/s); these values indicate a quasi-reversible one-electron transfer process, in agreement with previous findings [31]. Note that the kinetic constant for heterogeneous electron transfer, k°, at NEEs is substituted by an apparent constant $k°_{app}$. NEEs behave indeed as electrodes with partially blocked surface [32] and:

$$k°_{app} = k° \, f \qquad (1)$$

where f is the fractional electrode area. Eq. 1 explains the reason why quasi-reversible processes look less reversible at NEEs, as it is observed here for iodide oxidation.

The broken line CVs in the same Fig. 3 show the background currents before spiking with iodide, that is in the CV signal relevant to the background electrolyte (blank). As expected, no iodide signal is detected before spiking. The difference in current between the forward (I_f) and backward (I_b) scan in the blank is proportional to the double layer charging current and the electrode area (active area for NEEs) according to the following equation [33,34]:

$$(I_f - I_b) = 2 \, v \, C_{dl} \, A \qquad (2)$$

where v is the scan rate, C_{dl} is the double-layer capacitance and A is the metal surface exposed to the solution that is the active area for a NEE and geometric area for an Au-disk electrode.

Comparing data for the NEE and the Au-disk electrode, obtained operating under the same experimental conditions and using NEE and Au-disk with the same A_{geom} value, the ratio between background currents results:

$$(I_f - I_b)_{NEE}/(I_f - I_b)_{Au\text{-}disk} = A_{act}/A_{geom} = f \qquad (3)$$

By substituting data obtained from the CVs in Fig. 3, measured in correspondence of the $E_{1/2}$ for the I^-/I_2 couple, we can estimate that, for our NEEs, this ratio is 8×10^{-2}. Note that the $E_{1/2}$ of interest is quite positive and not far from the foot of the oxidation limit of the potential window

accessible with NEEs in chloride free solutions [17]. It was demonstrated that for NEEs operating close to this limit, the background current is given not only by the double layer charging current but also by a residual current related to background oxidation [17]. For this reason, the f value can be higher than the value expected only on the basis of geometric considerations (namely 1.3×10^{-2}). Therefore, f value can be considered as an *apparent* fractional electrode area, which however should correspond to the real improvement in signal to background current ratio achievable by NEEs, estimated specifically at the potential values where peak currents are really measured.

Focusing on signals recorded at NEEs, the oxidation peak current is directly proportional to the iodide solution concentration and a linear calibration plot is obtained (not shown), with a dynamic range extending over two orders of magnitude and a sensitivity (m, slope of the calibration plot) of 30 nA cm^{-2} μM. Current densities are calculated with respect to the overall geometric area of the ensemble. The detection limit DL, calculated as DL= 3σ/m (where σ is the standard deviation) resulted DL= 0.3 μM. Such a DL is almost one order of magnitude lower than the best literature datum at gold ultramicroelectrodes in water solution [35]. Note also that DL obtained by us at the Au-macro (not shown) is 4 μM, which is more than one order of magnitude higher than DL at NEEs and the ratio between the two DLs is very close to the f ratio calculated by equation (3). We wish to stress that no preconcentration of the iodide was employed in these analyses.

3.3 Lagoon water

The monitoring of iodide and its seasonal cycling in estuarine waters is the subject of specially devoted studies [36,37]; this prompted us to test the use of NEEs for performing the direct determination of iodide in lagoon waters.

Fig. 4a shows the CVs recorded in a water sample from the lagoon of Venice before and after spiking with standard additions of iodide. The sample was acidified to pH 1 by adding few drops of concentrated H_2SO_4. The first line CV refers to the sample, while the following ones to the sample spiked with known amount of iodide. The voltammetric oxidation of I^- is less reversible than in the synthetic samples [23] since the forward to backward peak separation increases to 280 mV; however, an oxidation peak is detected, whose current increases with the standard additions. The lower electrochemical reversibility of the CVs is probably due to other components such as organics or surfactants which can be present in this kind of rather raw sample, which underwent only filtration and acidification as pre-treatment. The iodide

voltammetric behavior, particularly the one observed after spiking, is very similar to the one observed previously in table salt samples [23]. The standard addition plot reported in Fig. 4b, allowed us to estimate a I^- concentration in the sample of (1.6 ± 0.5) μM i.e. (203 ± 63) μg/L for triplicate analysis. Interestingly, this concentration value is slightly higher than the detection limit with NEEs, but lower than DL with millimeter-sized Au disk electrodes (namely 4 μM [23]). The concentration determined by us in the studied sample compares with literature data from other marine areas [38], however, it is significantly higher than values measured by chromatography in the Venice Lagoon [39], that were between 14 and 32 μg/L.

Both the high standard deviation (31%) and the large difference with previous results from the same area prompted us to improve the determination, lowering the detection limit which, for CV, is too close to the concentration to be determined. It was recently shown that DLs achievable with NEEs can be improved by using pulsed voltammetric techniques instead of CV [19]. Preliminary experiments indicated that square wave voltammetry (SWV) at low frequency is suitable to the goal of determining trace iodide in lagoon waters.

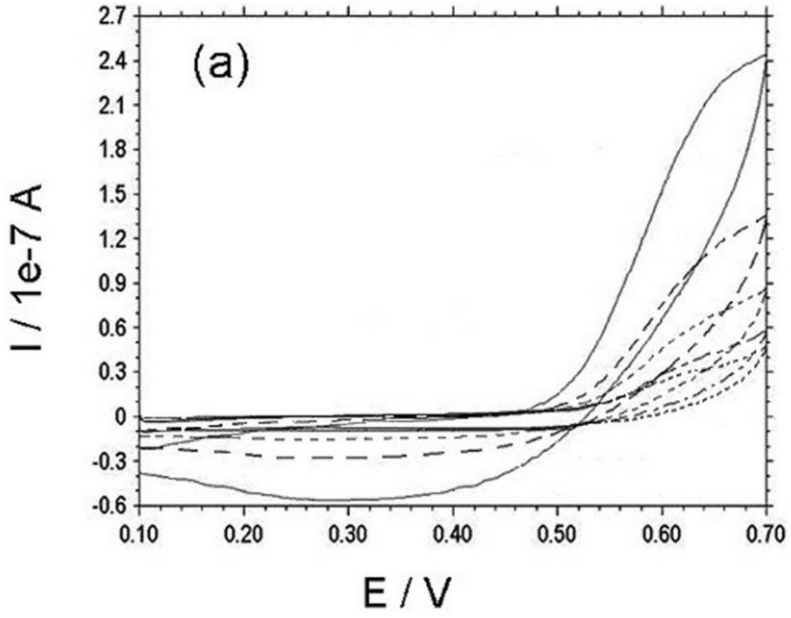

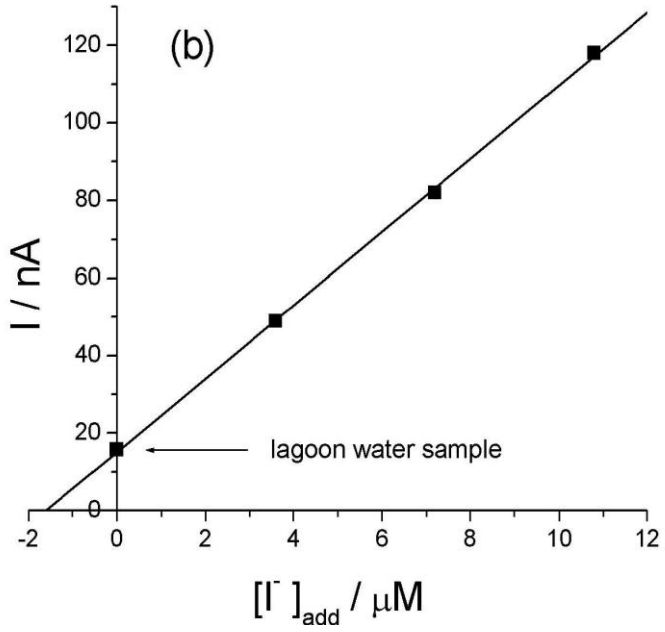

Figure 4. (a) Cyclic voltammograms recorded at 20 mVs^{-1} at a NEE in lagoon water acidified with sulphuric acid, pH 1.0, before (⋯⋯) and after standard additions of KI: 4 μM (– · – · –), 8 μM (- - -), 12 μM (– – –) and 24 μM (——). (b) Standard additions plot.

Fig. 5a shows the SW voltammograms recorded in acidified lagoon water before and after spiking with KI. A resolved although rather small peak is detected in the sample with E_p= 600 mV vs. Ag/AgCl. It was observed that both the peak height and resolution (given by the ratio $I_p/W_{1/2}$, where $W_{1/2}$ is the half-peak width) reach their maximum at low frequencies, namely 2 Hz. This is explained by the geometry of NEEs and on the time dependence of diffusion layers (see Fig.2). At low time scales, that is at low frequencies, diffusion hemispheres around each nanoelectrode are larger, so that the total overlap condition is achieved.

Note that under total overlap conditions, the 100% of A_{geom} contributes to the voltammetric signal [20,34], so that signals are higher than under partial overlap conditions. Another feature evident from the SWVs in Fig. 5a is the anticipation of the anodic limit of the accessible potential window to 0.700-0.720 V vs. Ag/AgCl (compare e.g. with Fig. 3). This is probably related to the easier oxidation of the gold nanoelectrodes caused by the high chloride concentration (~ 0.58 M) present in the sample.

Fig. 5b shows the standard additions plot from which the iodide concentration in the sample is evaluated to be (0.30 ± 0.05) μM for triplicate determinations. Detection limits calculated on the basis of 3σ/m criterion, result 0.10 μM and the quantification limit QL= 10σ/m= 0.30 μM. Therefore, the concentration determined by us is higher than DL, but close to QL.

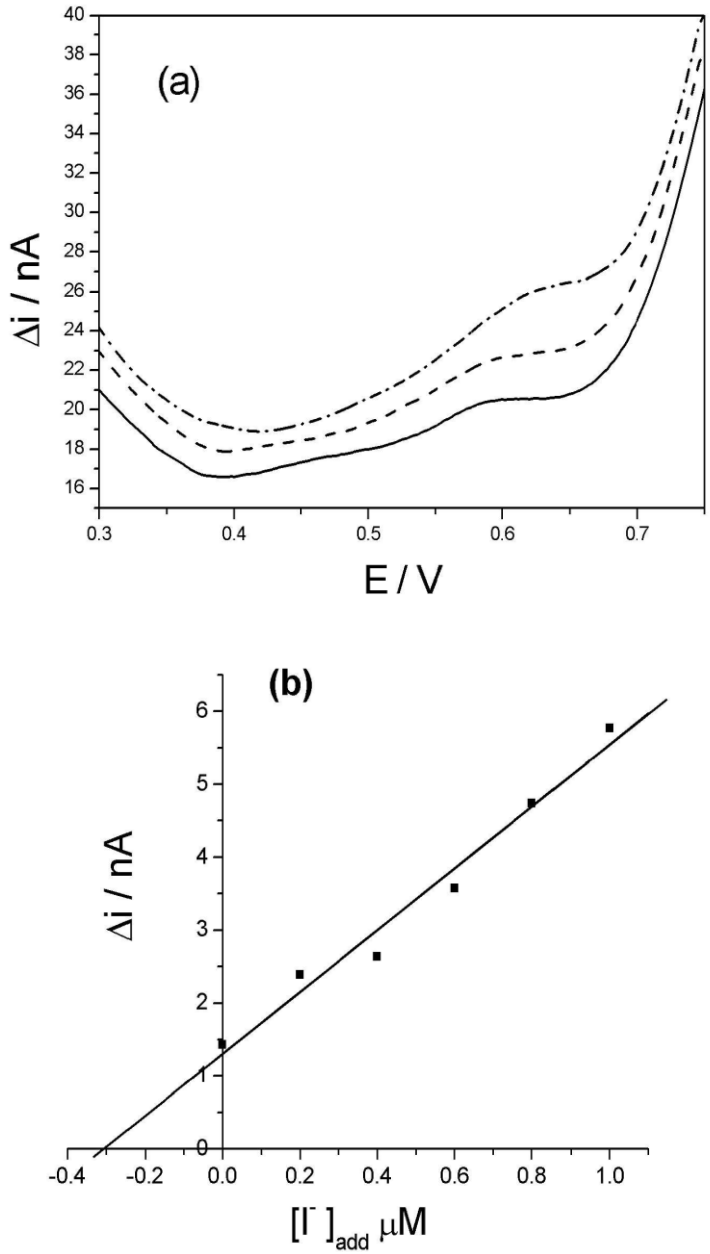

Figure 5. (a) Square wave voltammograms recorded at a NEE in lagoon water acidified with sulphuric acid, pH 1.0, (——) and spiked with 0.4 μM KI (- - -) and 0.8 μM KI (− · − · −). Scan parameters: pulse height 50 mV , frequency 2 Hz. (b) Standard additions plot.

As a comparison, the same sample was analyzed using the cathodic stripping method at the HMDE after addition of Triton-X 100, proposed by Luther and coworkers [13]. Fig. 6 shows the voltammetric pattern and the standard additions plot at the HMDE. The concentration determined resulted (0.40 ± 0.05) μM, that is in agreement with the value measured with the NEE by SWV.

Note that with NEE no preconcentration nor deoxygenation of the sample is required, while for cathodic stripping a 180 s preconcentration and deoxygenation of the sample for several minutes are necessary. However, peak current at the HMDE are better resolved and, indeed, detection limits can, in principle, be further lowered by increasing the preconcentration time.

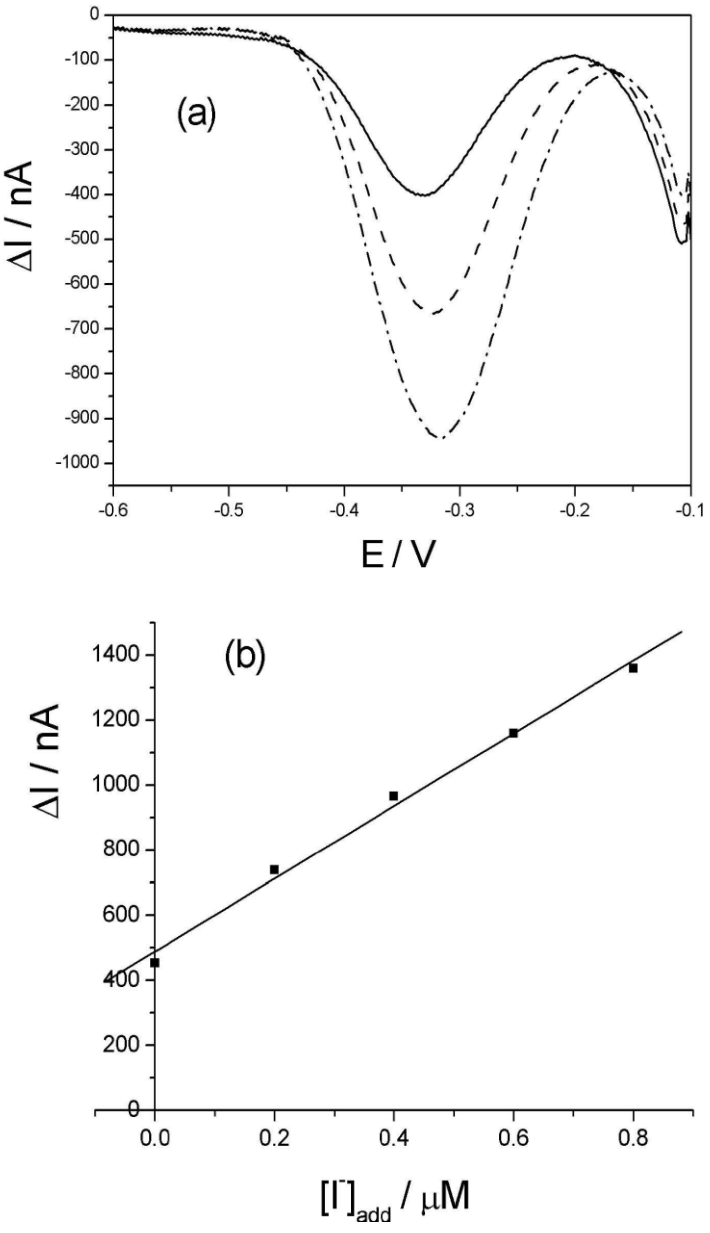

Figure 6. (a) Cathodic stripping square wave voltammograms recorded with a HMDE in lagoon water after the addition of Triton-X 100 (——) and spiked with 0.2 μM KI (- - -) and 0.4 μM KI (– · – · –). Scan parameters: pulse height 20 mV, frequency 100 Hz, deposition time 180 s at – 0.1 V (b) Standard additions plot.

4. Conclusions

Nanoelectrode ensembles are advanced nanotech electrochemical sensors which allows one to achieve low detection limits for the direct determination of iodide in water samples. Iodide is oxidized electrochemically both at gold macroelectrodes and at ensembles of gold nanodisks electrode; detection limits at NEEs are one order of magnitude improved with respect to DLs at Au- macro electrodes. The results presented here show that the use of gold NEEs allows indeed the direct determination of micromolar concentrations of iodide in water samples. In lagoon waters, a shortening of the potential window accessible makes somehow critical the determination when iodide concentration is in the submicromolar range. Under these conditions, the use of square wave voltammetry improves the detection capabilities. The comparison of the NEE-based method with literature methods at the HMDE [13], indicates that the latter is to be preferred when electrolytic preconcentration and deoxygenation of the sample are possible, while NEEs are to be preferred when the direct detection is required, and in samples where the iodide concentration is ≥ 0.30 μM.

References

[1] G.T.F. Wong, *Rev. Aq. Sc.* **4** (1991), 45.

[2] P. Pongpaew, S. Saowakontha, R. Tungtrongchitr, U. Mahaweerawat, F.P. Schelp, *Nutr. Res.* **22** (2002), 137.

[3] F. Delange, B. de Benoist, D. Alnwick, *Thyroid* **11** (2001), 437.

[4] J.L. Lambert, G.L. Hatch, B. Mosier, *Anal. Chem.* **47** (1975), 915.

[5] M. Haldimann, B. Zimmerh, C.Als, H.Gerber, *Clin. Chem.* **44** (1998), 817.

[6] K. Ito, T. Ichihara, H. Zhuo, K. Kumamoto, A.R. Timerbaev, T. Hirokawa, *Anal. Chim. Acta* **497** (2003), 67.

[7] K. Yokota, K. Fukushi, S. Takeda, S.I. Wakida, *J. Chromatogr. A* **1005** (2004), 145.

[8] G.T.F. Wong, P.G. Brewer, *Anal. Chim. Acta* **81** (1976), 81.

[9] K. Ito, *J. Chromatogr. A* **830** (1999), 211.

[10] L. Rong, T. Takeuchi, *J. Chromotogr. A* **1042** (2004), 131.

[11] J.P. Perchard, M. Buvet, K. Molina, *J. Electroanal. Chem.* **14** (1967), 57.

[12] K.Z. Brainina, Z. Fresenius, *Anal. Chem.* **312** (1982), 428.

[13] G.W. Luther, C.B. Swartz, W.J. Ullman, *Anal. Chem.* **60** (1988), 1721.

[14] R. D. Rocklin, E.L. Johnson, *Anal. Chem.* **55** (1983), 4.

[15] I. Svancara, J. Konvalina, K. Schachl, K. Kalcher, K. Vytras, *Electroanal.* **10** (1998), 435.

[16] A. Walcarius, G. Lefevre, J.P. Rapin, G. Renaudin, M. Francois, *Electroanal.* **13** (2001), 313.

[17] B. Brunetti, P. Ugo, L.M. Moretto, C.R. Martin, *J. Electroanal. Chem.* **491** (2000), 166.

[18] P. Ugo, N. Pepe, L.M. Moretto, M. Battagliarin, *J. Electroanal. Chem.* **560** (2003), 51.

[19] L.M. Moretto, N. Pepe, P. Ugo, *Talanta* **62** (2003), 1055.

[20] P. Ugo, L.M. Moretto, F. Vezzà, *ChemPhysChem* **3** (2002), 917.

[21] V.P. Menon, C.R. Martin, *Anal. Chem.* **67** (1995), 1920.

[22] W. Vastarella, L. Della Seta, A. Masci, J. Maly, M. De Leo, L.M. Moretto, R. Pilloton, *Intern. J. Environ. Anal. Chem.* **87** (2007), 701.

[23] F.C. Pereira, L.M. Moretto, M. De Leo, M.V.B. Zanoni, P.Ugo, *Anal. Chim. Acta* **575** (2006), 16.

[24] M. De Leo, F.C. Pereira, L.M. Moretto, P. Scopece, S. Polizzi, P.Ugo, *Chem. Mater.* **19** (2007), 5955.

[25] M. De Leo, A. Kuhn, P. Ugo, *Electroanal.* **19** (2007), 227.

[26] P. Ugo, L. M. Moretto, in *Handbook of Electrochemistry*, Ed. C. G. Zoski, Elsevier, **2007**, Cap. 16, Sezione 16.2.

[27] H.J. Lee, C. Beriet, R. Ferrigno, H.H. Girault, *J. Electroanal. Chem*. **502** (2001), 138.

[28] J.C. Hulteen, V.P. Menon, C.R. Martin, *J. Chem. Soc. Faraday Trans*. **92** (1996), 4029.

[29] M. De Leo, L.M. Moretto, O. Buriez, P. Ugo, *Electroanal.* **21** (2009), 392.

[30] P. Ugo, L.M. Moretto, S. Bellomi, V.P. Menon, C.R. Martin, *Anal. Chem*. **68** (1996), 4160.

[31] M.A. Tadayyoni, P. Gao, M.J. Weaver, *J. Electroanal. Chem*. **198** (1986), 125.

[32] C. Amatore, J.M. Saveant, D. Tessier, *J. Electroanal. Chem*. **147** (1983), 39.

[33] A.J., Bard, L. Faulkner, *Electrochemical Methods*, Wiley, New York (2000), 18.

[34] P. Ugo, L.M. Moretto, in *Handbook of Electrochemistry* (1st edn.), edited by C.G. Zoski, Elsevier, Amsterdam (2007) (Chapter 16.2).

[35] W. Zhang, H. Zha, B. Yao, C. Zhang, X. Zhou, S. Zhong, *Talanta* **46** (1998), 711.

[36] G.W. Luther III, H. Cole, *Mar. Chem*. **24** (1988), 315.

[37] G.T.F. Wong, L.-S. Zhang, *Est. Coast. Shelf Sc*. **56** (2003), 1093.

[38] L. Rong, L.W. Lim, T. Takeuchi, *Talanta* **72** (2007), 1625.

[39] E. Marengo, M.C. Gennaro, D. Giacosa, C. Abrigo, G. Saini, M.T. Avignone, *Anal. Chim. Acta* **317** (1995), 53.

Modification of nanoelectrode ensembles by thiols and disulfides to prevent non specific adsorption of proteins

1. Introduction

The nanoelectrode ensembles (NEEs), introduced by Chuck Martin's group in the mid nineties [1], have shown properties useful for many advanced applications. In the electroanalytical and sensor fields, NEEs are particularly attractive since they are characterized by highly improved signal-to-background current ratios and extremely low detection limits [1-4], they are suitable to extreme miniaturization [3], can be turned into 3-D nanoelectrode systems [5-8] or can be developed in groups of singly addressable arrays for multianalyte detection [9,10].

In the previous chapter, we demonstrated that NEEs can be successfully applied for the direct determination of trace iodide in water samples.

Thanks to their properties, NEEs are finding numerous applications in different fields [11-13] and among the others, they can be employed for preparing nanostructured electrochemical biosensors [5,7,14,15]. It is interesting to note that NEEs are indeed nanocomposite made by a pre-ordered arrangement of two different materials. On one side, there is the large surface of the templating membrane composed by an insulating organic polymer, typically track-etch polycarbonate (PC) [1,13]. On the other side, each pore of the starting membrane in the final NEE hosts a gold nanowire, suitable for electrochemical transduction. This duality in the structure of the NEEs surface was recently exploited in our laboratory to immobilize an antibody-based biorecognition layer onto the wide polycarbonate surface which surrounds the nanoelectrodes [14,15]. This allowed the preparation of an electrochemical immunosensor able to detect the receptor protein HER2, captured selectively by the monoclonal antibody Herceptin™ bound on the polycarbonate surface. It was shown that for the Herceptin™ case, the immobilization of the antibody did not hinder the electron transfer at the nanoelectrodes, thanks to the fact that this protein is characterized by a high isoelectric point (pI=9.2) [16] which helps in avoiding its adsorption on the gold surface. This is not necessarily the case for negatively charged polypeptides, that is for proteins with low pI, which are known to easily adsorb on gold. Several procedures have been indeed developed to prevent undesired protein adsorption on gold [17,18] as well as on other materials [19]. Note that, in the case of NEE-based biosensors, unwanted protein adsorption could constitute a problem for extending their use to the analysis of complex samples.

Pioneering studies developed on flat gold surfaces and microelectrodes [20-23] showed the possibility to modify electrode surfaces and to tune their ionic selectivity by using self-assembled monolayers (SAM) of thiols with carboxylate functionalities; indeed, by changing the solution pH it is possible to change the ionic charge of the monolayer. In the present research, we demonstrate the possibility to use SAMs of thiols and disulfides to furnish ionic permselectivity even to the surface of gold nanoelectrodes with diameter as small as 30 nm. In particular, in the present study we report for the first time on the modification of NEEs by self assembly of the cyclic disulfide thioctic acid (TA) and of the thiol 2-mercaptoethanesulfonic (MES) acid (Scheme 1).

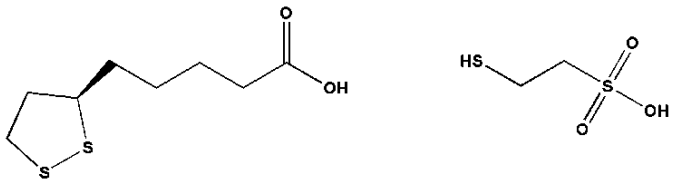

Scheme 1. Structural formula of the thiol derivatives used.

As said above, the majority of proteins adsorbable on gold are polyanionic at physiological pH, therefore, we focused on Au-SAMs formed by negatively charged sulphur compounds which could hinder such undesired protein adsorption. Note that TA is a weak acid, whose carboxylic group is characterized by a pK_a of 5.4 [24], therefore it is dissociated in neutral or basic solution while at low pH it is protonated, even when deposited as a SAM on Au [20]. On the other hand, MES is a strong acid whose sulphonic group is always deprotonated (anionic).

Moreover, we bring such a surface modification to a further goal, that is to generate on the NEEs more complex structures which exploit also the affinity of PC for proteins to create on the polymer membrane a protein layer which surrounds, but does not block the nanoelectrodes. The proteins studied to this aim are the globular proteins casein and bovine serum albumin (BSA), which present well known fouling properties with respect to gold surfaces and polycarbonate as well [25,26]. We demonstrate here the possibility to obtain on the NEE a complex structure in which the polycarbonate is coated by a sort of protein cushion (on which other biomolecules can be eventually bound), among which the nanoelectrodes, protected by suitable SAMs, remain free to act as efficient electrochemical transducers.

2. Experimental

2.1. Electrochemical apparatus

All electrochemical measurements were carried out at room temperature with a CH660A potentiostat controlled via personal computer by its own software, using a three-electrode single-compartment cell equipped with a platinum counter electrode and an Ag/AgCl (KCl saturated) reference electrode, to which all reported potential values are referred.

2.2. FTIR-ATR (attenuated total reflection)

The spectra were recorded by a Thermo Scientific Smart iTR equipped with a ZnSe crystal. The resolution of the instrument was adjusted to 4.0 cm^{-1} and every spectrum was collected with 64 scans.

2.3. AFM (atomic force microscopy)

AFM measurements were performed in air on samples dried at room conditions, using a Veeco NS IV Dimension 3100 Scanning Probe Microscope. Images were collected in Tapping mode™ using standard silicon cantilevers with typical resonant frequency 150 kHz, elastic constant 5 N/m. Tip curvature radius was 10 nm, length 6 μm, conical angle 22°. All the measurements were performed on NEEs fabricated with track-etched polycarbonate membranes with pores diameter of 80 nm. Preliminary electrostatic force measurements (EFMs) were performed with the same apparatus, but using cantilever tips metalized with a 20 nm Pt layer and applying a difference in potential of 20 V between the tip and the sample.

2.4. Materials

Thioctic acid 98% and ferrocenecarboxylic acid (FcCOOH) 97% were purchased from Aldrich; 3 M MES solution in water was from Sigma. The salt (ferrocenylmethyl) trimethylammonium hexafluorophosphate ($FA^+PF_6^-$) was prepared by metathesis of the (ferrocenylmethyl) trimethylammonium iodide (Alfa Aesar) with potassium hexafluorophosphate 99% (Alfa Aesar). Casein was from VWR International and was dissolved (4 mM) in 1 M maleic acid buffer. BSA was purchased from Sigma. Purified water was obtained using Milli-Ro plus Milli-Q (Millipore) water purification system. All other chemicals were reagent grade. Track-etch polycarbonate

(PC) membrane filters, thickness 6 μm, were obtained from SPI-pore™ with nominal pore diameter of 30 nm or 80 nm, average pore density 6×10^8 pores cm^{-2}, coated with polyvinylpyrrolidone (PVP) by the producer.

2.5. Template fabrication of NEEs

Polycarbonate membranes with 30 or 80 nm pore diameters were used for preparing NEEs used for CV and AFM characterization, respectively.

Ensembles of gold nanoelectrodes were prepared by electroless deposition as already described (ref. [7] and chapter 3, paragraph 2.3.). Handy NEEs were assembled as explained on chapter 3 (paragraph 2.3.) and as reported previously [13]. Note that the geometric area of the NEEs is 0.07 cm^2, while the calculated active area (surface of the nanoelectrodes) of the NEEs with 30 nm nanodisks diameter (used for the CVs) is 3×10^{-4} cm^2.

2.6. NEEs modification

NEEs coated with a SAM of TA (TA–NEEs) were prepared by overnight dipping in 0.01 M TA in 75% ethanol in water [27]. This was followed by rinsing with ethanol to remove any unbound molecule.

NEEs coated with MES (MES–NEEs) were prepared by overnight dipping in 0.01 M MES water solution, followed by repeated rinsing with water. Both procedures were carried out at room temperature.

NEEs treated with casein or BSA (Cas–NEEs and BSA–NEEs, respectively) were obtained by dipping in a stirred solution of 0.2 mM casein or BSA solution in 0.01 M phosphate buffer (pH 7.5) for 30 min. The NEEs were repeatedly rinsed with pure phosphate buffer before use. Some NEEs were pre-treated with MES, before the protein treatment, to obtain MES–Cas–NEEs or MES–BSA–NEEs.

In some preliminary experiments, the PVP which impregnates the commercially available track-etched membranes was removed by dipping the membranes in 50% (V/V) acetic acid (HAc) [28].

3. Results and discussion

3.1. Redox probes at SAM modified NEEs

At first, we studied the effect of TA and MES adsorbed on the surface of the nanoelectrodes by analyzing the cyclic voltammetric behavior of two ferrocene derivatives used as redox probes, that are the cationic probe FA^+ and the weak acid FcCOOH, which dissociates to the anion $FcCOO^-$ in slightly alkaline solutions (pK_a of FcCOOH is 6.7 in water/methanol [29]). Relevant CV patterns are reported in Fig. 1 and Fig. 2, while characteristic potential values, drawn from these CVs, are listed in Table 1.

Fig. 1a shows the comparison of the CVs of FA^+ in slightly alkaline solution at the bare NEE (full line), TA–NEE (dashed line) and MES–NEE (dotted line). The three patterns practically overlap, showing the characteristics typical of a one-electron reversible oxidation process at a NEE operating under total overlap diffusion conditions [1]. These results indicate that the presence of MES or TA, at pH 9, does not influence the voltammetric behavior of the cationic probe FA^+.

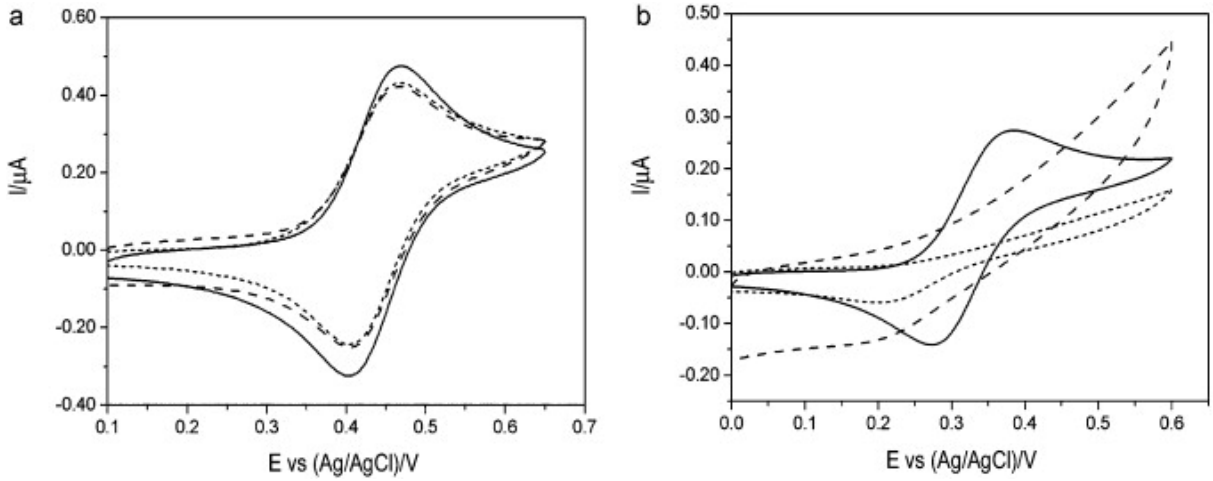

Figure 1. Cyclic voltammograms in 10^{-2} M carbonate buffer, pH 9.0, of 1.0×10^{-4} M FA^+PF_6 (a) and 0.7×10^{-4} M FcCOOH (b), with a bare NEE (full lines), a TA-NEE (dashed lines) and a MES-NEE (dotted lines). Scan rate 20 mVs^{-1}.

For $FcCOO^-$, the peak to peak separation at the bare NEE (see Fig. 1b, full line and Table 1), is slightly larger, suggesting a quasi-reversible behavior [1]. This can be attributed to the fact that NEEs are very sensitive to kinetics slow-down. Since the first studies on NEEs [1,30], it was indeed demonstrated that these ensembles of nanodisk electrodes behave as electrodes with

partially blocked surface [31], for which the true heterogeneous kinetic constant is substituted by an apparent one, the latter being smaller by a factor which corresponds to the fractional electrode area [1,30]. The validity of such a model was confirmed also by more recent theoretical studies [32-35]. The dashed and dotted lines in Fig. 1b, show that a completely different behavior is observed for $FcCOO^-$ at modified NEEs, with the CVs at the TA–NEE (dashed line) and MES–NEE (dotted line) becoming almost featureless.

All these evidences indicate that MES and TA are indeed bound on the gold surface of the nanoelectrodes forming a SAM. On the basis of electrostatic interactions, these SAMs do not affect the electrochemical behavior of the cationic probe FA^+ while they repel the anionic probe $FcCOO^-$.

Fig. 2 shows the CVs recorded with the same NEEs and with the same redox probes of Fig. 1, but in acidic solutions, namely in 10^{-2} M HCl. At the MES–NEE (dotted line in Fig. 2a) the CV of FA^+ does not change significantly from the one recorded in neutral (not shown) or slightly alkaline solution (see Fig. 1a) or at the bare-NEE (full line), while at the TA–NEE (dashed line) only a broad voltammetric signal is recorded. At pH 2 the carboxylic groups of the thioctic acid are protonated, therefore the TA layer is neutral and produces an insulating coating which hinders the electron transfer.

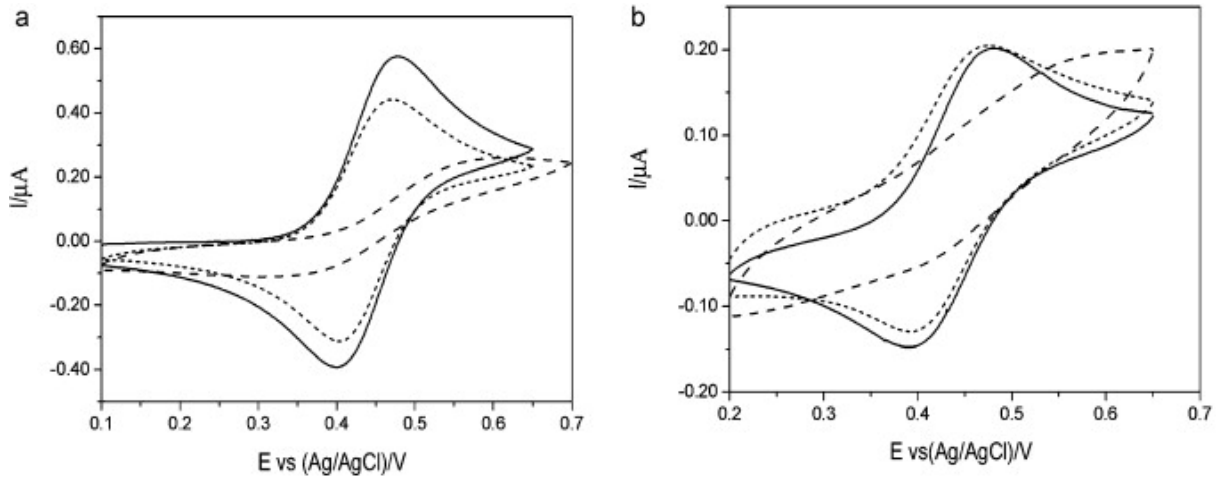

Figure 2. Cyclic voltammograms in 10^{-2} M HCl of 1.0×10^{-4} M FA^+PF_6 (a) and 0.7×10^{-4} M FcCOOH (b) at a bare NEE (full lines), a TA-NEE (dashed lines) and a MES-NEE (dotted lines). Scan rate 20 mVs^{-1}.

For FcCOOH (see Fig. 2b) a significant suppression of the signal is observed at the TA–NEE (dashed line), while the voltammetric features typical of a one electron-oxidation are detected at

the MES–NEE (dotted line) and bare NEE (full line). Note that the protonation of FcCOOH at pH 2 reflects in a shift of $E_{1/2}$ to more positive potential values (see 3rd column in Table 1).

The explanation for the voltammetric behavior of FcCOOH at the TA–NEE is analogue to that for FA^+: the SAM of TA is neutral and generates an insulating layer on the surface of the nanoelectrodes. In the case of the MES–NEE, a well resolved CV signal is detected also for FcCOOH due to the fact that at pH 2 the carboxylic group of the ferrocene derivative is protonated; the probe is neutral and it is no more repelled by the negatively charged MES layer.

pH	**Analyte**	**Bare NEE**		**TA-NEE**		**MES-NEE**	
		$E_{½}$ (V vs Ag/AgCl)	**ΔE_p** (V)	**$E_{½}$** (V vs Ag/AgCl)	**ΔE_p** (V)	**$E_{½}$** (V vs Ag/AgCl)	**ΔE_p** (V)
9	FA^+	0.440	0.060	0.440	0.060	0.440	0.060
	$FcCOO^-$	0.330	0.090	No peaks		Only a small reduction peak at 0.20 V	
2	FA^+	0.440	0.070	Broad peaks		0.440	0.070
	FcCOOH	0.430	0.090	No peaks		0.430	0.090

Table 1. Characteristic potential values relevant to the cyclic voltammograms in Figures 1 and 2.

All these results indicate that SAMs of suitable sulphur compounds give ionic charge selectivity to NEEs, furnishing to the nanoelectrodes the same permselectivity demonstrated previously for the case of individual μm-sized electrodes [20-23]. A MES layer allows only cationic or neutral probes to access the nanoelectrode surface to undergo successful electron transfer. Note that, for TA, the selectivity is pH dependent while for MES this property is pH independent; for this reason, in the following part of the study, we focused on MES.

3.2. Voltammetry at protein treated NEEs

Previous studies [26,36] reported that PVP, which impregnates the commercially available PC membranes, can somehow inhibit the adsorption of proteins on the polymer, even if such an adsorption is not completely prevented [37]. For this reason we performed some preliminary experiments comparing BSA and Cas adsorption on PVP coated vs. PVP-free PC membranes. In the latter case, PVP was removed from commercially available membranes by HAc treatment

(see Section 2). The amount of protein adsorbed was estimated by comparing the intensity of the color developed by staining with Fuchsin acid [38] and Naphthol blue black [39]. It was observed that the protein adsorption is slightly higher in the membranes treated with HAc, however this adsorption was not negligible on the untreated commercial membranes. On the basis of this result and taking into account that we are interested in studying the behavior of modified NEEs prepared from as-received commercially available membranes, in the following part of the research we focused on NEEs obtained using PVP-coated PC track-etched membranes.

Fig. 3 compares the voltammetric behavior of the redox probe FA^+ at a bare NEE (full line), a Cas–NEE (casein treated, not thiolated; dashed line) and a MES–Cas–NEE (MES and casein treated; dotted line).

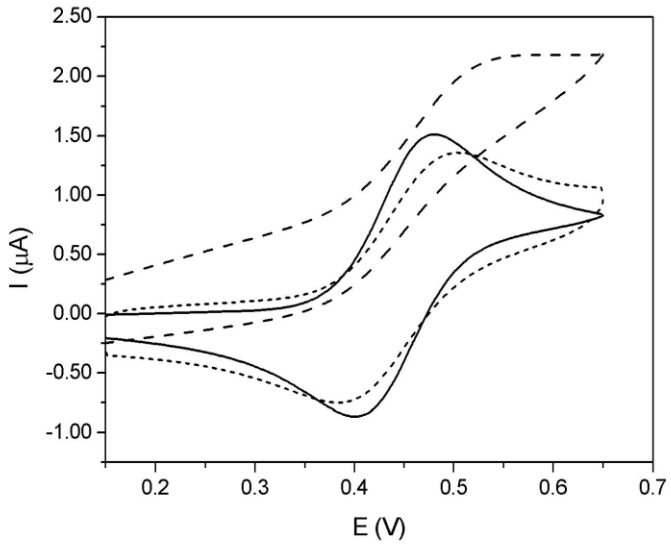

Figure 3. Cyclic voltammograms recorded in 5×10^{-4} M FA^+, 0.01 M phosphate buffer pH 7.5 with a bare NEE (full line), a Cas-NEE (dashed line) and a MES-Cas-NEE (dotted line). Scan rate 20 mV s^{-1}.

Heavy distortion and degradation of the CV pattern is indeed observed at the Cas–NEE. The capacitive current, estimated as the difference in the forward to backward CV pattern [40] before the upraise of the voltammetric peak (e.g., at 0.2 V), increases dramatically. With respect to the bare NEE, the peak signal for FA^+ becomes broader and less resolved from the background. Moreover, a significant ohmic drop contribution is observed, which causes the sloping of all the CV pattern. These evidences suggest that casein is strongly adsorbed on all the surface of the

NEE, forming a blocking layer which hinders the electron transfer at the surface of the Au nanoelectrodes. Similar characteristics were observed at BSA–NEEs (not shown).

The adsorption of the proteins was studied also by FTIR-ATR measurements performed on NEEs, before and after treatment with casein.

The gray-line spectrum in Fig. 4 shows the IR absorption features typical of bisphenol-A polycarbonate [41]. The spectra of the Cas–NEE (Fig. 4, black-line) and BSA–NEE (not shown) present additional absorption peaks which are indicative of the presence of a protein layer; they are: the broad absorption system in the 3100–3600 cm^{-1} range, due to N–H stretching with superimposed the absorption bands typical for residual water; the peaks at 1730 cm^{-1}, 1640 cm^{-1} and 1590 cm^{-1} which correspond to the amides I, II and III absorption peaks, respectively. Our results are comparable with those obtained by Kim et al. [41] for BSA adsorbed on virgin PC. The evidence that spectra recorded on NEEs and virgin PC displays the same features excludes any key-role for the adsorption of the protein related to the presence or absence of the gold nanoelectrodes.

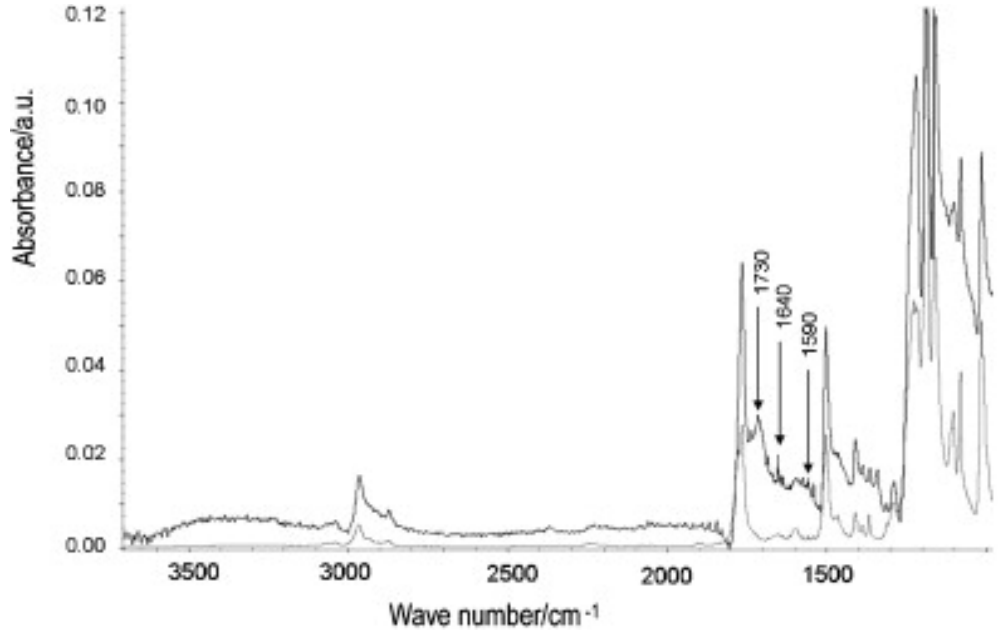

Figure 4. FTIR-ATR spectra of a bare NEE (gray-line) and a Cas-NEE (black-line).

The dotted line in Fig. 3 shows the CV recorded in FA^+ at a MES–Cas–NEE, that is a NEE in which the nanoelectrodes were coated with MES before being dipped in the casein solution. The comparison with the signal at the Cas–NEE with no previously adsorbed SAM, indicates that MES protects efficiently the nanoelectrodes from the adsorption of the protein, allowing one to

record perfectly reversible signals for FA^+ oxidation even after treating the NEE with the protein solution. Fully comparable results were obtained for BSA (not shown).

3.3. AFM characterization of NEEs

In order to investigate the morphology of the NEEs treated with MES and proteins, AFM characterizations were performed. The topography of a bare NEE prepared with track etched PC, with pores of 80 nm nominal diameter, is shown on the left side in Fig. 5a. The dark spots, of approximately 120 nm diameter, correspond to the nanoelectrodes, while the middle-toned flat surface corresponds to the surrounding PC. This image as well as the profile on the right (taken in correspondence of the white line on the topographic image), confirm that the majority of the pores are filled with nanowires. In particular, the profile shows that the heads of the wires are slightly recessed with respect to the outer surface of the membrane; for instance, the nanoelectrode in position around 0.10 μm is approximately 30–40 nm recessed, while the nanoelectrode in position 2.00 μm is approximately 20 nm recessed. Note that AFM profiles of virgin track-etched polycarbonate membranes (not shown) demonstrate that the cantilever penetrates into the empty pores up to a depth of 100 nm, which corresponds to the maximum depth accessible with the cantilever tips used here. Preliminary electrostatic force measurements (not shown) gave large electrical conductivity values only in correspondence of the position of the dark spots in Fig. 5a, so confirming that the pores are now filled with metal nanowires. The number of nanoelectrodes per unit area (surface density) was evaluated by counting the dark spots detected in a square 10 μm × 10 μm in the AFM and EFM topographic images; the measured surface density matches with the nominal pore density declared by the producer that is 6×10^8 pores (or nanoelectrodes) cm^{-2}. The average diameter of the nanoelectrodes, drawn from the AFM data, results slightly larger (approximately 120 nm) than the nominal diameter of the pores (80 nm). All these results agree with previous detailed studies performed by using a variety of electron microscopies [42,43] which demonstrated that, by performing gold deposition under the experimental conditions used here, the majority of the pores are indeed filled with gold and that the obtained nanoelectrodes have diameters slightly larger than the nominal values of the pores. The slight recession observed for the gold NEEs is probably due to the procedure used to clean the NEEs from the outer deposit of gold by peeling with scotch tape [1]. This agrees with previously reported evidences that the peeling of the NEE surface can break the very end of the gold nanowires; on one side Martin and co-workers showed this by careful FE-SEM analysis [44], on the other side, evidences of a slight recession were gained by the observation of some

peculiarities in the electrochemical behavior of NEEs in high viscosity ionic liquids [45], where NEEs operate under pure radial diffusion conditions. It must be emphasized that when NEEs operate in total overlap regime, this slight recession has no final effect on the voltammetric patterns [45].

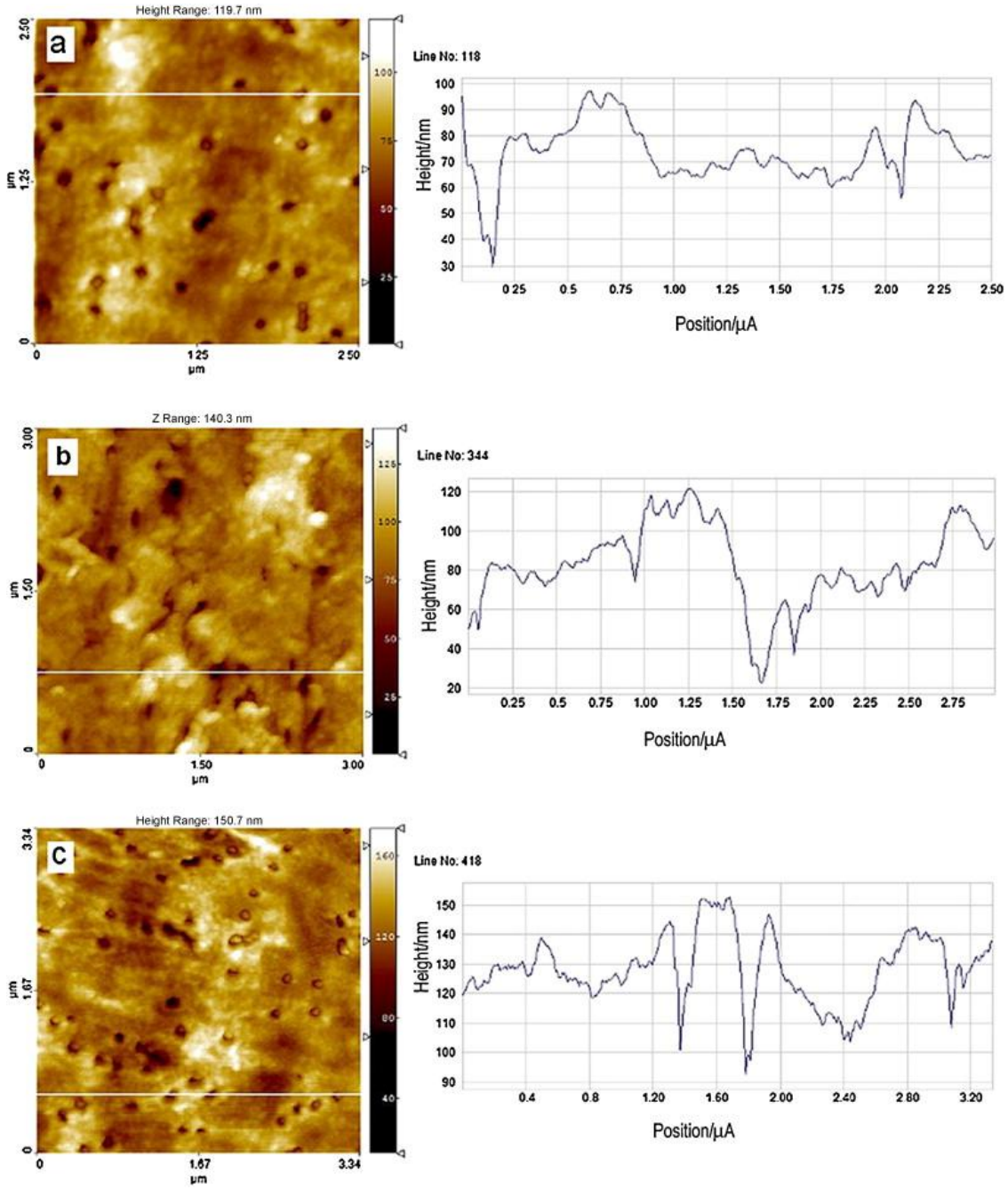

Figure 5. AFM of a bare NEE (a), of a BSA-NEE (b) and of a MES-BSA-NEE (c). On the left: the topography of the surface; on the right: profilometric sections obtained in correspondence of the white lines shown in the topographic images.

It should be noted that the same AFM measurements were performed on MES–NEEs, but data did not show relevant differences between not thiolated vs. thiolated electrodes (not shown), since the SAM is too thin (approximately, 5 Å thick [46]) to be detected.

To study the role of the adsorption of proteins and the efficiency of the protection by SAMs, a bare NEE and a MES–NEE were dipped for 30 min in a solution containing BSA. The obtained samples, named BSA–NEE and MES–BSA–NEE, respectively, were then analyzed by AFM and relevant results are shown in Fig. 5b and c, respectively.

The topography and profilometric pattern of the BSA–NEE (Fig. 5b) show that the protein molecules coat almost all the surface of the not thiolated NEE so causing an increase of the roughness of the outer surface. Only few nanoelectrodes (dark spots) can now be distinguished (such as those, for instance, at positions 0.00, 1.65 and 1.80 μm in the profile).

Fig. 5c shows that the situation changes dramatically for the MES–BSA–NEE. The topographic image demonstrates that, even after prolonged contact with the BSA solution, the thiolated nanoelectrodes remain free and their tips are clearly distinguishable from the surroundings. The roughness of the profile is still higher than in Fig. 5a (bare NEE), however, the height of the step which corresponds to the spatial transition between each nanoelectrode and the surrounding insulator, increases, being now approximately double than the height of the steps reported in Fig. 5a. In the profile on the right of Fig. 5c, the steps for the two nanoelectrodes in position 1.40 and 1.80 μm are now 50–60 nm high. All these evidences indicate that a protein layer is adsorbed on the MES–BSA–NEE, but it coats only the PC, while the thiolated nanoelectrodes are protein free. These observations fully match with the voltammetric evidences reported in the previous section.

4. Conclusions

The results here reported confirm the effectiveness of SAM of TA and MES to functionalize the gold surface of the very small nanoelectrodes that compose a NEE. This is useful, on one side, for protecting the Au nanoelectrode from undesired adsorption of proteins so avoiding interferences in the transduction of electrochemical signal. Note that, de-protection of the Au nanoelectrodes surface by electrochemical desorption of SAMs is, in principle, possible by performing the cathodic stripping of the SAM [47,48]. On the other hand, the present results open the way to the selective functionalization of NEEs, which can be performed by arranging different chemical functionalities on the gold of the nanoelectrodes vs. the organic surface of the polycarbonate. In the examples shown here, the final result of the modification of NEEs with MES and proteins can be imaged as a sort of protein cushion deposited on the PC with the SAM-coated gold nanoelectrodes remaining protein free. To the best of our knowledge, this is the first report showing the possibility to exploit NEEs for the controlled building of such a protein-thiols interconnected structure.

References

[1] V.P. Menon, C. Martin, *Anal. Chem.* **67** (1995), 1920.

[2] P. Ugo, L.M. Moretto, S. Bellomi, V.P. Menon, C.R. Martin, *Anal. Chem.* **68** (1996), 4160.

[3] L.M. Moretto, N. Pepe, P. Ugo, *Talanta* **62** (2004), 1055.

[4] F.C. Pereira, L.M. Moretto, M. De Leo, M.V. Boldrin Zanoni, P. Ugo, *Anal. Chim. Acta* **575** (2006), 16.

[5] R. Gasparac, B.J. Taft, M.A. Lapierre-Devlin, A.D. Lazareck, J.M. Xu, S.O. Kelley, *J. Am. Chem. Soc.* **126** (2004), 12270.

[6] K. Krishnamoorthy, C.G. Zoski, *Anal. Chem.* **77** (2005), 5068.

[7] M. De Leo, A. Kuhn, P. Ugo, *Electroanalysis* **19** (2007), 227.

[8] L.X. Cao, P.S. Yan, K. Sun, D.W. Kirk, *Electroanalysis* **21** (2009), 1183.

[9] C.G. Zoski, N. Yang, P. He, L. Bernardini, M. Koudelka-Hep, *Anal. Chem.* **79** (2007), 1474.

[10] L. Soleymani, Z. Fang, E.H. Sargent, S.O. Kelley, *Nat. Nanotechnol.* **4** (2009), 844.

[11] J.I. Yeh, H. Shi, *Nanomed. Nanobiotechnol.* **2** (2010), 176.

[12] P. Ugo, L.M. Moretto, B. Scrosati in *Encyclopedia of Electrochemical Power Sources*, edited by J. Garche, C. Dyer, P. Moseley, Z. Ogumi, D. Rand and B. Scrosati, Elsevier, Amsterdam **vol. 2** (2009), 92.

[13] P. Ugo, L.M. Moretto, in *Handbook of Electrochemistry* (1st edn.), edited by C.G. Zoski, Elsevier, Amsterdam (2007) (Chapter 16.2).

[14] S. Pozzi Mucelli, M. Zamuner, M. Tormen, G. Stanta, P. Ugo, *Biosens. Bioelectron.* **23** (2008), 1900.

[15] M. Zamuner, S. Pozzi Mucelli, M. Tormen, G. Stanta, P. Ugo, *Eur. J. Nanomed.* **1** (2008), 33.

[16] H. Wiig, C.C. Gyenge, O. Tenstad, *J. Physiol.* **567** (2005), 557.

[17] S. Yu, S.B. Lee, M. Kang, C.R. Martin, *Nano Lett.* **1** (2001), 495.

[18] S. Yu, S.B. Lee, C.R. Martin, *Anal. Chem.* **75** (2003), 1239.

[19] C.C.A. Ng, S. Ciampi, J.B. Harper, J.J. Gooding, *Surf. Sci.* **604** (2010), 1388.

[20] Q. Cheng, A. Brajter-Toth, *Anal. Chem.* **64** (1992), 1998.

[21] Q. Cheng, A. Brajter-Toth, *Anal. Chem.* **67** (1995), 2767.

[22] Q. Cheng, A. Brajter-Toth, *Anal. Chem.* **68** (1996), 4180.

[23] J. Zhao, L. Luo, X. Yang, E. Wang, S. Dong, *Electroanalysis* **11** (1999), 1108.

[24] M. Windholz, S. Budavari, R.F. Blumetti, E.S. Otterbein, *The Merck Index. An Encyclopedia of Chemicals, Drugs, and Biologicals (10th edn.)*, Merck & Co., Inc., Rahway, NJ (1983).

[25] J. Johansson, H.K. Yasuda, R.K. Bajpai, *Appl. Biochem. Biotechnol.* **70–72** (1998), 747.

[26] M. Henry, C. Dupont-Gillian, P. Bertrand, *Langmuir* **19** (2003), 6271.

[27] E. Chow, D. Ebrahimi, J.J. Gooding, D.B. Hibbert, *Analyst* **131** (2006), 1051.

[28] I.F. Cheng, C.R. Martin, *Anal. Chem.* **60** (1988), 2163.

[29] R.A. Benkeser, D. Goggin, G. Schroll, *J. Am. Chem. Soc.* **76** (1954), 4025.

[30] B. Brunetti, P. Ugo, L.M. Moretto, C.R. Martin, *J. Electroanal. Chem.* **491** (2000), 166.

[31] C. Amatore, J.-M. Saveant, D. Tessier, *J. Electroanal. Chem.* **147** (1983), 39.

[32] C. Amatore, A.I. Oleinick, I. Svir, *Anal. Chem.* **81** (2009), 4397.

[33] T.J. Davies, R.G. Compton, *J. Electroanal. Chem.* **585** (2005), 63.

[34] N. Godino, X. Borrise, F.X. Munoz, F.J. del Campo, R.G. Compton, *J. Phys. Chem. C* **113** (2009), 11119.

[35] J. Guo, E. Lindner, *Anal. Chem.* **81** (2009), 130.

[36] M. Henry, P. Bertrand, *Surf. Interface Anal.* **41** (2009), 105.

[37] S. Robinson, P.A. Williams, *Langmuir* **18** (2002), 8743.

[38] M.C. Gay, *Annales du Lab. de Recerche des Musées de France* (1970) 8.

[39] E. Martin, *Studies in Conservation* **vol. 22** (1977) 63.

[40] A.J. Bard, L.R. Faulkner, *Electrochemical Methods. Fundamentals and Applications* (2nd edn.), John Wiley & Sons, Inc., New York (2001).

[41] K.J. Kim, A.G. Fane, M. Nystrom, A. Pihlajamaki, *J. Membr. Sci.* **134** (1997), 199.

[42] P. Ugo, N. Pepe, L.M. Moretto, M. Battagliarin, *J. Electroanal. Chem.* **560** (2003), 51.

[43] M. De Leo, F.C. Pereira, L.M. Moretto, P. Scopece, S. Polizzi, P. Ugo, *Chem. Mater.* **19** (2007), 5955.

[44] S. Yu, N. Li, J. Wharton, C.R. Martin, *Nano Lett.* **3** (2003), 815.

[45] M. De Leo, L.M. Moretto, O. Buriez, P. Ugo, *Electroanalysis* **21** (2009), 392.

[46] A. Dalmia, C.C. Liu, R.F. Savinell, *J. Electroanal. Chem.* **430** (1997), 205.

[47] Y. Dong, S. Abaci,C. Shannon, *Langmuir* **19** (2003), 8922.

[48] J.J. Calvente, Z. Kovacova, M.D. Sanchez, R. Andreu, W.R. Fawcett, *Langmuir* **12** (1996), 5696.

Electrochemical DNA Biosensors Based on Ensembles of Polycarbonate Embedded Nanoelectrodes

1. Introduction

The development of electrochemical sensors for DNA detection is widely documented in the recent literature [1-3]. Such sensors are based on the immobilization of an oligonucleotide probe, containing the nucleotide sequence of interest, onto the surface of the transducer. In this way, in the presence of the complementary sequence in the sample, the hybridization process takes place directly on the electrode surface easing the subsequent detection.

Different approaches have been employed to detect electrochemically the hybridization event, many of them requiring the use of electrochemical labels such as redox or enzyme labels [4-6] or intercalation redox probes [7,8] and some of them enabling the label-free detection [9]. Recently, the DNA hybridization event was detected by binding the capture DNA onto the surface of the complex 3D-structures, such as carbon nanotubes [10,11] or metal nanowires [12]. In the latter work, arrayed gold nanowires were obtained by partial etching with oxygen plasma of the polycarbonate surface of membrane templated nanoelectrode ensembles (NEEs) [13]. This treatment led to an increase of the electrode active area by exposing the wires of approximately 150-250 nm length for further immobilization of the biorecognition layer.

However, it was successively demonstrated [14] that the increase in the active area obtained by physical or chemical etching usually leads to a significant decrease in signal to background current ratio [14], losing one of the advantages of NEEs.

In order to keep the geometric features intact and keep the signal to noise ratio at the maximum, therefore increasing the sensitivity of the method, we have developed an alternative approach of NEE use for DNA biosensor design. In here described approach, the polycarbonate (PC) membrane surrounding the nanoelectrodes is used for the direct immobilization of the biomolecules, which then in turn act as molecular recognition layer, leaving the role of producing the electrochemical signal to a redox mediator dissolved in the electrolyte and which shuttles electrons from the nanoelectrodes to an enzyme label bound via DNA to the PC surface. Polycarbonate is one of the most used polymeric platforms for the fabrication of bioanalytical microarrays for protein or DNA detection [15-19] and it is commonly employed as insulator in the preparation of ensembles and arrays of nanoelectrodes [13,20-22].

The exploitation of the polymeric surface of NEEs for the immobilization of biological macromolecules was successfully tested for the fabrication of electrochemical immunosensors able to detect the receptor protein HER2 [23]. To achieve that, the capture antibody Herceptin™ was immobilized by direct adsorption onto the PC surface, which surrounds the nanoelectrodes, without any pre-treatment leaving the electrodes free for the electron transfer. The biosensing capabilities of such NEEs were tested in tumor lysates allowing the detection of HER2 down to 100 pg/μL.

Preliminary attempts performed by us, aimed at immobilizing also $_{ss}$DNA probes by the same procedure used for Herceptin™ were unsuccessful. However, they pushed us into the present study, aimed at developing immobilization procedures more specifically devoted at binding DNA probes onto the PC of NEEs.

To this goal we explore for the first time the utilization of the PC surface of NEEs for immobilization of the capture oligonucleotide probes, which in turn, minimizes the fouling of the gold nanoelectrode surface. In particular, we focus on optimizing the conditions for reacting the oligonucleotide probe with the -COOH groups present on the PC surface. In addition, the hybridization of the complementary DNA strand containing glucose oxidase is achieved and the activity of the biosensor demonstrated.

Finally, a procedure able to increase the amount of carboxylic functionalities on the PC surface is described and the effect of this treatment on the following functionalization with DNA probes is discussed.

2. Experimental

2.1. Apparatus

All electrochemical measurements were carried out at room temperature with a PalmSens potentiostat controlled via personal computer by its own software, using a three-electrode single-compartment cell equipped with a platinum counter electrode and an Ag/AgCl (KCl saturated) reference electrode, to which all reported potential values are referred.

Fluorescence measurements were carried out with a Varian, Cary Eclipse Fluorescence Spectrophotometer.

NAP™-5 and NAP™-10 columns prepacked with Sephadex™ G-25 DNA Grade were from GE Healthcare. Ultrafiltration devices (Vivaspin6 30000 MWCO) were purchased from VWR.

The purification of the DNA-enzyme conjugate was carried out by Fast Protein Liquid Chromatography (FPLC) (GE Healthcare, Äkta Explorer) using a MonoQ 5/50 GL column.

2.2. Chemicals

Potassium permanganate ($KMnO_4$) was purchased from Carlo Erba. Thionin acetate (THA), *N*-ethyl-*N*′-(3-dimethylaminopropyl) carbodiimide hydrochloride (EDC), *N*-hydroxysulfosuccinimide sodium salt (sulfo-NHS), ethanolamine and glucose oxidase (GOx) from *Aspergillus niger* were from Sigma-Aldrich. The salt (ferrocenylmethyl) trimethylammonium hexafluorophosphate ($FA^+PF_6^-$) was prepared by metathesis of the (ferrocenylmethyl) trimethylammonium iodide (Alfa Aesar) with potassium hexafluorophosphate 99% (Alfa Aesar). Amino-end DNA (acD1 and acD2) and thiolated DNA (SHD1) were purchased from Sigma Aldrich and had the following sequences:

acD1: [AmC6T]CTTATCGCTTTATGACCGGACC

acD2: [Am5T]TTGTTATACGCC

SHD1: [ThiolC6]GGTCCGGTCATAAAGCGATAAG

Stock solutions of oligonucleotides (100 μM) were prepared in TE buffer (50 mM Tris, 100 mM NaCl, 1 mM EDTA in pH 7.4) and kept frozen until use.

Dithiothreitol (DTT) was from AppliChem. N-2-Hydroxyethyl piperazine-N'-2-ethane sulphonic acid (HEPES) ≥99.5 %, p.a. was purchased from Carl ROTH. The cross-linker sulfosuccinimidyl 4-[N-maleimidomethyl]-cyclohexane-1-carboxylate was purchased from Sigma Aldrich.

Purified water was obtained using Milli-Ro plus Milli-Q (Millipore) water purification system. All other chemicals were reagent grade.

Track-etch polycarbonate (PC) membrane filters were obtained from SPI-pore™ with nominal pore diameter of 30 nm, average pore density of 6×10^8 pores cm^{-2} and coated with polyvinylpyrrolidone (PVP) by the producer.

2.3. Synthesis of $_{ss}$DNA conjugated with GOx (D1-GOx)

Glucose oxidase-DNA conjugates were prepared using sulfoSMCC methodology as previously described [24]. Briefly, 100 μL of a 100 μM SHD1 solution was incubated with DTT (60 μL of a 1 M DTT) overnight at 37° C to allow for the reduction of disulfide bonds. Before coupling, reduced SHD1 was purified by use of NAP5 and NAP10 size exclusion column. GOx was firstly

desalted through a short size exclusion column (NAP5) and then 400 μL of the final solution (60 μM ca.) were added to 100 μL of 2 mg sSMCC in dimethylformamide. The activation reaction was allowed to proceed for 1 h in dark at RT and during this step, sSMCC is coupled to the GOx surface through reaction with lysine amino groups. After the reaction completion, activated GOx was purified by NAP5 and NAP10 column using 0.01 M PBS pH 7.4 as elution buffer. The buffer solutions of SHD1 and activated GOx were immediately combined and incubated in the dark for 3 h at RT. After incubation, the buffer was exchanged to 20 mM Tris pH 8.2 using an ultrafiltration device (Vivaspin6 30000 MWCO) and D1-GOx purified using FPLC (fast protein liquid chromatography) system with an ion exchange column. The fractions containing the conjugate were collected, concentrated and redissolved in 0.01 M PBS, pH 7.4.

2.4. Fabrication, activation and functionalization of NEEs

2.4.1. Template fabrication of NEEs

NEEs were prepared by template gold electroless deposition using previously described procedure [14] and assembled as previously reported [25]. Both procedures are described on chapter 3 (paragraph 2.3).
Also in this case, the whole surface of the device was insulated with Monokote (Topflite), apart a hole (diameter 3 mm) which defines the geometric area of the ensemble (A_{geom}= 0.07 cm^2).

2.4.2. Characterization and activation of PC membrane of NEEs

The amount of -COOH groups present on the PC membrane of NEEs was measured by reacting the membrane with thionin acetate (THA) [26] as follows: a NEE was immersed into 800 μL of a THA solution in ethanol (concentration 0.1 mg mL^{-1}) and shaken overnight at room temperature in dark. The electrode was then removed, washed three times with ethanol and transferred into 800 μL of a 0.01 N HCl solution in a mixture ethanol/water 1:1. After shaking for 1.5 h, the NEE was removed and a fluorescence spectrum of the final acidic solution was recorded.
In order to study the possibility to increase the number of –COOH groups present on the polymeric surface, a chemical activation was done following the procedure used by Papra et al. [27], with some modifications. NEEs were immersed into a 0.32 M $KMnO_4$ solution in 0.75 N

H_2SO_4 at RT for different times (90 and 150 min), without shaking. Before the treatment, the insulating tape which surrounds the geometric area of each NEE was covered by an adhesive tape (which was removed after the treatment) in order to prevent its oxidation. Subsequently, the electrodes were rinsed with water and 3 M HCl to remove any oxidation residues from the polymeric surface. Finally, the NEEs were rinsed with water, ethanol and allowed to dry in air.
A further spectrochemical and electrochemical characterization of the activated NEEs was performed and the results were compared with those obtained with non-activated NEEs.

2.4.3. Functionalization of NEEs

Before proceeding with the immobilization of the oligonucleotide probes, the carboxylic groups were activated by immersion of NEEs into a 0.1 M HEPES buffer solution (pH 7.5) containing 0.5 mM EDC and 0.8 mM sulfo-NHS. The incubation was allowed to proceed for 20 min under shaking (at RT). The addition of the succinimide derivative stabilizes the intermediate ester obtained by reaction between EDC and carboxylate groups [28], thus increasing the efficiency of the coupling reaction with the amino-$_{ss}$DNA (acD1).
The functionalization was done transferring the electrodes into a 0.1 M HEPES buffer solution (pH 7.5) containing 400 pmol of acD1 strands and incubated for 2 h under shaking, at 37° C. The NEEs were finally rinsed with buffer.
In order to prevent any non-specific adsorption of the target $_{ss}$D1 conjugated with GOx (D1-GOx) on the activated polymeric surface, a blocking treatment was performed. The NEEs were immersed into a 20 mM ethanolamine in 0.01 M PBS solution (pH 7.4). The reaction was allowed to proceed for 30 min at RT, under shaking. Ethanolamine is used to deactivate the remaining NHS-activated carboxylic groups [29] onto the polymeric membrane. The advantage of ethanolamine is that it is a small molecule and unlike BSA, casein or other protein blocking systems, it does not interfere with biological macromolecules present on the surface of the NEE. In example, Liberelle et al. have shown that the blocking procedure with this molecule did not induce any significant change in the thickness of the surface protein layer [30].
The hybridization reaction was carried out by spotting 10.5 µL of a 0.01 M PBS solution (pH 7.4) containing 20 pmol D1-GOx onto the capture DNA containing surface for 2 h at RT. Resulting DNA-modified NEEs were rinsed five times in 0.01 M PBS over 10 minutes.

3. Results and Discussion

3.1. Characterization and functionalization of NEEs

At first, the PC surface of a NEE was characterized by spectrochemical titration with thionin acetate (see experimental) in order to estimate the amount of the surface carboxylic groups available for the probe immobilization. The thionin procedure has previously been used for the quantitative determination of carboxylic groups on activated polymers [31-33] and involves the formation of ion pairs between the cationic dye and carboxylate moieties. A calibration curve was first obtained and subsequently employed for the quantification of the carboxylic groups. The obtained concentration of -COOH groups determined on the polymeric surface of the NEE was about 9.7×10^{-10} mol/cm^2.

These functional groups present on the surface of the template material as terminal groups of the polymeric chains were then exploited for the immobilization of the single-stranded DNA (acD1) strands using EDC/NHS strategy [28] (Scheme 1a).

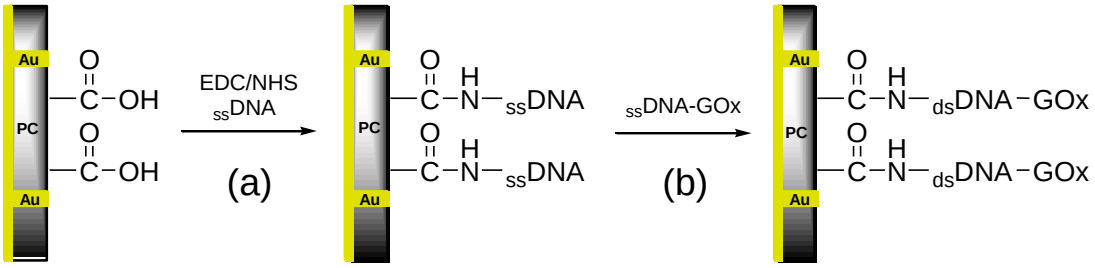

Scheme 1. Design of DNA hybridization sensor based on NEE assembly: a) activation of -COOH groups of the PC surface and immobilization of the capture complementary $_{ss}$DNA onto the activated carboxylic functionalities and b) hybridization of DNA-GOx conjugate onto modified PC surface.

To enable the detection of the DNA hybridization event, thiolated complementary DNA (SHD1) was modified with glucose oxidase (GOx) using sulfoSMCC methodology [24] (Scheme 2),

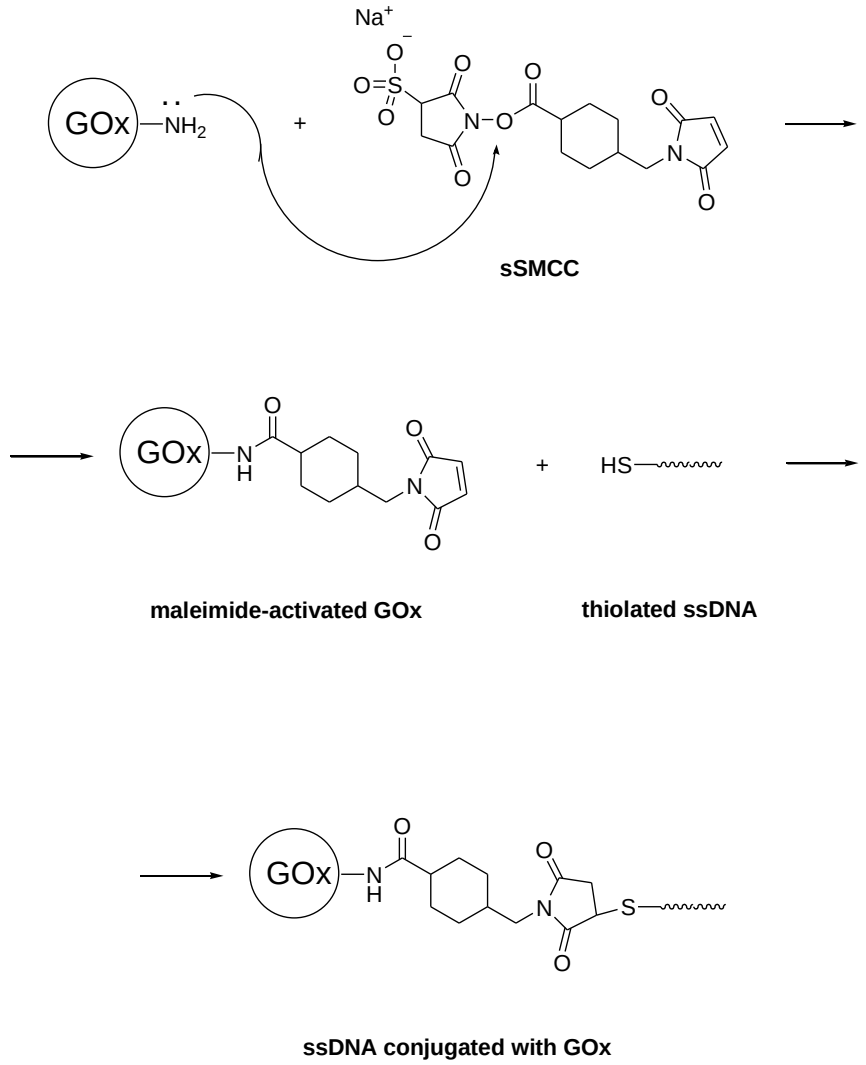

Scheme 2. Modification of $_{ss}$DNA with glucose oxidase using sSMCC methodology [24].

and subsequently hybridized to the capture acD1 immobilized on the PC (Scheme 1b). Glucose oxidase was chosen as the enzymatic label as it is readily available, the modification with single-stranded DNA is simple and it enables the amplification of the signal of redox probes [34] through the mechanism represented on Scheme 3.

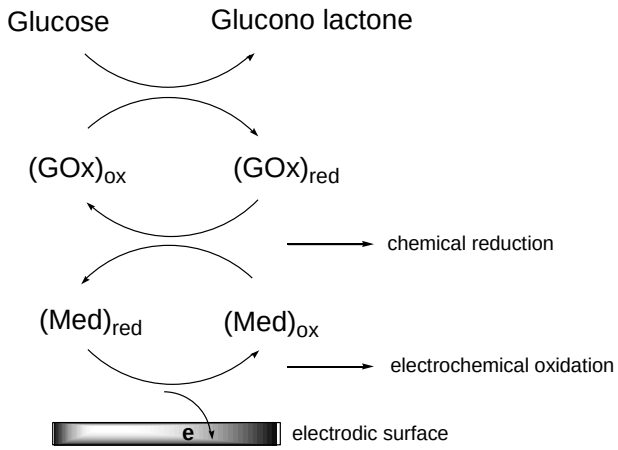

Scheme 3. Mechanism of mediated electron transfer to detect GOx enzymatic activity.

Electrochemical characterization of functionalized NEEs was performed in a deoxygenated 10 mM PBS solution (pH= 7.4) containing 0.1 mM FA^+ as redox mediator. It is worth noting that nitrogen was purged into the solution in order to prevent the inhibition of GOx enzymatic activity by H_2O_2 which is produced by reaction between the enzyme and the substrate in presence of oxygen acting as electron acceptor [35].

The voltammogram reported in Figure 1 (full line), shows the CV behavior of FA^+ recorded with the NEE functionalized with double-stranded DNA-GOx. The voltammetric pattern is fully reversible and diffusion controlled (ΔE_p= 0.067 V, $E_{1/2}$= (E_{pa} + E_{pc})/2= 0.42 V, I_{pc}/I_{pa}= 1). I_p scales linearly with v½ (data not shown), indicating that the functionalization of the NEE with the DNA probe does not interfere with the total overlap diffusive regime [13] which characterizes the FA^+ voltammetric behavior at non-functionalized NEEs [36]. Note that the same CV pattern is recorded also with a bare NEE (Fig. 1, dotted line).

In the presence of 50 mM glucose (dashed line, Figure 1), the voltammetric pattern changes dramatically: the oxidation peak increases partially tending to a sigmoidal shape while the reduction peak disappears. The shape of the voltammogram is typical for an electrocatalytic process: in the presence of both enzyme label and the enzymatic substrate, the mediator is reduced chemically at the electrode/solution interface to be oxidized again directly at the electrodic surface (see Scheme 3). Therefore, the above described voltammetric evidences indicate that the functionalization with the capture probe and the subsequent hybridization with the GOx labeled target on the NEE were successful. Moreover, the GOx acts as a sensitive and efficient label, suitable to detect the hybridization event.

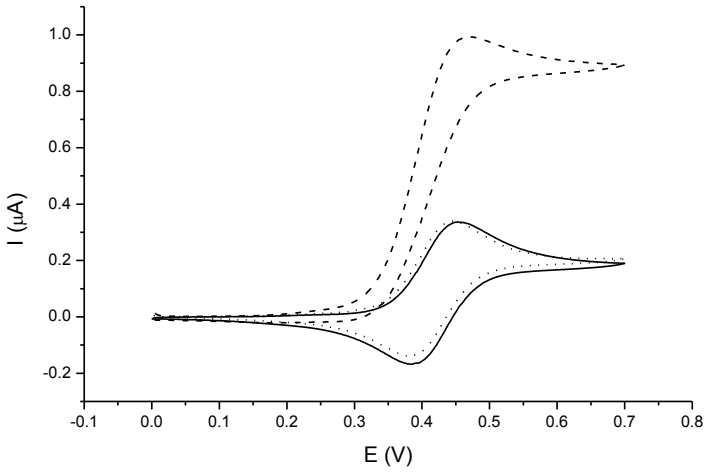

Figure 1. Cyclic voltammograms recorded with a functionalized NEE in a 10 mM PBS solution (pH= 7.4) containing 0.1 mM FA^+ PF_6^-, before (full line) and after (dashed line) the addition of 50 mM glucose and, for comparison, with a bare NEE in absence of substrate (dotted line). Scan rate 5 mVs^{-1}.

The anodic current value measured with the DNA functionalized NEE in the presence of the glucose substrate (0.96 μA) is higher than the current values recorded with non-functionalized NEEs both when mediator, substrate and 20 pmol enzyme (Figure 2a, 0.42 μA) or mediator, substrate and 20 pmol D1-GOx (Figure 2b, 0.55 μA) are all present in the solution.

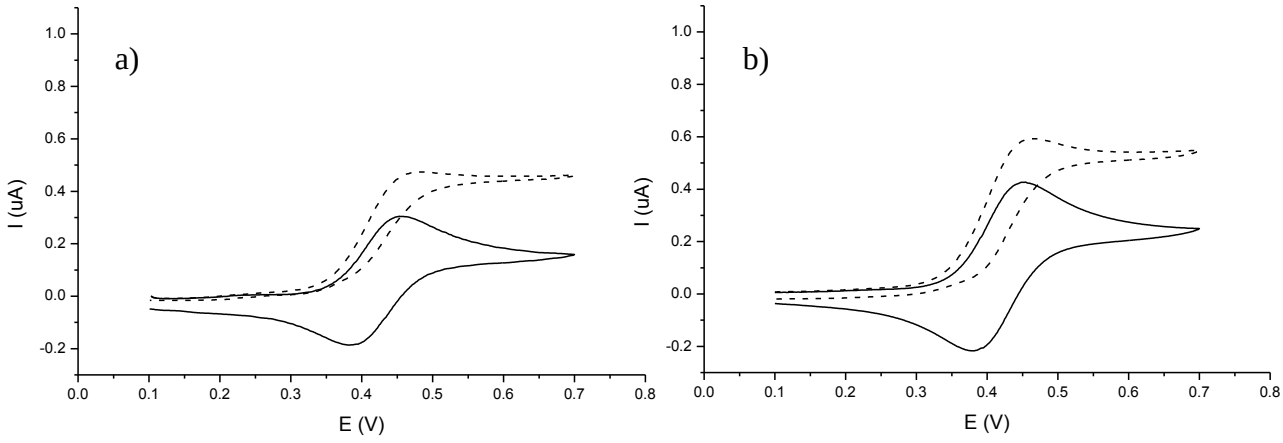

Figure 2. Cyclic voltammograms recorded with a bare NEE in a deoxygenated 10 mM PBS solution (pH= 7.4) containing 0.1 mM FA^+ PF_6^- and 50 mM glucose before (full line) and after (dashed line) the addition of 20 pmol GOx (a) and 20 pmol D1-GOx (b). Scan rate 5 mVs^{-1}.

In order to achieve a comparable catalytic current value as in Fig. 1, the GOx concentration in solution, in experiments like those in Fig. 2a, must be increased up to between 80-200 pmol (Figure 3). These results confirm the operability of a capture/preconcentration effect of D1-GOx by the acD1 functionalized NEE.

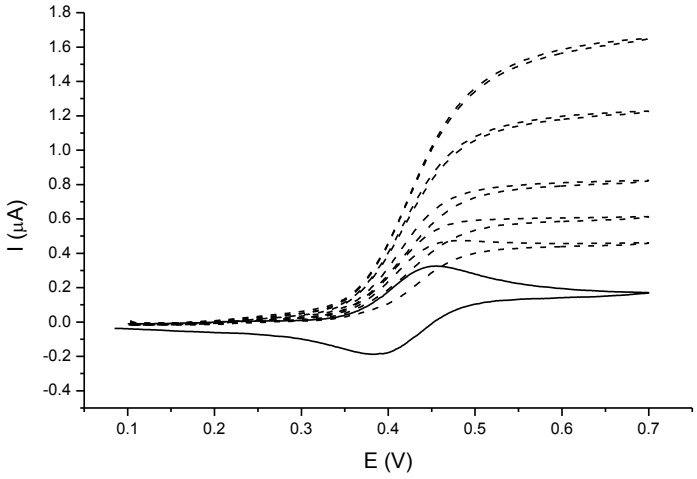

Figure 3. Cyclic voltammograms recorded with a bare NEE in a deoxygenated 10 mM PBS solution (pH= 7.4) containing 0.1 mM FA^+ PF_6^- and 50 mM glucose (full line). The dashed lines are recorded after consecutive additions of GOx (20/40/80/200/400 pmol). Scan rate 5 mVs^{-1}.

To prove that the active GOx is introduced via the hybridization of the D1-GOx target with the capture acD1 immobilized on the NEE surface and not via the non-specific interactions, two different control experiments were performed.

Figure 4 shows the voltammograms recorded with a bare NEE (i.e. non-functionalized with the capture probes, acD1) (a) and with a NEE functionalized with not complementary capture strand, acD2 (b), both treated also with after the addition of D1-GOx solution.

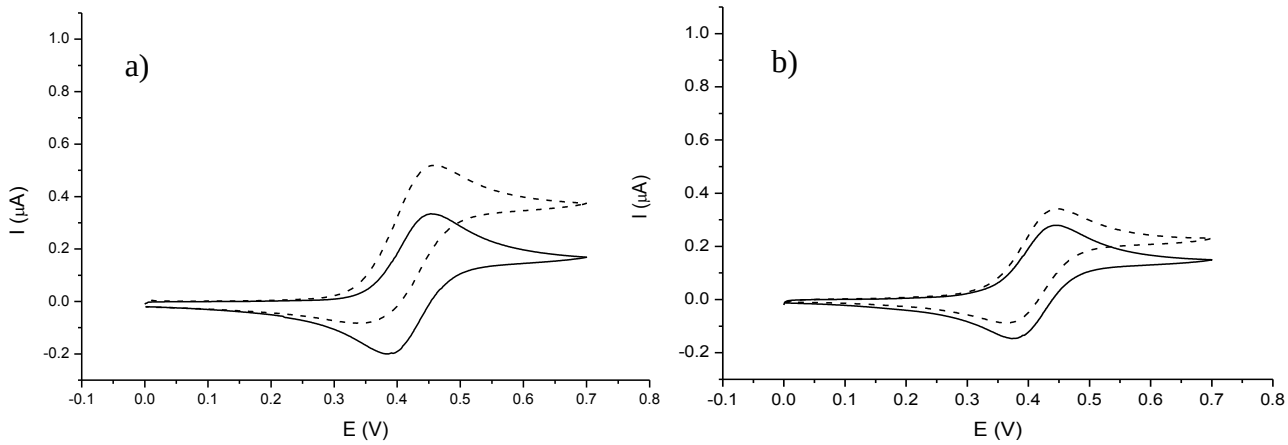

Figure 4. Cyclic voltammograms recorded with a bare NEE (a) and a NEE modified with not complementary strand acD2 (b), after treatment with D1-GOx solution. Measurements were performed in a 10 mM PBS solution (pH= 7.4) containing 0.1 mM $FA^+PF_6^-$ before (full line) and after (dashed line) the addition of 50 mM glucose. Scan rate 5 mVs^{-1}.

The comparison of the signals recorded before (full lines) and after (dashed lines) the addition of glucose, shows a small catalytic effect, which indicates that there is some amount of non-specific adsorption of the D1-GOx. This could indicate that there is some interaction of the enzyme with the polymeric surface. In fact, it was previously reported that the roughness of the membrane surface or the presence of other functional groups, namely carbonyl groups, could promote a small adsorption of the protein, in this case GOx, onto the polycarbonate [15].

3.2. Characterization and functionalization of chemically activated NEEs

In order to test the possibility of increasing the surface concentration of –COOH groups on the PC surface and, consequently, the amount of probe which can be bound on the NEE, the polymeric surface of NEEs was chemically oxidized by treatment with $KMNO_4$. The number of generated carboxylic groups was then determined by fluorescence labeling (see experimental). The fluorescence intensities of the acidic solutions containing THA and the relative calculated amounts of -COOH per cm^2, obtained after 90 and 150 minutes of oxidative treatment of the NEEs with $KMnO_4$, are listed in Table 1 and compared with those measured for the non-activated NEE.

Treatment	Intensity	Concentration of THA in solution (nM)	Concentration of COOH groups (mol/cm^2)
Untreated NEE	7.7	85	~ 9.7×10^{-10}
90 min	21.1	232	~ 2.7×10^{-9}
150 min	26.9	294	~ 3.4×10^{-9}

Table 1. Concentration of –COOH groups obtained with and without activation of PC surface and quantification using THA dye. Fluorescence excitation 594 nm, emission 620 nm.

These data show a significant increase in surface -COOH concentration upon $KMnO_4$ activation; for instance, a 150 min treatment causes a three-fold increase in the surface concentration of carboxylic groups.

These activated electrodes were functionalized with the acD1 probe and hybridized with the D1-GOx target using the same procedure described above for the non-activated NEE.

Figure 5a shows the voltammetric responses recorded in FA^+ solution at such DNA-GOx modified NEE, activated for 90 min., before and after the addition to the electrolyte solution of excess glucose (full and dashed lines, respectively). The voltammetric signal of the mediator recorded before adding glucose differs from the one reported in Figure 1, mainly for the larger capacitive current detected between approximately 0.0 and 0.2 V, i.e. before uprising of the Faradaic signal (CV peaks).

After adding excess glucose, the Faradaic anodic current increases up to reading 1.24 µA and the peak tends to become sigmoidally shaped, while the associated cathodic peak (return scan) disappears. All these features compare with those observed for the DNA-GOx non-activated NEE apart, again, a significant increase in the double-layer (background) charging current. Note that the ΔI value (difference in anodic current with and without glucose) is now slightly higher at the activated NEE, being 0.8 µA in Fig. 5a vs. 0.64 µA in Fig. 1.

Figure 5b reports the result obtained at an activated NEE, but not functionalized with the acD1 probe, i.e. treated only with the D1-GOx target. Again, the results compare with those obtained in the same experimental conditions at the non-activated NEE (see Fig. 4a), apart a higher background current in the CVs of Fig. 5b.

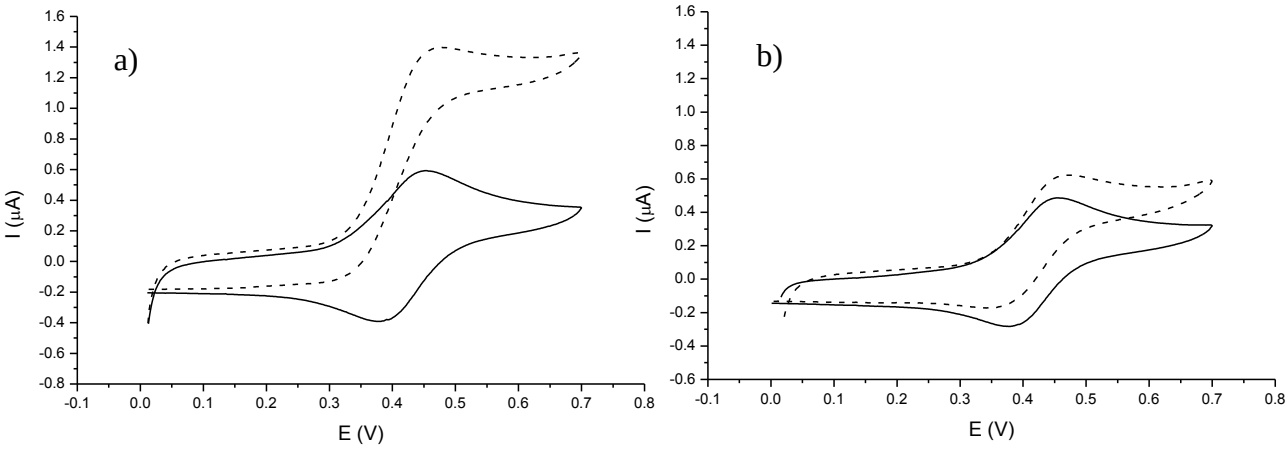

Figure 5. Cyclic voltammograms recorded with an activated NEE functionalized with acD1 (a) and an activated NEE non-functionalized with acD1 (b), both submitted to spotting with D1-GOx solution. Measurements were performed in a 10 mM PBS solution (pH= 7.4) containing 0.1 mM $FA^+PF_6^-$ before (full line) and after (dashed line) the addition of 50 mM glucose. Scan rate 5 mVs^{-1}.

All these evidences indicate that, at the activated NEE:

- both the functionalization with the probe and the hybridization with the GOx labeled target are successfully performed;
- the amount of DNA captured by the activated electrode is slightly higher than without activation, with a ~20% Faradaic current increase with respect to the non-activated NEE;
- non-specific adsorption of the target is limited to quite low value;
- however, the activation of the NEE with $KMnO_4$ causes an undesired increase in the background current.

In order to investigate the latter point, i.e. the double-layer charging current increase, a series of background CV were recorded at bare NEEs in pure supporting electrolyte (0.01 M KNO_3), before and after the chemical activation; relevant results are reported in Fig. 6.

The dashed curve in Fig. 6a and the full line in Fig. 6b show the voltammograms recorded with a NEE after 90 and 150 min activation, respectively. It is evident that the double layer charging current, which can be measured as the half difference between the forward to backward currents [37], increases in comparison with the untreated NEE (full line, Fig. 6a).

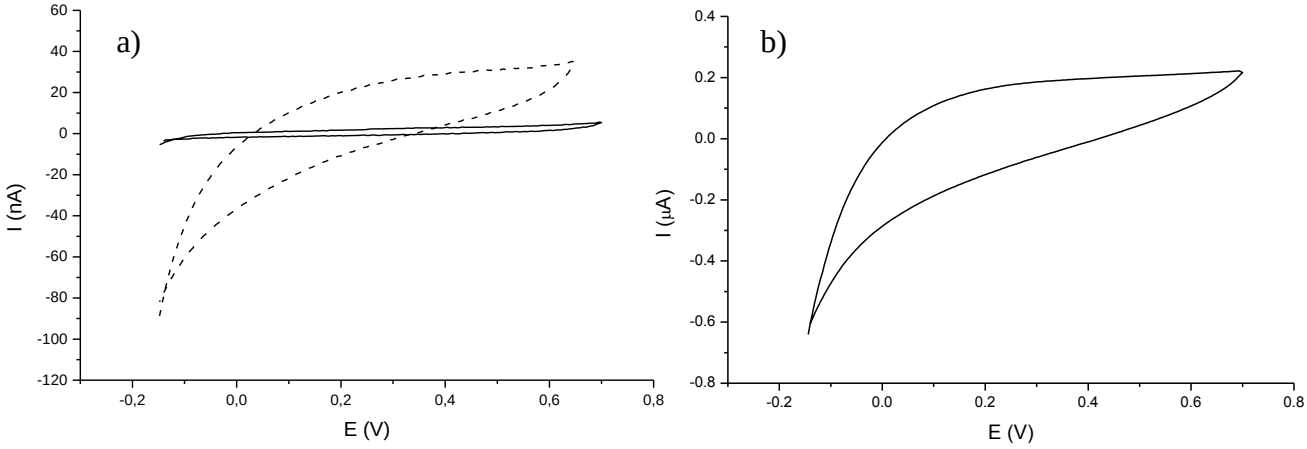

Figure 6. a) CVs recorded in 0.01 M KNO_3 at a non-activated NEE (full line) and a NEE activated for 90 minutes (dashed line); b) CV recorded in 0.01 M KNO_3 at a NEE chemically activated for 150 min. Scan rate 20 mVs^{-1}. Note the different scale of y-axis.

Since the capacitive current at a NEE is proportional only to the active area [25], according to the following equation,

$$I_{cap} = vC_{dl}A_{act} \qquad (1)$$

where C_{dl} is the double-layer capacitance of gold in 50 mM $NaNO_3$ [13], this increase could be due either to the partial etching of the outer layer of the polymer and/or the loss in sealing between the Au nanofibers and the surrounding membrane. In fact, both these conditions cause a partial exposure of the fibers, increasing the area of the metal surface in contact with the solution [14]. If the activation time is extended to 150 minutes, the capacitive current increases dramatically, as shown in Figure 6b (see current scale)

Table 2 lists the capacitive current values obtained from the voltammograms in Fig. 6, measured at 0.2 V, as well as relevant active area values calculated by eq. 1, using a C_{dl} value of 21 µF cm^{-2} [13].

Samples	I_{cap} (μA)	A_{act} (cm^2)
Non-activated NEE	1.3×10^{-3}	3.2×10^{-3}
NEE activated for 90 min	1.6×10^{-2}	3.7×10^{-2}
NEE activated for 150 min	1.4×10^{-1}	0.3

Table 2. Double layer charging current values and active areas calculated from the cyclic voltammograms in Figures 6 a and b.

These data indicate a significant increase in active area with increasing activation time, with a roughly, one order of magnitude increase when passing from 0 to 90 min to 150 min activation time. The background current can decrease dramatically if the NEE is subjected to a heat-treatment at ~155° C for 15 minutes after the activation step. The heating step carried out at a temperature higher than the glass transition temperature of PC, improves the sealing between the nanowires and the template, favoring the decrease of the exposed active area. This treatment, however, contributes to the decrease of the -COOH concentration on the polymeric surface down to less than 4×10^{-10} mol/cm^2. This phenomenon could be explained by surface reorganization of the 3-D polymer structure induced by the heat.

In order to compare the analytical performances of non-activated and $KMnO_4$ activated NEEs for the application of interest here, that is DNA hybridization detection, peak currents and electrocatalytic peak current increments at all the NEEs described above are reported in Table 3, and were also compared in terms of current densities (J and ΔJ); these values were calculated by voltammetric peak currents divided by the active area values (see Table 2).

NEE	Functionalization steps	I_p (μA)	ΔI_p (μA)	J (A/cm^2)	ΔJ (A/cm^2)
No chemical activation	cD1 + D1-GOx	0.96	0.64	3×10^{-4}	2×10^{-4}
	D1-GOx (no acD1)	0.51	0.18	1.6×10^{-4}	6×10^{-5}
	cD2 + D1-GOx	0.33	0.06	1×10^{-4}	2×10^{-5}
Chemical activation	cD1 + D1-GOx	1.24	0.80	3×10^{-5}	1.8×10^{-5}
	D1-GOx (no acD1)	0.49	0.12	1×10^{-5}	3×10^{-6}

Table 3. Current intensities and densities relative to dashed lines in Figures 1, 4 and 5.

It is evident that the current density in the case of the non activated NEEs is one order of magnitude higher than for the activated NEEs, due to the change of the active surface area which is almost ten times smaller (Table 2).

4. Conclusions

We have, for the first time, shown that the polymer surface of nanoelectrode ensembles can be bio-functionalized with DNA, by utilizing the amide coupling strategy to immobilize the capture, single-stranded DNA onto the PC, instead onto the gold electrode surface [38]. Subsequent to the immobilization, complementary strand containing a reporter enzyme GOx was successfully hybridized and the hybridization process electrochemically detected with the help of a redox mediator which aids the electron exchange between the active site of the enzyme and unmodified gold nanoelectrodes.

Furthermore, the activation of the polymer surface by permanganate treatment was preformed and the comparison between non activated and activated NEEs showed that there are more active -COOH groups present on the surface upon the activation. At the same time, the activation of the surface was shown to cause an increase in the capacitive current. However, we have shown that this is not a limiting factor in design of DNA biosensing platform since the non activated NEE contain enough active -COOH groups to enable the immobilization of tens of pmol of DNA. When larger amounts of biomolecules need to be captured, the activation of PC can be additionally optimized to allow the design of more sensitive sensors.

In this proof of concept study, $_{ss}$DNA was captured and complementary strand hybridized and the hybridization even detected electrochemically. Our future work is focus in applying described methodology for design of the electrochemical DNA biosensor with improved sensitivity.

References

[1] K. Kerman, M. Kobayashi, E. Tamiya, *Meas. Sci. Technol*. **15** (2004), R1.

[2] F. Lucarelli, G. Marrazza, A.P. Turner, M. Mascini, *Biosens. Bioelectron.* **19** (2004), 515.

[3] M. Pedrero, S. Campuzano, J.M. Pingarrón, *Anal. Methods* **3** (2011), 780.

[4] G. Carpini, F. Lucarelli, G. Marrazza, M. Mascini, *Biosens. Bioelectron*. **20** (2004), 167.

[5] P.M. Levine, P. Gong, R. Levicky, K.L. Shepard, *Biosens. Bioelectron*. **24** (2009), 1995.

[6] L. Tang, G. Zeng, G. Shen, Y. Li, C. Liu, Z. Li, J. Luo, C. Fan, C. Yang, *Biosens. Bioelectron.* **24** (2009), 1474.

[7] S. Girousi, V. Kinigopoulou, *Cent. Eur. J. Chem*. **8** (2010), 732.

[8] M.-Y. Wei, L.-H. Guo, P. Famouri, *Microchim Acta* **172** (2011), 247.

[9] K. Kerman, Y. Morita, Y. Takamura, E. Tamiya, *Electrochem. Commun*. **5** (2003), 887.

[10] J. Li, H. Tee Ng, A. Cassell, W. Fan, H. Chen, Q. Ye, J. Koehne, J. Han, M. Meyyappan, *Nano Lett.* **3** (2003), 597.

[11] T.I. Abdullin, I.I. Nikitina, D.G. Ishmukhametova, G.K. Budnikov, O.A. Konovalova, M.K. Salakhov, *J. Anal. Chem.* **62** (2007), 599.

[12] M.A. Lapierre-Devlin, C.L. Asher, B.J. Taft, R. Gasparac, M.A. Roberts, S.O. Kelley, *Nano Lett.* **5** (6) (2005), 1051.

[13] V.P. Menon, C.R. Martin, *Anal. Chem.* **67** (1995), 1920.

[14] M. De Leo, A. Kuhn, P. Ugo, *Electroanalysis* **19** (2007), 227.

[15] V.C. Rucker, K.L. Havenstrite, B.A. Simmons, S.M. Sickafoose, A.E. Herr, R. Shediac, *Langmuir* **21** (2005), 7621.

[16] S. Morais, R. Marco-Molés, R. Puchades, A. Maquieira, *Chem. Commun*. (2006), 2368.

[17] Z. Wang, R-X Li, *Nanoscale Res. Lett.* **2** (2007), 69.

[18] Y. Li, Z. Wang, L.M.L. Ou, H.-Z. Yu, *Anal. Chem.* **79** (2007), 426.

[19] S. Morais, L.A. Tortajada-Genaro, T. Arnandis-Chover, R. Puchades, A. Maquieira, *Anal. Chem.* **81** (2009), 5646.

[20] K. Krishnamoorthy, C.G. Zoski, *Anal. Chem*. **77** (2005), 5068.

[21] M. De Leo, F.C. Pereira, L.M. Moretto, P. Scopece, S. Polizzi, P. Ugo, *Chem. Mater.* **19** (2007), 5955.

[22] L.M. Moretto, M. Tormen, M. De Leo, A. Carpentiero P. Ugo, *Nanotechnology* **22** (2011), 185305.

[23] S.P. Mucelli, M. Zamuner, M. Tormen, G. Stanta, P. Ugo, *Biosens. Bioelectron*. **23** (2008), 1900.

[24] Lj. Fruk, J. Müller, G. Weber, A. Narvaez, E. Dominguez, C.M. Niemeyer, *Chem. Eur. J.* **13** (18) (2007), 5223.

[25] P. Ugo, L.M. Moretto, in *Handbook of Electrochemistry* (1st edn.), edited by C.G. Zoski, Elsevier, Amsterdam (2007) (Chapter 16.2).

[26] V.B. Ivanov, J. Behnisch, A. Holländer, F. Mehdorn, H. Zimmermann, *Surf. Interface Anal*. **24** (1996), 257.

[27] A. Papra, H.-G. Hicke, D. Paul, *J. Appl. Polym. Sci*. **74** (1999), 1669.

[28] J.V. Staros, R.W. Wright, D.M. Swingle, *Anal. Biochem.* **156** (1986), 220.

[29] J.-S. Park, N. L. Abbott, *Adv. Mater*. **20** (2008), 1185.

[30] B. Liberelle, C. Boucher, J. Chen, M. Jolicoeur, Y. Durocher, G. De Crescenzo, *Bioconj. Chem*., **21** (2010), 2257.

[31] N. Médard, M. Aouinti, F. Poncin-Epaillard, P. Bertrand, *Surf. Interface Anal*. **31** (2001), 1042.

[32] C. Geismann, M. Ulbricht, *Macromol. Chem. Phys*. **206** (2005), 268.

[33] N. Médard, J.-C. Soutif, F. Poncin-Epaillard, *Surf. Coat. Technol*. **160** (2002), 197.

[34] A.E.G. Cass, G. Davis, G.D. Francis, H.A.O. Hill, W.J. Aston, I.J. Higgins, E.V. Plotkin, L.D.L. Scott, A.P.F. Turner, *Anal. Chem*. **56** (1984), 667.

[35] K. Kleppe, *Biochem.* **5** (1966), 139.

[36] M. Silvestrini, P. Schiavuta, P. Scopece, G. Pecchielan, L.M. Moretto, P. Ugo, *Electrochim. Acta* **56** (2011), 7718.

[37] A.J. Bard, L.R. Faulkner, *Electrochemical Methods. Fundamentals and Applications* (2nd edn.), John Wiley & Sons, Inc., New York (2001) (Chapter 1).

[38] R. Gasparac, B.J. Taft, M.A. Lapierre-Devlin, A.D. Lazareck, J.M. Xu, S.O. Kelley, *J. Am. Chem. Soc.* **126** (2004), 12270.

Biosensors Based on the Modification of Ensembles of Nanoelectrodes with Gold Nanoparticles

1. Introduction

How already explained in the previous chapters of this thesis, a NEE is a two-dimensional composite device (herein called 2D-NEE), constituted by inlaid nanodisk electrodes embedded in the insulating polycarbonate membrane [1].

2D-NEEs present some unique characteristics, such as highly improved signal-to-background current ratio, very low detection limits, high sensitivity to charge transfer kinetics [2]; moreover, they are suitable to extreme miniaturization. However, 2D-NEEs show some limits in all those applications where systems with high electroactive area are required, for instance, in the case of electrochemical devices and sensors based on the use of electroactive molecules or redox mediators immobilized on electrode surfaces.

Recently, it was shown that 3D ensembles of metal nanowires can be obtained by plasma or chemical etching of 2D-NEE. Such 3D-NEEs have been successfully applied to prepare advanced electrochemical sensors [3,4]. However, electrode systems with large surface area and controlled nano-geometries can further improve the electrochemical and sensing capabilities of these devices.

In this chapter, a new strategy to fabricate 3D nanostructures on NEEs is presented and discussed. This approach is based on the immobilization of gold nanoparticles (AuNPs) on the metal surface of "conventional" 2D-NEEs; this is achieved by exploiting the binding properties of bifunctional thiols [5]. The increase in active area is then verified by CV, using adsorbed redox species.

After immobilization of the nanoparticles, the metal surface is further functionalized with suitable biomolecules, namely thiolated oligonucleotides. It is known that AuNPs can be used either for the immobilization of oligonucleotides [6] and as labels for the detection of the DNA hybridization [7,8].

In particular, we immobilized single-stranded DNA ($_{ss}$DNA) probes on the AuNPs deposited on the NEE. The hybridization with complementary target strands is then verified electrochemically using glucose oxidase (GOx), as the enzyme label bound to the target sequences. A ferrocene derivative is used as redox mediator to shuttle electrons from the enzyme to the nanoelectrodes.

Experimental results obtained by this system constitute a proof of concept of feasibility of a rather complex NEE-based nanostructure. Moreover, they allow one to verify and compare the analytical potentialities of AuNPs-NEEs vs. conventional 2D-NEEs.

2. Experimental

2.1. Materials

Trisodium citrate dihydrate was from Merck; cysteamine hydrochloride and phosphomolybdic acid, $H_3PMo_{12}O_{40}$ (PMA), were purchased from Sigma Aldrich. All other reagents were of analytical grade and were used as received. Purified water was obtained using a Milli-Ro plus Milli-Q (Millipore) water purification system.

Chloroauric acid was prepared dissolving an amount of metallic gold in aqua regia, heating the acidic solution under stirring and concentrating it by evaporation. Afterward, three subsequent additions of 1.2 M HCl and two additions of water were done. The solution was concentrated every time. The gold plating solution (sodium gold sulfite, $Na_3[Au(SO_3)_2]$), was easily prepared starting with the reaction of chloroauric acid and a slight excess of sodium bicarbonate. This reaction allows the formation of sodium chloroaurate ($Na(AuCl_4)$). The solution was allowed to concentrate, until orange crystals were formed. At this point, the procedure reported by J.A. Abys et al. [9] was followed, adapting the various concentrations at the initial concentration of metallic gold used by us for the synthesis of chloroauric acid.

The chloroaurate crystals were dissolved in water, heated at 80° C under stirring and then barium hydroxide was added to the stirred solution, causing a colour change to brown. Subsequently, NaOH, preferably as concentrated aqueous solution, was added and the temperature was increased to boiling. The pH of this solution should be between 6 and 8. After adjusting of pH, the solution was cooled and filtered. The precipitate was repeatedly rinsed with small amounts of cold water. Then, the precipitate was dissolved in water and the solution was heated at 50° C under stirring. The solution was then cooled and the precipitate was collected. Heating, cooling and filtration were repeated two times.

The final precipitate was dissolved in water, brought to 60-65° C and subsequently Na_2SO_3 was added under stirring. The solution was kept at this temperature until a purple precipitate was formed, with disappearance of the previous brown precipitate. The solution was finally filtrated and kept in the dark until use.

Thiolated $_{ss}$DNA (SHD1) and complementary thiolated $_{ss}$DNA (SHD2) were purchased from Sigma Aldrich and had the following sequences:

SHD1: HS-5' GTGGAAAGTGGCAATCGTGAAG 3'

SHD2: HS-5' TTTTTTCTTCACGATTGCCACTTTCCAC 3'

All oligonucleotides stock solutions (100 uM) were prepared in TE buffer (50 mM Tris, 100 mM NaCl, 1 mM EDTA in pH 7.4) and kept frozen until use.

The complementary strand (SHD2) was conjugated with glucose oxidase (GOx) as already described in the previous chapter (paragraph 2.3.).

Track-etched polycarbonate (PC) membrane filters were obtained from SPI-pore™ with nominal pore diameter of 30 nm, average pore density of 6×10^8 pores cm^{-2} and coated with polyvinylpyrrolidone (PVP) by the producer.

2.2. Electrochemical apparatus

All electrochemical measurements were carried out at room temperature with a CH660A potentiostat controlled via personal computer by its own software, using a three-electrode single-compartment cell equipped with a platinum counter electrode and an Ag/AgCl (KCl saturated) reference electrode, to which all reported potential values are referred.

2.3. Synthesis of gold nanoparticles (AuNPs)

AuNPs were synthesized following the method described by Gooding et al. [10], with some modifications. Briefly, 100 mL of a 1 mM $HAuCl_4$ solution was heated to boiling under stirring.

4 mL of 0.05 M trisodium citrate were added to the first solution with constant stirring. A color change was evident after the addition of citrate, from yellow to colorless, then grey, black and finally red vine. The solution was kept under heating and stirred for 10 minutes. After this time, the heat was turned off and the solution was stirred for 10 more minutes. Finally, the colloidal solution was cooled at RT and the volume was adjusted. The solution was kept in the dark until use.

2.4. Electrode preparation and functionalization

2.4.1. Fabrication of NEEs and modification with AuNPs

2D-NEEs were fabricated using a well known electroless plating procedure and assembled as previously described (ref. [11] and chapter 3, paragraph 2.3.). The geometric area (A_{geom}) of the NEEs used here is tipically 0.07 cm^2.

NEEs modified with AuNPs (AuNPs-NEEs) were prepared exploiting the formation of interactions between the gold surface (the metal surface of either NPs and nanodisks) and specific functional groups (-SH, -NH_2). In this case, self-assembled monolayers (SAMs) furnished a simple method to obtain surfaces with composition, structure and thickness well defined.

For the modification of NEE with SAMs, the electrode was dipped overnight (16 h ca.), into a 10 mM cysteamine solution in water. Being a small molecule, this bifunctional thiol forms SAMs that don't interfere with the electronic transfer between electrode and redox species in solution. Cysteamine is to prefer to dithiols, because it cannot form multilayers or disulfide bridges that can decrease the efficiency in the cross-linking. Moreover, SH terminal groups bind preferentially to the metal surface of NEEs leaving the amino groups free for the subsequent NPs immobilization.

The NEE modified with SAMs (cyst-NEE) was then immersed into the colloidal gold solution, prepared as described before. The incubation was allowed to proceed for 8 h at RT. The formation of a 3D-structure takes place through the attachment of the nanoparticles to the free amino functionalities present on the monolayers, by weak covalent bonds [12,13].

The general scheme of an AuNPs-NEE is shown here:

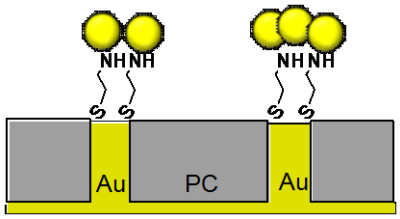

Scheme 1. Representation of an AuNPs-NEE. *Note*: the dimensions are not in scale.

In order to ascertain that the presence of SAMs effectively favors the immobilization of NPs, also a not thiolated NEE was incubated into the colloidal solution for 8 h.

2.4.2. Functionalization of AuNPs-NEEs with oligonucleotides

5 µL of a 2 µM SHD1 solution in 10 mM TE buffer (pH= 7.2) with 1 M NaCl, were spotted onto the geometric area of an AuNPs-NEE, at RT. It is important to note that the concentration of the buffer containing the strands has a significant influence in the immobilization step. In fact, in high ionic strength solutions, the electrostatic repulsions between oligonucleotides are minimized [14], and a high coverage of the electrodic surface can be achieved.

After 1 h, the electrode was rinsed dipping into pure TE buffer for 10 minutes and subsequently spotted with 5 µL of 2 µM target conjugated with GOx, in 10 mM TE buffer (pH= 7.2) with 1 M NaCl. Finally, the NEE was immersed in TE buffer for 10 more minutes and allowed to dry in air. The same functionalization steps were performed, for comparison, on a bare NEE.

3. Results and discussion

3.1. Characterization of the colloidal solution

The AuNPs solution was characterized by UV-vis spectroscopy. Figure 1 shows the absorbance spectrum where a single peak with a maximum at 525 nm was detected, that corresponds to the excitation surface plasmon resonance of the gold nanoparticles [15]. The shape of the observed spectrum is typical of a system with a quite narrow size distribution [16].

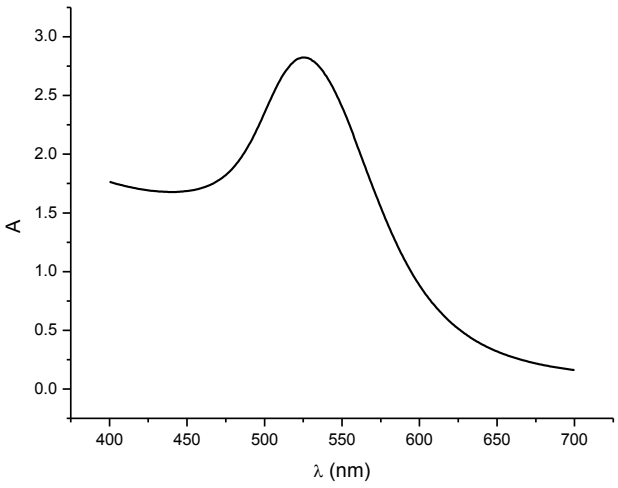

Figure 1. Absorbance spectra relative to the colloidal gold solution.

The average diameter of the nanoparticles was calculated from the spectrum, by using the following equation proposed by Haiss [17]:

$$d = \exp (B_1 A_{spr}/A_{450} - B_2) \qquad (1)$$

where the numerical parameters B_1 and B_2 were determined experimentally. Using these values (B_1= 3.00 and B_2= 2.20), the diameter can be calculated with an error of ~ 11%. In our case, the equation allowed to obtain a value of *d* equal to 16 nm.

This value is in quite agreement with TEM images reported in Figure 2, where a prevalence of rotund nanoparticles with a diameter of almost 20-30 nm are shown.

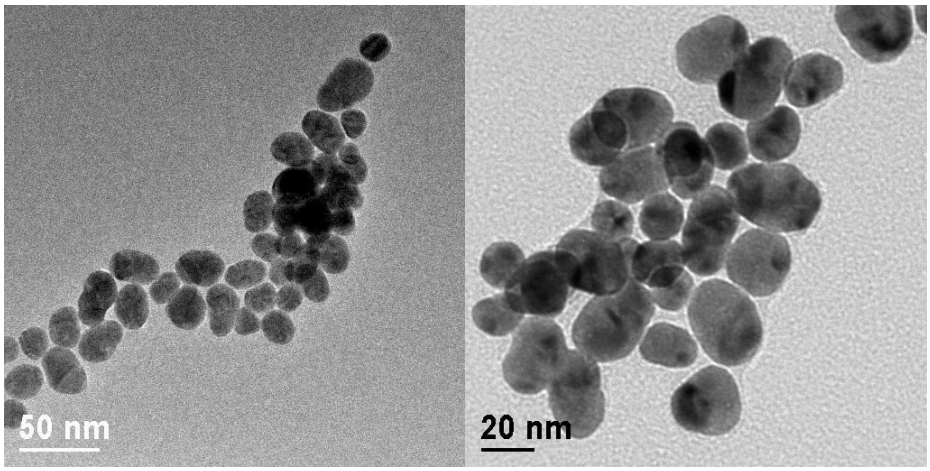

Figure 2. TEM images of gold nanoparticles at different magnifications.

3.2. Electrochemical characterization of AuNPs-NEEs

Figure 3 compares the cyclic voltammograms recorded at a bare NEE (Fig. 3a and b, full lines), with those obtained with a not thiolated NEE (Fig. 3a, dashed curve) and a cyst-NEE (Fig. 3b, dashed curve), both immersed for 8 h into the colloidal gold solution. The characterization was performed into pure supporting electrolyte (1 mM KNO_3), at 50 mV/s.

It is evident that in the absence of monolayers of cysteamine, the nanoparticles cannot bind to the gold surfaces of the NEE and its active area (A_{act}) doesn't change. This is demonstrated by the fact that the capacitive current (I_C), which is proportional to the active area (eq. 2, chapter 1), remains unchanged.

On the contrary, the presence of the amino groups on the nanoelectrode surfaces allows the immobilization of the AuNPs, causing a dramatic increase in the capacitive current.

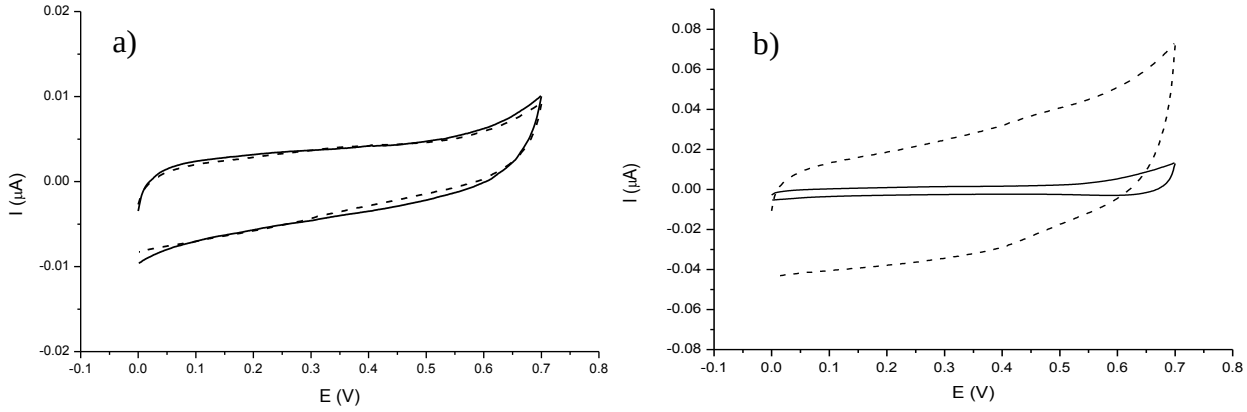

Figure 3. Cyclic voltammograms recorded in 1 mM KNO_3 at a not thiolated NEE (a) and a cyst-NEE (b), before (full lines) and after (dashed lines) the incubation into the colloidal solution. Scan rate 50 mVs^{-1}. Note the scale of y-axis.

The analysis of the blank CV at different scan rates, allows one to calculate A_{act} of the electrodes. As shown in Figure 4, I_C scales linearly with v both for the bare NEE and for the AuNPs-NEE.

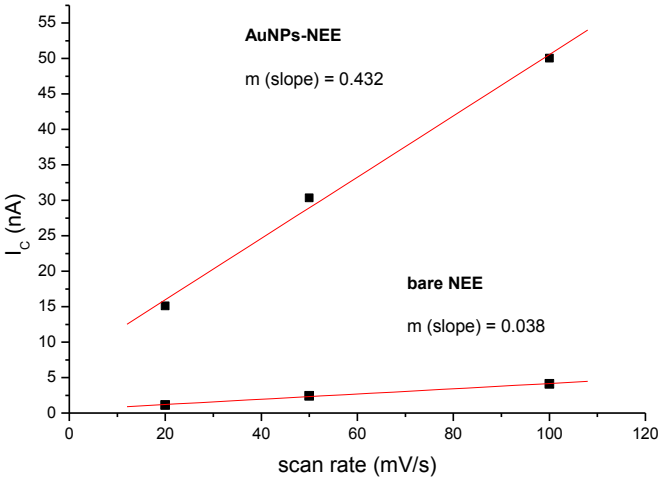

Figure 4. Plots I_C vs. scan rate.

By using equation 2, from the slopes of the straight lines, it was possible to calculate A_{act} values for the bare NEE and the AuNPs-NEE, that are 1.4×10^{-3} cm^2 and 16×10^{-3} cm^2, respectively.

$$m = C_{dl} \times A_{act} \qquad (2)$$

A C_{dl} value of 21 μF cm^{-2} [1] was used for the calculations.

It was demonstrated that the average diameter of the nanoelectrodes in our ensembles is really 50 ± 10 nm [18]. Taking into account this value and the experimental nanoelectrode density (6.5 × 10^8 pores cm^{-2} [18]), one can calculate a value of almost 1.2 × 10^{-3} cm^2 for expected A_{act} of the bare NEE. This result is in accordance with the value calculated by equation 2.

The above results indicate that the AuNPs-NEE presents an one-order of magnitude increase in A_{act}, caused by the treatment with AuNPs.

Both electrodes were then compared into a solution containing a redox mediator. Figure 5 shows the CVs recorded in 10^{-4} M FA^+ in 10^{-2} M phosphate buffer (pH 7.0) at 10 mV/s. In presence of SAMs of cysteamine (dashed line) it is evident a decrease of the anodic peak of the mediator. This could be due to the fact that at pH 7.0, the amino group of cysteamine is protonated (pKa_{amino}= 10.7 [19]), so it partially repels the positively charged mediator from the electrodic surface.

In presence of the AuNPs the active area increases, consequently the capacitive current increases (dotted curve). However, the reversible oxidation of FA^+ is still well detectable and its oxidation peak current is comparable to the one recorded with the bare unmodified NEE.

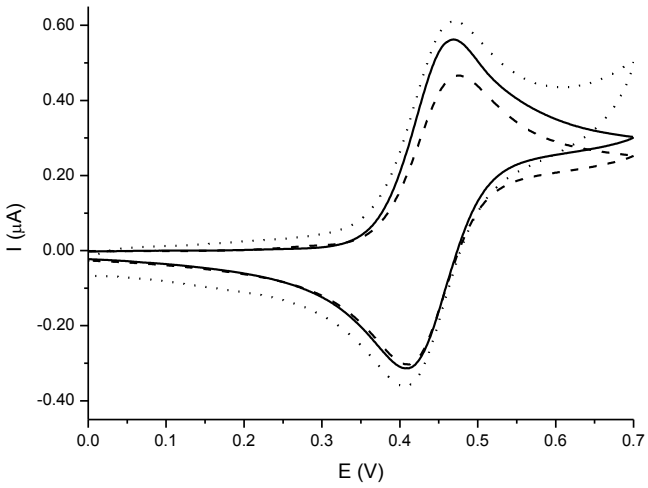

Figure 5. Cyclic voltammograms recorded with a bare NEE (full line), a cyst-NEE (dashed line) and an AuNPs-NEE (dotted line) in a 10^{-2} M phosphate buffer solution (pH= 7) containing 10^{-4} M $FA^+PF_6^-$. Scan rate 10 mVs^{-1}.

A further characterization was made in order to study the increase in the active area, passing from a 2D to a more complex 3D-structure.

A bare NEE and an AuNPs-NEE were immersed for 1 h at RT, into an aqueous solution containing 5 mM phosphomolybdic acid (PMA). Subsequently, the electrodes were rinsed with water and characterized by cyclic voltammetry in 0.5 M H_2SO_4 [4].

Figure 6a reports a comparison between the CVs relative to the bare NEE treated with the polyoxo-metalate, at different scan rates. The voltammograms obtained show two reversible processes, which correspond to the following consecutive reduction steps:

$$PMo_{12}O_{40}^{3-} + 2e^- \leftrightarrow PMo_{12}O_{40}^{5-}$$

$$PMo_{12}O_{40}^{5-} + 2e^- \leftrightarrow PMo_{12}O_{40}^{7-}$$

The peak current values depend linearly on the scan rate, indicating a surface process related to molecules adsorbed on the gold surface of the NEE.

The electrochemical signal of the PMA increases dramatically at the AuNPs-NEE (Figure 6b), in agreement with the higher active area due to the presence of the nanoparticles.

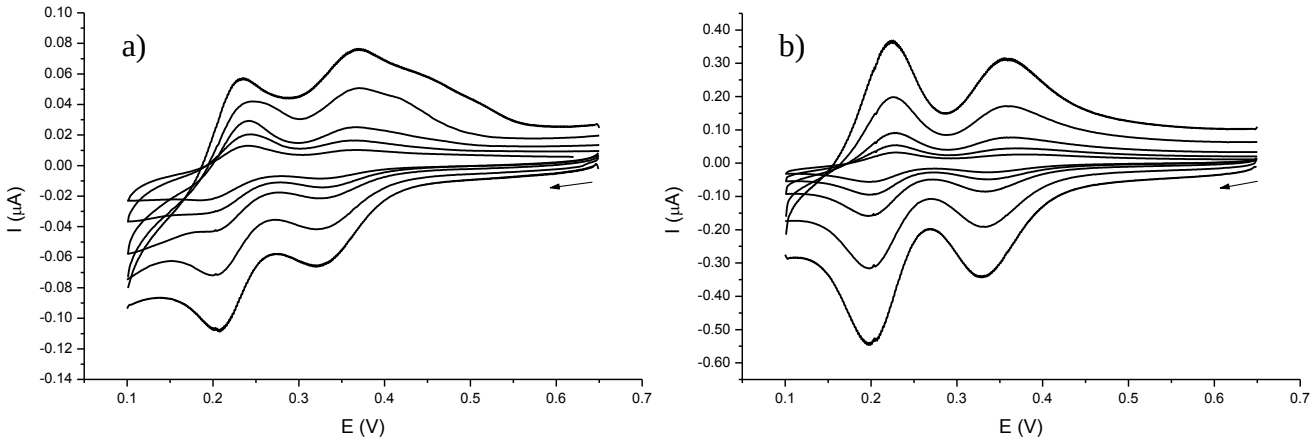

Figure 6. Cyclic voltammograms recorded in 0.5 M H_2SO_4 with a bare NEE (a) and an AuNPs-NEE (b) both treated with PMA. Scan rates: 5, 10, 20, 50 and 100 mV/s.

Figure 7 shows the comparison between the voltammograms relative to both NEEs, recorded at 10 mV/s.

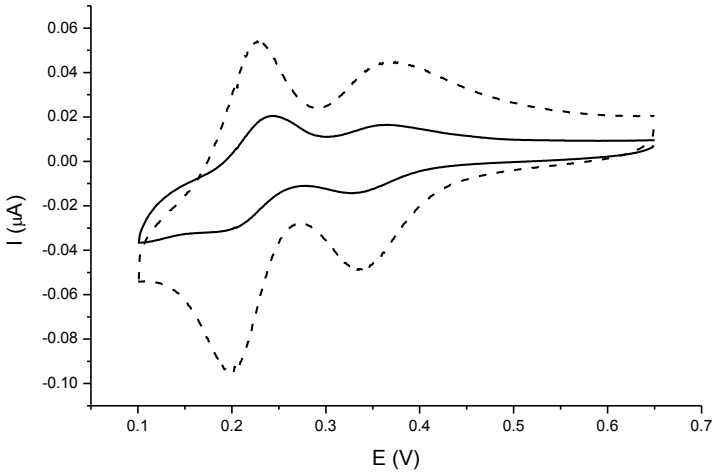

Figure 7. Cyclic voltammograms recorded in 0.5 M H_2SO_4 with a bare NEE (full line) and an AuNPs-NEE (dashed line), both treated with PMA. Scan rate 10 mV/s.

By integrating the first reduction peak, it was possible to obtain the charge value (Q) associated with the peak. From this value, the number of moles adsorbed (m) onto both NEEs was then calculated, with the following equation:

$$m = Q/ nF \qquad (3)$$

where n is the number of electrons exchanged in the reaction (in this case two) and F is the Faraday constant.

By the Avogadro's number one can also calculate the total number of molecules adsorbed on both electrodes (Table 1).

	I_{pc1} (A)	**Q (C)**	**m (mol)**	**molecules**
Bare NEE	1.1×10^{-8}	9.3×10^{-8}	4.8×10^{-13}	2.9×10^{11}
AuNPs-NEE	3.7×10^{-8}	3.3×10^{-7}	1.7×10^{-12}	1.0×10^{12}

Table 1. Values relevant for the calculation of molecules adsorbed on both electrodes.

Both, charge and number of moles increase at the AuNPs-NEE, confirming the possibility to immobilize a larger amount of electroactive molecules (almost three times higher) onto the 3D structure, respect to a bare 2D-NEE.

PMA is a Keggin-type heteropoly anion [20] characterized by a spherical structure with size of about 1 nm [21]. Only for simplification, we considered this polyoxometalate as a sphere with d = 1 nm, therefore with a cross area of approximately 0.78×10^{-14} cm^2. In this way, we were able to estimate a theoretical two-dimensional area covered by the molecules, that was 23×10^{-4} cm^2 for the bare NEE and 78×10^{-4} cm^2 for the AuNPs-NEE.

The first value is larger than the active area of the bare NEE calculated before. Since POMs adsorb onto a surface through the formation of a monolayer [20-22], the higher value obtained can be due to the fact that the heads of the nanodisks are not perfectly flat but with rounded heads, as already seen by AFM measurements (see chapter 4 and ref. [23]). Consequently, the gold surface area available for PMA adsorption is larger than the calculated A_{act} of the assembly.

On the other hand, the total area covered by POMs on the AuNPs-NEE, is less than half of the value calculated with the capacitive current method. This can be easily explained considering that the A_{act} value calculated by equation 2, and relative to the electrode modified with nanoparticles, corresponds to the whole metal surface of the particles, while the gold surface available for the adsorption of PMA is only the surface of the nanoparticles in direct contact with the solution, since a significant part of them is involved in the cross-linkage with SAMs or can be covered by the other ones.

3.3. Preliminary results on the use of AuNPs-NEEs as biosensors

Once verified the possibility to build nanostructures aimed at increasing the metal surface of NEEs, preliminary tests for the use of these devices as platforms to produce electrochemical biosensors were performed. The procedure consisted in the direct immobilization of thiolated oligonucleotides (SHD1) directly onto the metal surfaces of a 2D and a 3D-NEE and the subsequent hybridization with complementary target sequences conjugated with GOx (see the experimental section).

A blocking step with thiols is often carry out between the immobilization of $_{ss}$DNA onto the electrodic surface and the hybridization with the target. This procedure is used both, to prevent any non specific adsorption of the target labeled with enzymes and to favor a higher accessibility of the probes bound to the Au surface [24].

In our case, the introduction of the blocking step, carried out by immersion (1 h) of the electrode into a 1 mM 6-mercaptohexanol solution in TE buffer, 1 M NaCl, didn't show any advantage in the functionalization.

Electrochemical characterization of both functionalized electrodes was performed into a

deoxygenated 10 mM phosphate buffer solution (pH= 7), containing 0.1 mM FA^+.

Figure 8 shows the comparison between the results obtained with the 2D-NEE (Fig. 8a) and the NEE modified with AuNPs (Fig. 8b).

The full line voltammograms show the reversible oxidation of FA^+ recorded at both NEEs. In the presence of 0.05 M glucose (dashed lines) the curve shape changes significantly: the oxidation peak increases while the reduction peak disappears.

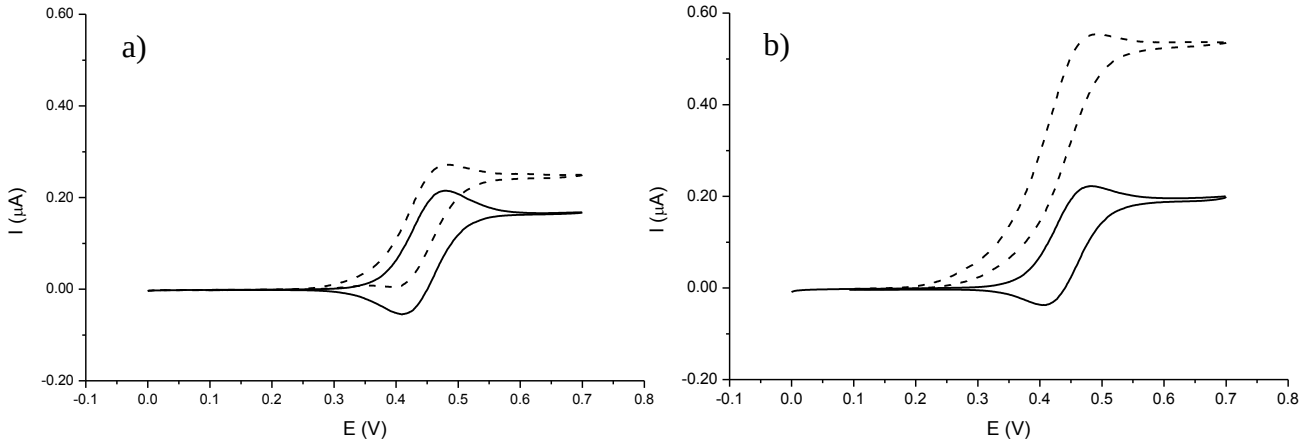

Figure 8. Cyclic voltammograms recorded with a 2D-NEE (a) and an AuNPs-NEE (b) in a 10 mM phosphate buffer solution (pH= 7) containing 0.1 mM FA^+ PF_6^- before (full lines) and after (dashed lines) the addition of 0.05 M glucose. Scan rate 2 mVs^{-1}.

The voltammogram shape changes because in co-presence of both enzyme and substrate, the mediator is reduced chemically at the interface electrode-solution to be then re-oxidized exchanging electrons with the electrodic surfaces (Scheme 2).

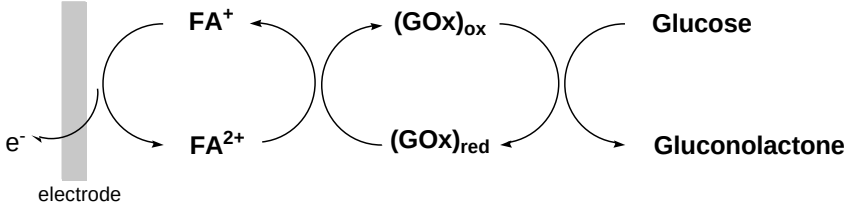

Scheme 2. Mechanism of mediated electron transfer.

It is important to note that with NEEs modified only with the probe sequences, consequently without hybridization with the complementary strands conjugated with GOx, no catalytic signal was observed.

Figure 8 also puts in evidence a larger catalytic current at the AuNPs-NEE, that is almost 2 times higher than that recorded with the conventional 2D-NEE.

The comparison between the oxidation peak current values relative to both NEEs, at different concentrations of glucose (Figure 9), shows that the catalytic current value increases up to a glucose solution concentration of 0.01 M reaching, afterwards, a plateau. A similar behavior is observed for the 2D-NEE with a plateau current that is, how said before, half of the one at the AuNPs-NEE.

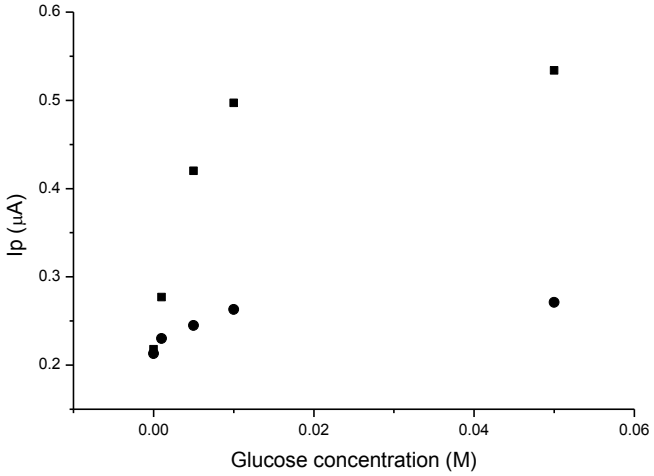

Figure 9. Oxidation peak current values recorded with a bare NEE (circles) and an AuNPs-NEE (squares) in a 10 mM phosphate buffer solution (pH= 7) containing 0.1 mM FA^+ PF_6^- at increasing glucose concentrations (0 M; 1 mM; 5 mM; 0.01 M and 0.05 M). Scan rate 2 mVs^{-1}.

The higher catalytic effect recorded at the 3D-NEE is more evident if we plot ΔI_p vs. glucose concentration (Figure 10). In this way, the anodic current peak value recorded at both NEEs, before the addition of glucose, is subtracted to the catalytic current values measured in presence of increasing concentrations of substrate.

For the AuNPs-NEE, the plateau current is more than 5 times bigger than the one at the 2D-NEE.

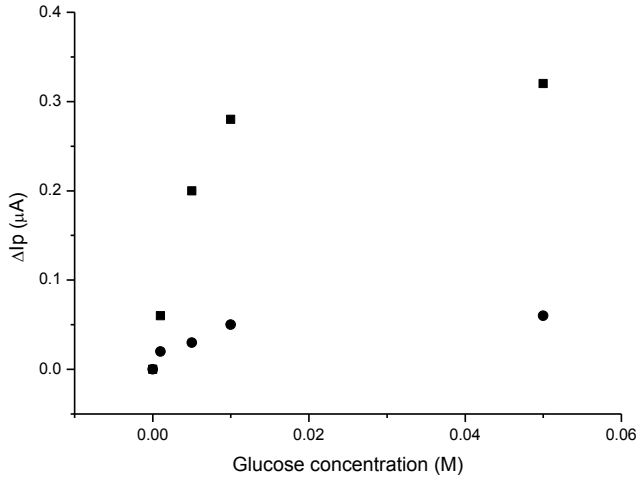

Figure 10. ΔI_p values relative to the bare NEE (circles) and the AuNPs-NEE (squares) in a 10 mM phosphate buffer solution (pH= 7) containing 0.1 mM FA^+ PF_6^- at increasing glucose concentrations (0 M; 1 mM; 5 mM; 0.01 M and 0.05 M). Scan rate 2 mVs^{-1}.

All these results indicate the higher efficiency in the immobilization on the nanoparticles, especially thanks to the larger surface area.

4. Conclusions

The preliminary results shown here confirm the possibility to easily modify "conventional" NEEs with gold nanoparticles, in order to fabricate 3D-NEEs useful for sensing or biosensing applications. In this way, no polymer etching to obtain three-dimensional structures is necessary, therefore any treatment than can make worse the performances of the electrodes is avoided. In fact, the two widely used etching procedures, i.e. O_2 plasma and chemical etching with dichloromethane, both cause a partial loss in the sealing between PC membrane and gold nanofibers [4]. The formation of holes around the electrodes exposes to the solution a wider electrodic surface, making difficult the control of the active area of the NEE.

It is also important to note that these electrode constructs maintain an "ensemble" structure, consequently keeping all the advantages typical of such a geometry. Moreover, the AuNPs don't block the electron transfer with redox species present in solution.

Finally, the experiments reported herein put in evidence as these devices are suitable platforms for the immobilization and detection of a bigger amount of redox species or biological molecules, respect to 2D-NEEs.

References

[1] V.P. Menon, C. Martin, *Anal. Chem*. **67** (1995) 1920.

[2] L.M. Moretto, S. Panero, B. Scrosati, P. Ugo, in *Handbook of Electrochemical Nanotechnology*, edited by Y. Lin, H.S. Nalwa, ASP, Stevenson Ranch **vol. 1** (2009), 87.

[3] R. Gasparac, B.J. Taft, M.A. Lapierre-Devlin, A.D. Lazareck, J.M. Xu, S.O. Kelley, *J. Am. Chem. Soc.* **126** (2004), 12270.

[4] M. De Leo, A. Kuhn, P. Ugo, *Electroanalysis* **19** (2007), 227.

[5] J. Dyne, Y.-S. Lin, L. M. H. Lai, J. Z. Ginges, E. Luais, J. R. Peterson, I. Y. Goon, R. Amal, J. J. Gooding, *ChemPhysChem*, **11** (2010), 2807.

[6] S.-f. Liu, Y.-f. Li, J.-r. Li, L. Jiang, *Biosens. Bioelectron*. **21** (2005) 789.

[7] F. Wang, S. Hu, *Microchim. Acta* **165** (2009), 1.

[8] M.T. Castaneda, S. Alegret, A. Merkoci, *Electroanalysis* **19** (2007), 743.

[9] J.A. Abis, J.J. Maisano, US Patent N° 6,126,807 (2000).

[10] J.B. Shein, L.M.H. Lai, P.K. Eggers, M.N. Paddon-Row, J.J. Gooding, *Langmuir* **25** (2009), 11121.

[11] P. Ugo, L. M. Moretto, in *Handbook of Electrochemistry*, Ed. C. G. Zoski, Elsevier, **2007**, Cap. 16, Sezione 16.2.

[12] D.V. Leff, L. Brandt, J.R. Heath, *Langmuir* **12** (1996), 4723.

[13] R.C. Hoft, M.J. Ford, A.M. McDonagh, M.B. Cortie, *J. Phys. Chem. C* **111** (2007) 13886.

[14] A.W. Peterson, R.J. Heaton, R.M. Georgiadis, *Nucleic Acids Res*. **29** (24) (2001), 5163.

[15] S. Mandal, S. Phadtare, M. Sastry, *Curr. Appl. Phys.* **5** (2005), 118.

[16] C. Cao, S.J. Sim, *Biosens. Bioelectron.* **22** (2007), 1874.

[17] W. Haiss, N.T.K. Thanh, J. Aveyard, D.G. Fernig, *Anal. Chem*. **79** (2007), 4215.

[18] P. Ugo, N. Pepe, L.M. Moretto, M. Battagliarin, *J. Electroanal. Chem.* **560** (2003), 51.

[19] T.-C. Huang, L.-Z. Huang, C.-T. Ho, *J. Agric. Food Chem.* **46** (1998), 224.

[20] M.S. Kaba, I.K. Song, M.A. Barteau, *J. Phys. Chem.* **100** (1996), 19577.

[21] G. Zhang, T. He, Y. Ma, Z. Chen, W. Yang, J. Yao, Phys. Chem. Chem. Phys. **5** (2003), 2751.

[22] D. Martel, N. Sojic, A. Kuhn, *J. Chem. Ed.* **79** (2002), 349.

[23] M. Silvestrini, P. Schiavuta, P. Scopece, G. Pecchielan, L.M. Moretto, P. Ugo, *Electrochim. Acta* **56** (2011), 7718.

[24] T.M. Herne, M.J. Tarlov, *J. Am. Chem. Soc.* **119** (1997), 8916.

Concluding remarks

This thesis demonstrates the possibility to extend the applications of NEEs, in the field of environmental application (chapter 3), from analytical chemistry to bio-sensing (chapters 4-6).
In the first case, thanks to their particular geometry, NEEs allow the direct analysis of trace elements in samples, in our case iodide, by a simple method that doesn't require any additional preconcentration or deoxigenation step. In fact, under well defined diffusion conditions, these devices show enhanced detection limits relative to mm-sized electrodes.
With respect to biosensing applications of NEEs in samples containing biological molecules which can adsorb on gold, poisoning the surface of the nanoelectrodes, in this thesis we demonstrate that the protection of the metal surface of NEEs with self-assembled monolayers (SAMs) of thiols or disulfides, constitutes an easy and efficient way to overcome such a fouling problem.
NEEs show to be useful and applicable also the DNA-hybridization detection. To this goal, we demonstrate the feasibility of two different approaches, where either the polycarbonate (PC) surface or the gold nanodisks are alternatively used as platform to immobilize the biorecognition elements.
Polycarbonate is a suitable substrate for the functionalization of both, proteins or DNA sequences, mainly because possesses functional groups that can be used for the direct linkage of the macromolecules. Moreover, because of its wide surface available for the functionalization, it allows the immobilization of a large amount of biomolecules.
The collaboration with the Fruk Group (Karlsruhe Institute of Technology (KIT), DFG - Centre for Functional Nanostructures), allowed the development of a protocol suitable for an efficient immobilization of DNA probes on the PC of NEEs.
Instead, the functionalization of the gold surface with thiolated DNA has required an increase in active area of the ensemble. This has been done by fabricating more complex 3D-structures starting from conventional 2D-NEEs, modified with gold nanoparticles (AuNPs). An interesting feature is that the modification didn't change the geometric features of the assembly, leaving unchanged all the advantages of these kind of sensors.
In both cases (functionalization of PC or gold), the use of NEEs allowed the detection of few tens of picomoles of target DNA.
Further efforts should be done in order to apply these procedures to the fabrication of biosensors suitable for the electrochemical detection of longer DNA strands, as well as to test and validate

the quantification limits of the proposed sensors with respect to their application as real diagnostic tools, to be employed also in clinical analyses.

Appendix

Publications in international journals

- ✓ P. Ugo, L.M. Moretto, M. Silvestrini, F.C. Pereira, Nanoelectrode Ensembles for the Direct Voltammetric Determination of Trace Iodide in Water, *Intern. J. Environ. Anal. Chem.* **90** (9) (2010), 747-759.

- ✓ M. Silvestrini, K. Bortolozzo, D. Paladin, P. Ugo, Biofunctionalization of Nanoelectrode Ensembles: Protection of the Nanoelectrodes with Self-Assembled Monolayers, *ECS Transactions* **25** (17) (2010), 1-9.

- ✓ M. Silvestrini, P. Schiavuta, P. Scopece, G. Pecchielan, L.M. Moretto, P. Ugo, Modification of Nanoelectrode Ensembles by Thiols and Disulfides to Prevent non Specific Adsorption of Proteins, *Electrochim. Acta* **56** (2011), 7718-7724.

- ✓ M. Silvestrini, L. Fruk, P. Ugo, Electrochemical DNA Biosensors Based on Ensembles of Polycarbonate Embedded Nanoelectrodes, in preparation.

Oral presentations to national/international scientific meetings

- ✓ YISAC 2009, Graz (June 29th – July 2nd 2009): "Nanoelectrode Ensembles for the Direct Voltammetric Determination of Trace Iodide in Water", M. Silvestrini, P. Ugo, L.M. Moretto.

- ✓ YISAC 2010, Venice (June 29th – July 1st 2010): "Functionalization and Protection of Nanoelectrodes Ensembles by SAMs", M. Silvestrini, P. Schiavuta, D. Paladin, P. Ugo.

- ✓ SCI 2010, Como (September 12th – 16th 2010): "Functionalization of Nanoelectrode Ensembles for Biosensing Purposes", M. Silvestrini, P. Schiavuta, L.M. Moretto, P. Ugo.

Poster contributions to national/international scientific meetings

- ✓ SCI 2009, Sorrento (July 5th – 10th 2009): "Nanoelectrode Ensembles for the Direct Voltammetric Determination of Trace Iodide in Water", M. Silvestrini, L.M. Moretto, P. Ugo.

- ✓ ISE 2010, Nice (September 26th – October 1st 2010): "Use of Nanoelectrode Ensembles as Electrochemical Biosensors", M. Silvestrini, K. Bortolozzo, D. Paladin, P. Ugo; "Direct Voltammetric Determination of Trace Iodide in Water by Nanoelectrode Ensembles", M. Silvestrini, L.M. Moretto, P. Ugo.

- ✓ Summer School on Nano-Biology 2010, Bad Herrenalb (September 7th – 11th 2011): "Functionalization of Nanoelectrode Ensembles for Biosensing Purposes", M. Silvestrini.

- ✓ NanotechItaly 2011, Venice (November 23th – November 25th 2011): "Advanced Applications of Ensembles of Electrochemical Nanoelectrodes: from Biosensors to Photoelectrochemical Devices", M. Silvestrini, M. Ongaro, L.M. Moretto, P. Ugo, K. Bortolozzo, D. Paladin.